BROADBAND IMPEDANCE MATCHING OF ANTENNA RADIATORS

by

Vishwanath Iyer

A Dissertation

Submitted to the Faculty

of the

WORCESTER POLYTECHNIC INSTITUTE

in partial fulfillment of the requirements for the

Degree of Doctor of Philosophy

in

Electrical and Computer Engineering

August 2010

Approved:

Dr. Sergey N. Makarov (Advisor) _____

Dr. Reinhold Ludwig (WPI) _____

Dr. William Michalson (WPI) _____

Dr. Faranak Nekoogar (LLNL) _____

To my wife, Smita

Abstract

In the design of any antenna radiator, single or multi-element, a significant amount of time and resources is spent on impedance matching. There are broadly two approaches to impedance matching; the first is the distributed impedance matching approach which leads to modifying the antenna geometry itself by identifying appropriate degrees of freedom within the structure. The second option is the lumped element approach to impedance matching. In this approach instead of modifying the antenna geometry a passive network attempts to equalize the impedance mismatch between the source and the antenna load.

This thesis introduces a new technique of impedance matching using lumped circuits (passive, lossless) for electrically small (short) non-resonant dipole/monopole antennas. A closed form upper-bound on the achievable transducer gain (and therefore the reflection coefficient) is derived starting with the Bode-Fano criterion. A 5 element equalizer is proposed which can equalize all dipole/monopole like antennas. Simulation and experimental results confirm our hypothesis.

The second contribution of this thesis is in the design of broadband, small size, modular arrays (2, 4, 8 or 16 elements) using the distributed approach to impedance matching. The design of arrays comprising a small number of elements cannot follow the infinite array design paradigm. Instead, the central idea is to find a single optimized radiator (unit cell) which if used to build the 2x1, 4x1, 2x2 arrays, etc. (up to a 4x4 array) will provide at least the 2:1 bandwidth with a VSWR of 2:1 and stable directive gain ($\leq$ 3 dB variation) in each configuration. Simulation and experimental results for a solution to the 2x1, 4x1 and 2x2 array configurations is presented.

Acknowledgement

This dissertation describes the research work done during my time at the Antenna Lab, in the ECE department at WPI.

I thank Prof. Sergey Makarov for agreeing to be my advisor, for allowing me to observe and learn, for being generous with his time and energy, for having faith in me, for giving me the space to explore, and contribute to a variety of different topics (indeed, only after we had pinned down my thesis topic), and for asking more of me. I also want to thank his wife Natasha for her warmth and kindness.

I thank Prof. Reinhold Ludwig, Prof. William Michalson and Dr. Faranak Nekoogar for agreeing to serve on my thesis committee and providing me with feedback. I was fortunate enough to assist Prof. Ludwig with ECE 2112 and ECE 3113 as a TA. I thoroughly enjoyed my interactions with him and with the students. I also thank him for giving me the opportunity to help out with the course instruction for ECE 2112 and see up close the classroom dynamic from the other side!

I thank Prof. Michalson for entertaining the initial email from me, accepting me as a Ph.D. student, and advising me.

I thank Dr. Nekoogar for interacting with me on several occasions regarding my thesis work and also for giving me the opportunity to collaborate on the book chapter.

My time during the Ph.D. would not have materialized if not for the support from the ECE department for my education in the form of the Teaching Assistantship. I thank Prof. Fred Looft for his continuous support. I would also like to thank Cathy, Colleen, Brenda and Stacie in the ECE office for the assistance, conversations and of course for being the keepers of all things sweet. Many thanks to Bob Brown for his assistance with the all important ECE server cluster.

My friends in the Antenna Lab, Daniel Harty, Brian Janice, Ed Oliveira and Tao Li made this experience richer. Special thanks to Daniel - the big array guy, who helped me with experimentally verifying the lumped component and distributed matching techniques presented in this thesis. A big thank you to Brian – super god balun steiner for his help with the modular array analysis and the simulation of the Dorne-Margolin blade monopole. I have enjoyed each and every crazy conversation we have had over the past 3 years ! Thank you and good luck for everything in the future.

I am glad I pursued the Ph.D. in the company of my friends Abhijit, Hemish, Jitish, and Shashank. Our discussions on everything technological and non-technological will always be cherished by me.

I would like to thank my mother, father, and sister for giving me the support and encouragement to pursue my goals. Finally, I want to thank my wife Smita for the sacrifices she has made. Thank you for your immeasurable contributions to this thesis. You are amazing!

Table of Contents

List of Figures

List of Tables

Chapter 1. Introduction to impedance matching of antenna radiators

The Maxwell equations are truly the foundation on which much of mankind's technological prowess rests on. The unification of electricity and magnetism, two very mysterious forces of nature in the late 1800's, achieved by James Clerk Maxwell, has withstood the significant revisions in our understanding of the universe. The invariance of his equations to General relativity put Maxwell's theory on a firm pedestal and being a part of one of the four fundamental forces of nature along with its unification to quantum mechanics has ensured its timelessness.

The original Maxwell equations were in a very different format than how we recognize it today. They were 20 equations in total and were written with the help of '*quaternions*', a four dimensional number system much like vectors. These twenty equations were recast into the four popular equations by Oliver Heaviside and Gibbs. In doing so, the quaternion representation was done away with and in its place the vector notation was instituted. This modification gave a far more intuitive appeal to the equations and helped the world of electrical engineering to develop and exploit it to its full potential. While it is true that to Maxwell goes the credit for unifying electricity and magnetism, we would be remiss in not stating that his theory rests on the work of such giants as Carl Friedrich Gauss, André Marie Ampère, and Michael Faraday.

It was Heinrich Hertz, Nikola Tesla, J. C. Bose, Alexander Popov, Thomas Edison and others who provided the physical manifestation for these mathematical entities. The twin pillars of electric power and communications (both wired and wireless) on which much

of mankind's current condition rests on, owes itself to the foundations laid down by these early pioneers. A common requirement for both is the need to ensure an efficient transfer of power from a source to a load. This can be succinctly stated as impedance matching. If the load and the source are purely resistive we can relate this to the maximum power transfer theorem and the need to keep the load resistance the same as the source resistance. In the case when there are reactive elements present in the circuit, the condition for maximum power transfer occurs with the use of conjugate impedance matching. We will delve into this topic in more detail in chapter 2 and 3.

1.1 Impedance matching – the beginnings

The period between 1890 and 1920 was a very significant one for experimental electrical engineering. It is during this fruitful period that the means for generating, delivering and using DC (Direct Current) power and AC (Alternating Current) power were invented. In addition the wireless revolution sweeping across the globe today has its technological underpinnings also situated during this period. While it is debatable as to the extent to which impedance matching was used in electric power, wired and wireless communications applications during this era, it undoubtedly spurred the theoretical investigations that soon followed.

In [1]-[6] some of the fundamental concepts in electric network theory were presented and explained. There was a great deal of interest in techniques that could extract a circuit topology if provided with the required transfer function and the driving point impedance functions. The invention of the vacuum tube in the early 1900's and its subsequent maturity by the 1920's resulted in a lot of interest in RF power amplifiers. Expectedly, the impedance matching problem had also to be dealt with. An example of T and Π

circuits being employed at the output stage of an RF power amplifier is shown in [7]. The author suggests their use and also discusses in detail the utility of such circuits to couple the power from the output of the power amplifier to an antenna. Note that the load and source are both assumed to be resistive. Some of these concepts such as in [1] have undergone a great deal of scrutiny as seen by the work done by Papoulis [8] from a purely mathematical perspective, and more recently by Geyi et. al. and Best [9], [10] for specifically the antenna impedance.

Since the design of filters was relatively well understood, it was but natural for using the body of work devoted to their design, in order to design impedance matching networks [11], [12]. Particularly, [12] has a good review of some basic lumped element filter building blocks and then proceeds to outline two applications which involve impedance matching inspired from the basic low-pass filter half-sections; one of these is an impedance matching problem between an RF transmission line and an antenna while the second one is for building coupling units between video amplifiers.

1.2 Impedance matching categories

In general impedance matching between an arbitrary pair of source and load can be classified into three categories. These are shown in Fig. 1.1 and outlined below:

a) The resistive matching problem – source and load are both resistive and unequal
b) The single matching problem – source is resistive and the load is complex
c) The double matching problem – source and load are both complex

Here we assume that an RF voltage source V_g with an internal resistance R_G or impedance Z_G has to be impedance matched to either a resistive load R_L or a complex impedance Z_L respectively.

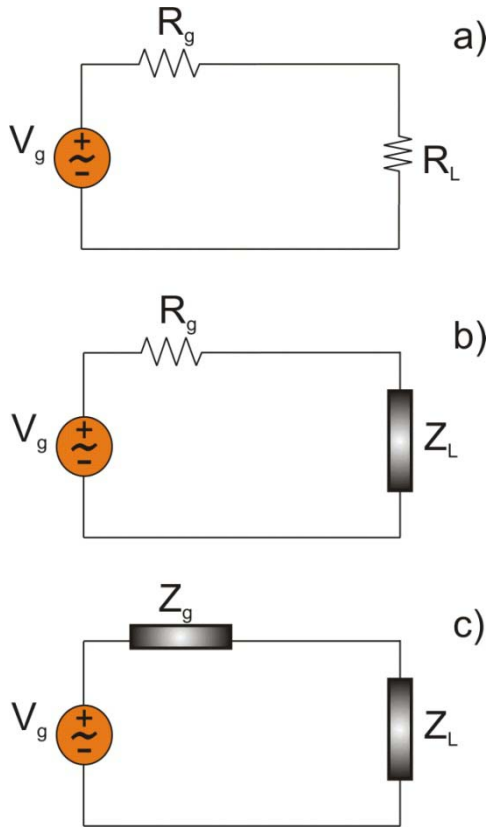

Fig. 1. 1 The three categories of impedance matching: a) purely resistive, b) single matching, and c) double matching.

The first case requires a network that will simply adjust the load resistance such that it is equal to the source resistance. The single matching and double matching cases however are a little more complicated. The single matching case is typically the most common impedance matching scenario encountered in antenna and RF circuit design. Since the load is complex and the source is resistive, there is reactance cancellation required. Additionally if the source and load resistances are not equal, there is the need for a step

up or step down network to maximize the power transfer (assuming narrowband single frequency). The double matching case could arise in an RFID (Radio Frequency IDentification) application where the tag has a chip connected to an antenna. The output impedance of the chip is usually complex. Ideally, the tag antenna if resonant should have purely resistive feed point impedance. However, such antennas are sensitive to their environment and can easily be detuned thus resulting in complex impedance being presented to the chip's input. A non-resonant antenna might be a better solution in this case since it would get rid of the antenna's sensitivity to its surrounding environment and we would still end up with a double matching problem.

1.3 Bode-Fano theory and the analytic approach

The first steps towards a theoretical basis for broadband matching were taken by Bode [13]. While this work considered a simple load (parallel combination of resistor and capacitor) under the single matching category, it was significant because for the first time engineers had a bound, cast in a gain-bandwidth formulation, for a given load. Central to Bode's work is the analytical approach which requires a circuit approximation of the load impedance as it uses the data in the complex frequency plane; it has been developed for simple load circuits only. This approach, unlike [7], [11], [14], and [15], did not provide the techniques to build a good impedance matching network. It did however give the designer a mathematical tool to compare the performance of a designed impedance matching network with a specified bandwidth in terms of the gain or the reflection coefficient. This approach was further investigated by Fano [16] and Youla [17].

Of particular importance is the utilization of Darlington's powerful theorem [6] (Sidney Darlington is arguable more famous for the transistor configuration '*Darlington pair*') by Fano together with the work done earlier by Bode, to convert the broadband impedance matching problem into a filter design problem. This theorem states that any physically realizable impedance function can be decomposed into a purely reactive lossless network terminated into a 1Ω resistor (done so by including a transformer in to the reactive network). Since the source resistance can also be changed to 1Ω by including a transformer, the impedance matching problem gets converted to a filter design problem. As shown in Fig. 1. 2, this is a partial filter design problem pertaining to the design of the first network, since the second network is already discovered through application of Darlington's theorem.

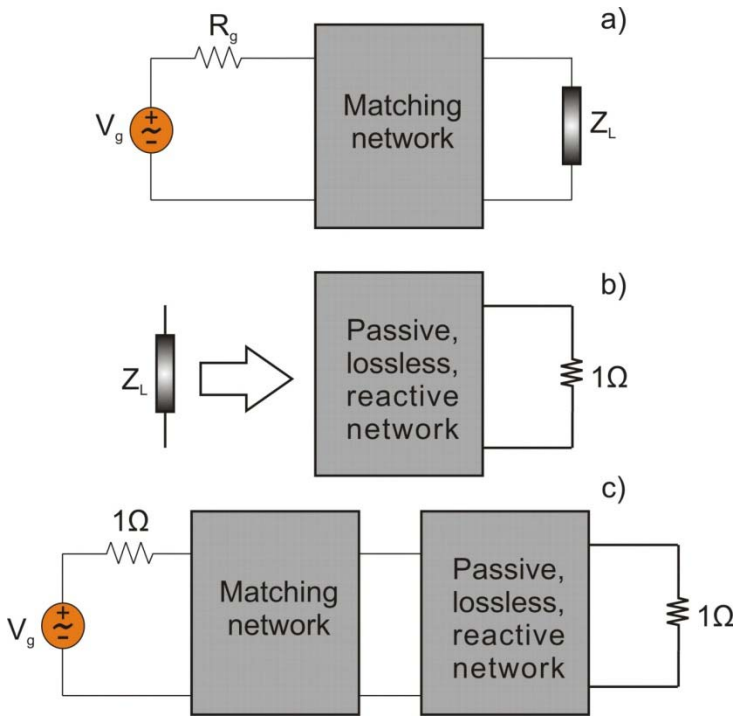

Fig. 1. 2. The broadband impedance matching problem a) as tackled by Fano, by applying Darlington's theorem to the load shown in b) thus converting it into a filter design problem seen in c).

As filter design was a mature art by this period, it was a tremendous boost to this nascent field of broadband impedance matching. Later, Chen and co-authors implemented Youla's theory for LCR loads of the type (C||R) +L [18], [19], and [20]. Of special note is Ref. [21], where a band-pass Chebyshev equalizer was presented for a Darlington type-C load, i.e. for $R_1 + C||R_2$. This load can reference the input impedance of a small dipole or monopole. Also to be noted are the Takahasi design formulas for wideband bandpass Chebyshev ladder networks, which are matching series and parallel LCR loads, see Ref. [22]. This method bypasses the gain – bandwidth theory and directly produces lumped lossless equalizers.

1.4 The Real Frequency Technique

The progress in analytic approaches to broadband impedance matching was tempered by the fact that designers needed to approximate the load with a circuit model. As noted in section 1.3 the analytic techniques work well for simple load types. However, for more complicated loads the analytic approach is too difficult. The Carlin's Real Frequency Technique (RFT) based gain-bandwidth optimization approach [22]-[25] is a numerical technique that does not require any circuit approximation of the load impedance. Instead, it relies on the actual measurement data of the load. A comprehensive review has been recently provided by Newman [26]. Although being quite versatile, this approach, along with the pure optimization step, still requires non-unique operations with rational polynomial approximations, and further extraction of equalizer parameters using the Darlington procedure [26]. Moreover, a transformer is required to match the obtained equalizer to the fixed generator resistance of $50\,\Omega$ [26].

1.5 Wideband matching of antenna radiators

For modern wideband or multiband hand-held radios typically used in either civilian or military roles, it is often desired to match a non-resonant (i.e., relatively short) monopole, or dipole-like, antenna over a wide frequency band. Current impedance matching techniques involve modifying the antenna structure and are in fact quite popular. Fig. 1.3 captures the state of the art in impedance matching (narrowband and wideband) for antennas.

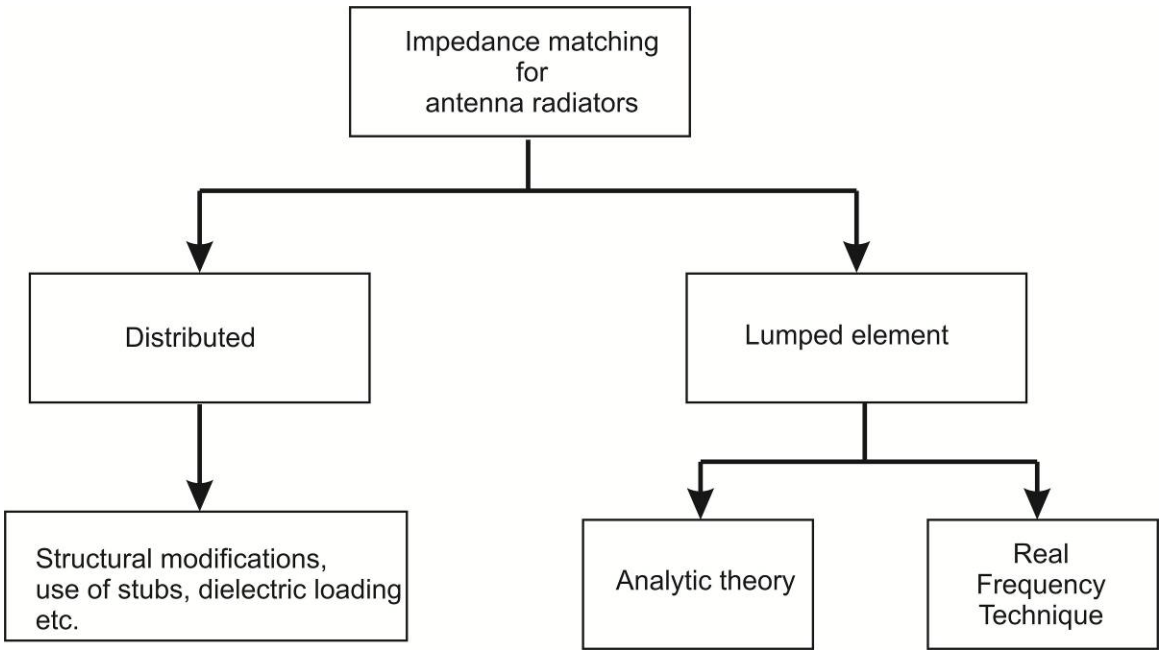

Fig. 1. 3. The impedance matching approach for typical antenna radiators.

Both approaches to impedance matching can be implemented either by including loss within the structure/network, or by a completely lossless approach. In the distributed approach to impedance matching, loss can be included, either intentionally or by circumstance, through the use of dielectric materials. The lumped element approach to lossy matching involves the inclusion of a properly chosen resistance located strategically within the network of inductors and capacitors. This is to be differentiated from the

lossless matching networks which are designed only with inductors and capacitors. Naturally, these components have a finite Q (Quality factor) and therefore some degree of loss does exist even in otherwise lossless networks.

This thesis makes contributions to both the lumped element and distributed approaches to impedance matching for antenna radiators. Two interesting and challenging problems have been considered; namely, the broadband impedance matching for electrically small (short) non-resonant dipoles/monopoles and the design of small sized resonant antenna arrays of a modular architecture. The problem of wideband matching for short non-resonant dipoles/monopoles is tackled using lumped element lossless equalizers. In addition we also provide insight into a lossy matching approach using lumped element circuits, for a blade monopole and compare it to the performance of a novel dielectrically loaded (truncated hemisphere) top-hat monopole antenna. The broadband modular array design focuses on a distributed approach to impedance matching.

1.5.1 Motivation for wideband matching of an electrically small (short) dipole/monopole using a lumped circuit

Our motivation for pursuing this goal is three-fold, namely:

I. For electrically small, non-resonant antennas distributed impedance matching techniques that involve modifying the antenna structure, together with optimization carried out within a full-wave electromagnetic simulation environment, are sometimes complicated to design, build, and analyze. The approach suggested in this thesis would minimize the complexity in wideband matching of short, non-resonant antennas.

II. Resonant antennas are extremely sensitive to their surroundings. For hand held radios, smart phones etc., the antenna is usually electrically small (short) and is indeed resonant. These antennas are exposed to different materials such as the human body, wood, metal, liquids etc. on a regular basis and as a result, they get detuned regularly. To compensate for this, the designer must take into account the different conditions that maybe most often encountered by the antenna for the specified application and model these within the full wave EM simulator. Depending on the kind of objects that might be modeled, the simulation complexity increases. It may be a better alternative in to deploy a non-resonant antenna with the kind of matching network suggested in this thesis.

III. This approach could also serve as a basis for building adaptive matching networks that modify the antenna response dynamically.

The standard narrowband impedance matching techniques include L, T, and Π sections of reactive lumped circuit elements, which may also include transformers with single- and double-stub tuning of transmission lines [27], [28]. The ever growing trend of miniaturization of wireless devices ensures that size remains an important constraint to satisfy. In the VHF-UHF bands, where there is a high concentration of wireless services, lumped circuits are preferable as they have a smaller size. However, the narrowband matching circuits are usually non-applicable when the bandwidth is equal to 20% or higher.

The notion of wideband antenna matching to a generator with a fixed generator resistance of $50\,\Omega$ is a classical impedance matching concept. As discussed earlier in sections 1.3 and 1.4 respectively as well as in Ref. [29] in general, wideband matching circuit design

methods can be classified into two groups: the analytical approach and the Real Frequency Technique (RFT) numerical approach. When the load is such a well-known subject as a short dipole or monopole, we can capitalize on prior experience with its impedance matching, and thus considerably simplify the problem.

This thesis studies the wideband matching problem for short dipoles or monopoles and does not use the two approaches discussed above. Instead, we prefer to introduce the equalizer topology up front: the equalizer's first section is the *L* section with two inductors. This section is adopted from the analysis of whip monopoles. Its double-tuning version has shown excellent performance for impedance matching and tuning of a whip monopole antenna over a wide band of frequencies [30]. The second and last section is a high-pass *T*-section with a shunt inductor and two capacitors. This section is intended to broaden the narrowband response of the *L*-section. The equalizer has only five lumped elements: three inductors and two capacitors. A direct numerical optimization technique is then employed to find the circuit parameters for wideband impedance matching. Here, the antenna impedance is approximated by an accurate analytical expression [31]. This matching network topology can be used for all dipole-like antennas. We will show that the present simple circuit yields an average band gain that is virtually identical to the gain obtained with an improved Carlin's equalizer [26]. This result is shown to be valid for a wide range of antenna lengths and radii (or widths for a blade dipole/monopole).

1.5.2 Motivation for design of modular arrays of resonant antenna radiators and broadband matching using the distributed approach

This thesis proposes a new approach to the design of small size wideband arrays of planar dipoles situated over a ground plane. The individual radiator which we refer to as the *unit*

cell, is resonant. The unit cell terminology is also commonly used for the individual radiator within large size finite arrays, and therefore not to be confused with it. Incidentally the design of those large arrays follows the Floquet theoretic infinite array simulation methodology which we propose and show to be inapplicable for the design of small size modular arrays. The motivation for pursuing this problem is three-fold:

I. There is much interest in the design of small size arrays in either linear or planar configurations in the wireless industry. This can be seen with the advent of MIMO (Multiple Input Multiple Output) systems for 4G, digital TV reception and also wireless positioning.

II. A modular architecture as proposed in this thesis could be a good solution as it is inherently flexible. Particularly, it is very easy to change the array configuration from a 2x2 to a 4x1 (planar to linear).

III. The key aspect of this approach is that a single optimized *unit cell* could be used in different configurations without degrading the performance objectives.

The modular design results in increased impedance bandwidth ($\geq 2:1$), as well as higher directive gain at the low frequencies. We also seek a maximum gain variation over the band of up to 3dB. Furthermore, we show that the careful design of the individual radiator may achieve such high bandwidths for the 2x1 array, 2x2 array, and 4x1 array of the same radiators respectively. The dipole and ground plane within each unit cell can be mounted on a thin, low epsilon and low loss dielectric material such as Poly methyl methacrylate (PMMA), commonly known as Plexiglass or on PVC (Polyvinyl Chloride). An analytical model for the power combiner is introduced and used during optimization of the arrays. Such a modular approach is well suited for low-cost large-volume small

broadside array design. The arrays presented here are intended for use in the UHF region of the spectrum but can be easily scaled and optimized for other bands.

1.6 Thesis organization

The thesis is organized as follows:

In chapter 2 the theoretical limit to wideband matching of an electrically small (short) non-resonant dipole/monopole is introduced. The matching circuit for such antennas is developed in chapter 3. In chapter 4 the simulation results and the experimental results are provided along with a discussion on the performance. Large portions of the content in chapters 2- 4 have been drawn from [70]. The modular array concept is introduced in chapter 5 along with the design approach. A model for the power combiner is also introduced. In chapter 6 simulation and experimental results are presented. Chapter 7 concludes the thesis and includes suggestions for future research efforts.

Chapter 2. Theoretical limit on wideband impedance matching for a non-resonant dipole/monopole

To understand the limitations on wideband impedance matching for a non-resonant dipole/monopole, it is important to first grasp its impedance behavior. The impedance behavior is the variation of the resistance, denoted as R and the reactance, denoted as X, with frequency. The impedance behavior is directly linked (as to be expected) with the current and voltage standing waves that are setup over the physical extent of the antenna, in this case the dipole/monopole. In this chapter, we attack this question of the impedance behavior initially from first principles by using Maxwell's equations, and subsequently by the use of a semi-empirical analytical expression. Confirmation between the analytical formulation and a full wave EM (Electromagnetic) simulation is also provided. The necessary conditions upon which the model depends on will be established. The reflective equalizer will be introduced and the analysis using Bode-Fano theory will be described. To understand the effect of geometry three different cases of the dipole will be considered for wideband matching. Last, but not the least, an introduction to the Chu limit and a discussion on the results within this context is provided.

2.1 The electrically small dipole

We will begin our discussion on dipoles with the small dipole. The small dipole is also referred to in literature as the *electrically small* dipole. This definition implies that the length of the dipole is much smaller than the wavelength at which it operates. While this definition is qualitatively satisfying, a quantitative justification is however required

regarding what constitutes the electrically small limit. There is much to be said in this regard. We will defer this discussion for now and simply state that for the purpose of the next few sections our definition of electrically small assumes that the length of the dipole, denoted as $l_A << \lambda$, where λ is the free space wavelength of operation.

A fundamental quantity of interest for any antenna is its input impedance. The input impedance allows us to view the antenna from a circuit theoretic perspective and therefore give us all the well developed circuit analysis techniques to analyze it with. Once the input impedance is derived, we can replace the antenna with an equivalent circuit representative of the impedance (at least for the small antenna case) and derive useful parameters such as reflection coefficient (return loss), efficiency, gain etc. To begin the analysis however, we will start with the Maxwell's equations.

2.2 Analytical solution for the input impedance of a small dipole

Consider the cylindrical dipole shown in Fig. 1. As mentioned earlier the length of the dipole is specified as l_A, the diameter is denoted by $d = 2a$, and a is the radius of the cylinder. The dipole is positioned at the origin of the co-ordinate system and the spherical co-ordinates (r, φ, θ) are used to identify any observation point in the surrounding space.

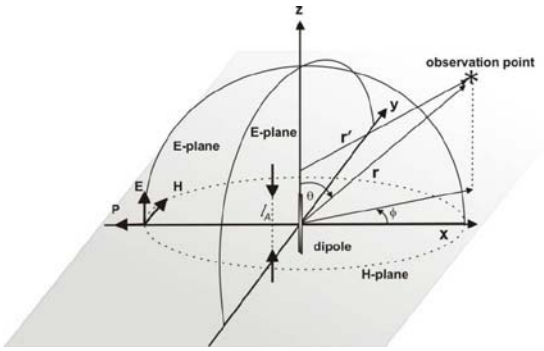

Fig. 2. 1.Dipole in radiating configuration.

Our first attempt at solving for the dipole fields and hence the impedance begins with the current density being assumed to be constant (an infinitesimally small dipole). To do so we define the current density to be

$$\vec{J}(\vec{r}) = \delta(x)\delta(y)\hat{z}I_0, \quad \forall -l_A/2 < z < l_A/2 \tag{2.1}$$

This is shown in Fig. 2.2, graphically,

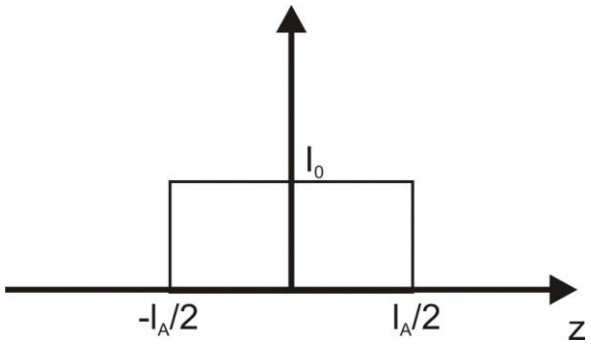

Fig. 2. 2. Uniform current distribution on the infinitesimally small dipole.

The integral

$$\vec{A}(\vec{r}) = \mu_0 \iiint \frac{\exp(-jk|\vec{r}-\vec{r}'|)}{4\pi|\vec{r}-\vec{r}'|}\vec{J}(\vec{r}')d\vec{r}' \tag{2.2}$$

is found analytically as (when $l \to 0$)

$$\vec{A}(\vec{r}) = \int_{-l_A/2}^{l_A/2} \frac{\exp(-jk|\vec{r}-(0,0,z')|)}{4\pi|\vec{r}-(0,0,z')|}dz' \approx \hat{z}\frac{\mu_0 I_0 l_A}{4\pi|\vec{r}|}\exp(-jk|\vec{r}|) \tag{2.3}$$

The magnetic field is found by taking the curl of the magnetic vector potential

$$\vec{H} = \frac{1}{\mu_0}\nabla \times \vec{A} \tag{2.4}$$

Before this is done, we first switch to the spherical coordinate system from the current

rectangular coordinate system (notice the unit vector for identification). The standard conversion approach utilizing the matrix-vector notation, is shown in Eq. (2.5).

$$\begin{bmatrix} A_r \\ A_\theta \\ A_\phi \end{bmatrix} = \begin{bmatrix} \sin\theta\cos\phi & \sin\theta\sin\phi & \cos\theta \\ \cos\theta\cos\phi & \cos\theta\sin\phi & -\sin\theta \\ -\sin\phi & \cos\phi & 0 \end{bmatrix} \begin{bmatrix} A_x \\ A_y \\ A_z \end{bmatrix} \tag{2.5}$$

Since Eq. (2.3) has only the z-component of the magnetic vector potential, we write the three components in the spherical coordinate system as,

$$\begin{aligned} A_r &= A_z \cos\theta = \frac{\mu_0 I_0 l_A}{4\pi|\vec{r}|}\exp\left(-jk|\vec{r}|\right)\cos\theta \\ A_\theta &= -A_z \sin\theta = -\frac{\mu_0 I_0 l_A}{4\pi|\vec{r}|}\exp\left(-jk|\vec{r}|\right)\sin\theta \\ A_\phi &= 0 \end{aligned} \tag{2.6}$$

We now use Eq. (2.4) to calculate the magnetic field $\vec{H}$. The curl expansion in spherical coordinates is as follows:

$$\nabla\times\vec{A} = \hat{r}\frac{1}{|\vec{r}|\sin\theta}\left[\frac{\partial}{\partial\theta}\left(A_\phi\sin\theta\right) - \frac{\partial A_\theta}{\partial\phi}\right] + \hat{\theta}\frac{1}{|\vec{r}|}\left[\frac{1}{\sin\theta}\frac{\partial A_r}{\partial\phi} - \frac{\partial}{\partial r}\left(|\vec{r}|A_\phi\right)\right] + \hat{\phi}\frac{1}{|\vec{r}|}\left[\frac{\partial}{\partial r}\left(|\vec{r}|A_\theta\right) - \frac{\partial A_r}{\partial\theta}\right] \tag{2.7}$$

Note, that from Eq. (2.6) the azimuthal component of the vector potential is zero while the radial and elevation component do not have any azimuthal variation. Applying this knowledge to Eq. (2.7) we find that only one component exists i.e.

$$\vec{H} = \nabla\times\vec{A} = \hat{\phi}\frac{1}{\mu|\vec{r}|}\left[\frac{\partial}{\partial r}\left(|\vec{r}|A_\theta\right) - \frac{\partial A_r}{\partial\theta}\right] = \hat{\phi}\frac{jkI_0 l_A\sin\theta}{4\pi|\vec{r}|}\left[1+\frac{1}{jk|\vec{r}|}\right]\exp(-jk|\vec{r}|) \tag{2.8}$$

The electric field is found using the expression for the magnetic field. Ampere's law modified by displacement currents $\varepsilon\frac{\partial\vec{E}}{\partial t} = \nabla\times\vec{H} - \vec{J}$ in the phasor form reads (in the free space where there are no currents)

$$\vec{E} = \frac{1}{j\omega\varepsilon}\nabla \times \vec{H} \tag{2.9}$$

To evaluate Eq. (2.9) we apply the similar procedure as before and recognize that the radial and elevation components of the magnetic field are zero. The expression for the curl becomes

$$\nabla \times \vec{H} = \hat{r}\frac{1}{|\vec{r}|\sin\theta}\left[\frac{\partial}{\partial\theta}\left(H_\phi \sin\theta\right)\right] + \hat{\theta}\frac{1}{|\vec{r}|}\left[-\frac{\partial}{\partial r}\left(|\vec{r}|H_\phi\right)\right] \tag{2.10}$$

Calculating the various partial derivatives in Eq. (2.10) and substituting $k/\omega\varepsilon = \eta$ we get

$$\vec{E} = \hat{r}\frac{\eta I_0 l_A \cos\theta}{2\pi|\vec{r}|^2}\left(1+\frac{1}{jk|\vec{r}|}\right)\exp(-jk|\vec{r}|) + \hat{\theta}\frac{j\eta k I_0 l_A \sin\theta}{4\pi|\vec{r}|}\left(1+\frac{1}{jk|\vec{r}|}-\frac{1}{k^2|\vec{r}|^2}\right)\exp(-jk|\vec{r}|) \tag{2.11}$$

The radiated power is obtained in the form

$$P_{rad} = R^2\int_0^{2\pi}\int_0^{\pi}\vec{P}\cdot\vec{n}\,d\varphi\sin\theta d\theta, \quad \vec{P} = \frac{1}{2}\mathrm{Re}\left[\vec{E}\times\vec{H}^*\right] \tag{2.12}$$

which after integration yields

$$P_{rad} = \frac{\pi\eta_0}{3}\frac{l_A^{\,2}}{\lambda^2}|I_0|^2 \equiv R|I_0|^2 \tag{2.13}$$

Therefore, the input resistance R of the small dipole antenna has the form

$$R = \frac{2\pi\eta_0}{3}\frac{l_A^{\,2}}{\lambda^2} = 80\pi^2\left(\frac{l}{\lambda}\right)^2 \tag{2.14a}$$

The reactance of the small dipole antenna may be obtained through the reactive power, which yields

$$X = -j\left[\frac{\eta_0}{3\pi}\left(\ln\frac{l_A}{2a}-1\right)\frac{\lambda}{l_A}\right] \tag{2.14b}$$

where *a* is the antenna radius for the cylindrical dipole. The reactance is capacitive and large. The width of the blade dipole *t* is related to the radius of the equivalent cylindrical dipole by making the static capacitance equal in both the cases. This yields ([32], p. 514):

$t = 4a = 2d$

2.3 Antenna impedance model

For a wire or strip dipole, the input impedance, Z_A, can be approximated with a high degree of accuracy [31] as

$$Z_A = R(z) - j\left[120\left(\ln\frac{l_A}{2a} - 1\right)\cot z - X(z)\right]$$

$$R(z) \approx -0.4787 + 7.3246z + 0.3963z^2 + 15.6131z^3 \qquad (2.15a)$$

$$X(z) \approx -0.4456 + 17.00826z - 8.6793z^2 + 9.6031z^3$$

In Eq. (2.15a), l_A is the dipole length, *a* is the dipole radius, $z = kl_A/2$, and $k = 2\pi/\lambda$ is the wavenumber. The accuracy of Eq. (2.15a) quickly degrades above the first resonance [31]; thus, at the high-frequency end, very small dipoles cannot be considered. At the lower end, Eq. (2.15a) is only valid when the dipole radiation resistance is positive and does not approach zero. This gives us 2 complex roots which and one real root. discarding the complex roots, we get the condition

$$z = kl_A/2 > 0.07 \text{ or } \frac{l_A}{0.5\lambda} > 0.05 \qquad (2.15b)$$

If a strip or blade dipole of width *t, is* considered, then $a_{\text{eq}} = t/4$ [32]. We note here that *a*, is the radius of a cylindrical dipole, whilst a_{eq} is the equivalent radius of a wire approximation to the strip dipole. In this study, the first result is used. Thus, Eq. (2.15a)

holds for relatively small non-resonant dipoles and for half-wave dipoles, i.e. in the frequency domain approximately given by

$$0.05 \leq f_C / f_{\text{res}} \leq 1.2 \qquad (2.15c)$$

where $f_{\text{res}} \equiv c_0 /(2l_A)$ is the resonant frequency of an idealized dipole having exactly a half-wave resonance (c_0 is the speed of light) and f_C is the center frequency. When a monopole over an infinite ground plane is studied, the impedance is half.

2.4 Comparison of impedance model with full wave EM simulation

To confirm the performance of the semi-analytical expression for the impedance behavior of a dipole, provided in Eq. (2.15a), we plot the resistance and reactance as a function of frequency (20 - 400 MHz) and compare it to the results from a full wave electromagnetic simulation model. A dipole of length $l_A = 150\,\text{mm}$ and resonant frequency of 1 GHz is considered. The full wave simulation model is of a blade dipole of appropriate width, *t* calculated using the relation $t = 2d$. To illustrate the difference in the impedance properties, four cases were considered in which the length to diameter ratios were varied, i.e. the cases considered were $\frac{l_A}{d} = [7.5, 10, 30, 60]$.

The resulting data for the resistance and reactance are plotted as a function of frequency in Fig. 2.3(a)-(d). Overall, there is excellent agreement between the analytical expression and the full wave simulation model for the reactance. We clearly see that the dipole thickness (diameter in case of cylinder or the width in the case of a planar (blade) dipole) has a significant impact on the reactance, namely the thicker dipoles have lower reactance. The resistance is primarily a function of the total length of the dipole

(inclusive of the feed width) and therefore doesn't display any significant variation with changing radii/widths.

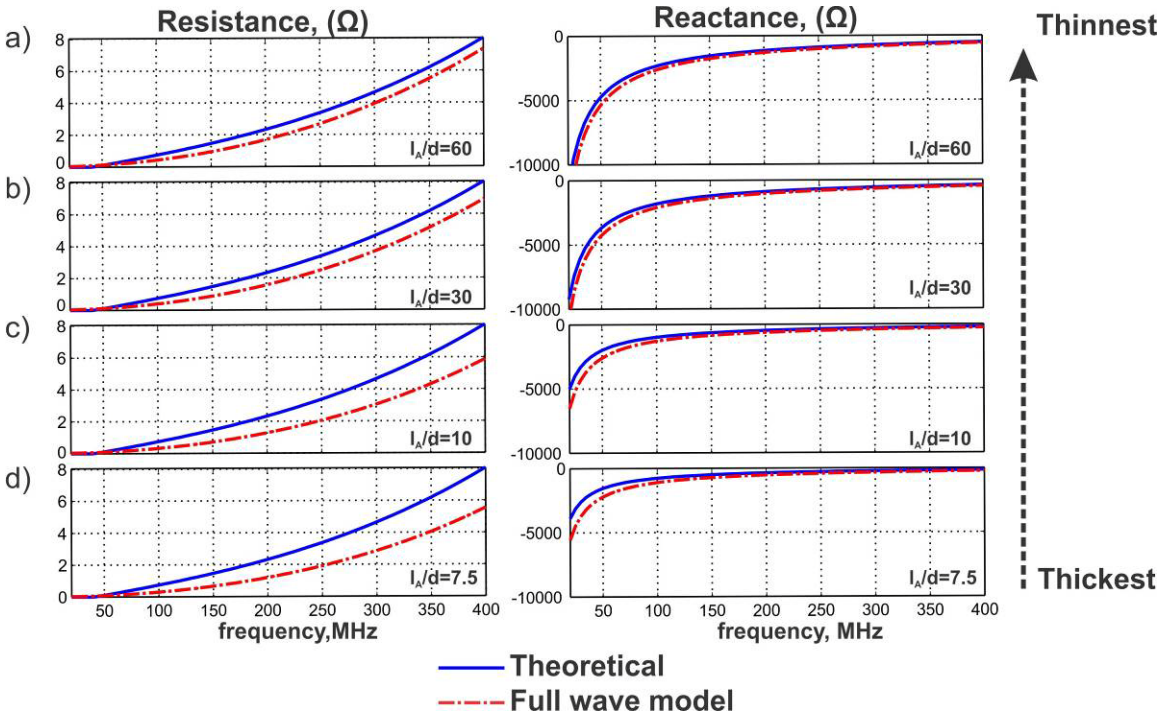

Fig. 2. 3. Comparison between the analytical expression for impedance of a dipole/monopole in Eq. (8a) (solid-blue curve) and the result of a full-wave EM simulation in Ansoft HFSS (dash-dotted red curve). The dipole is resonant at 1 GHz and 4 geometries have been considered (a - d).

2.5 Wideband impedance matching – the reflective equalizer

The reactive matching network is shown in Fig. 2.4(a) [23]. The generator resistance is fixed at $50\,\Omega$. This network does not include transformers. Following Ref. [23], the reactive matching network is included into the Thévenin impedance of the circuit as viewed from the antenna, see Fig. 2.4(b).

In fact, the network in Fig. 2.4(a) is not a matching network in the exact sense since it does not match the impedance exactly, even at a single frequency. Rather, it is a reflective (but lossless) equalizer familiar to amplifier designers, which matches the impedance equally well (or equally "badly") over the entire frequency band. The

equalizer network is reflective since a portion of the power flow is always being reflected back to generator and absorbed. Following Ref. [23], we can consider the generator or transducer gain in the form

$$T(\omega^2) = \frac{\text{Power to load}}{\text{Power to conjugate - matched load } Z_T^*} = \frac{4R_T(\omega)R(\omega)}{\left|Z_A(\omega) + Z_T(\omega)\right|^2} = 1 - \left|\Gamma(\omega)\right|^2 \quad (2.16)$$

The gain *T* is the quantity to be uniformly maximized over the bandwidth, *B*. In practice, the minimum gain over the bandwidth is usually maximized [23], [26].

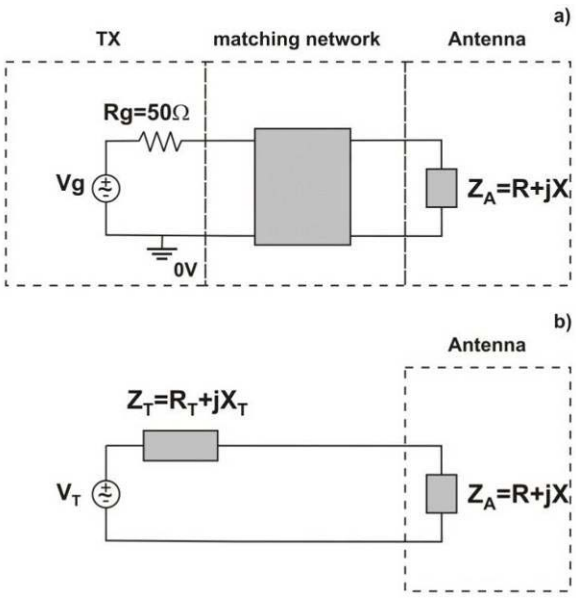

Fig. 2. 4. Transformation of the matching network: a) reactive matching network representation, b) Thévenin-equivalent circuit representation. The matching network does not include transformers.

The problem may be also formulated in terms of the power reflection coefficient $\left|\Gamma(\omega)\right|^2$, viewing from the generator with the equalizer into the antenna. Obviously, the power reflection coefficient needs to be minimized. Note that the transducer gain is none other than the square magnitude of the microwave voltage transmission coefficient. In this text, we follow the "generator gain" terminology in order to be consistent with the background research in this area.

2.6 Bode-Fano bandwidth limit

The Bode-Fano bandwidth limit of broadband impedance matching ([16], [28]) only requires knowledge of the antenna's input impedance; it approximates this impedance by one of the canonic *RC*, *RL*, or *RLC* loads ([16], and [28], p. 262). The input impedance of a small- to moderate-size dipole or monopole is usually very similar to a series *RC* circuit, as seen from Eq. (2.15a). When $f_C / f_{\text{res}} \le 0.5$ or $z = kl_A / 2 < 0.75$ (a small antenna or an antenna operated below the first resonance), the antenna resistance is usually a slowly-varying function of *z* (almost a constant) over the limited frequency band of interest whereas the antenna's reactance is almost a pure capacitance. This observation is valid at a common geometry condition: $\ln\left(l_A/(2a)\right) > 1.5$. The Bode-Fano bandwidth limit for such a *RC* circuit is written in the form [28] and restated here in Eq. 2.17. Fig. 2.5 illustrates the equivalent circuit for the electrically short antenna and an appropriate matching circuit to be found so as to achieve the input reflection coefficient level $\Gamma(\omega)$.

$$\int_0^\infty \frac{1}{\omega^2} \ln\left[\frac{1}{|\Gamma(\omega)|}\right] d\omega < \pi RC \tag{2.17}$$

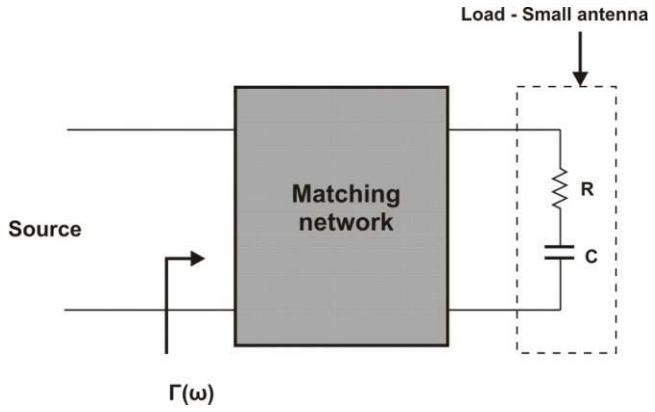

Fig. 2. 5. Low frequency *RC* circuit model for an electrically short dipole/monopole antenna**.**

Note, that Eq. (2.17) does not depend on the matching network (other than the fact that it is assumed to be passive and lossless) or on the source. It is purely a function of the load alone. For a rectangular band-pass frequency window $[f_C - B/2, f_C + B/2]$ of bandwidth B and centered at f_C, with $T = T_0$ within the window and $T = 0$ otherwise, Eq. (2.17) and Eq. (2.15a) allow us to estimate approximately the theoretical limit to the gain-bandwidth product as long as the dipole or monopole size remains smaller than approximately one quarter or one eight wavelength, respectively. This is shown in Fig. 2.6 along with two other realizations that illustrate the utilization of the available matching area in terms of the gain and bandwidth sought.

2.7 Gain-bandwidth product (small fractional bandwidth, small gain)

Let us first obtain the simple closed-form estimate for the gain bandwidth product. Using the expression for gain, T, in terms of power reflection coefficient $|\Gamma(\omega)|^2$, in Eq. (2.16) we rewrite Eq. (2.17) as,

$$\int_0^\infty \frac{1}{\omega^2} \ln\left[\frac{1}{\sqrt{1-T}}\right] d\omega < \pi RC \tag{2.18}$$

Substituting $T = T_0$ over the bandwidth B and applying the appropriate limits for ω to the integral in Eq. (2.18) we arrive at

$$\ln\left[\frac{1}{\sqrt{1-T_0}}\right] \int_{\omega_L}^{\omega_U} \frac{1}{\omega^2} d\omega < \pi RC \quad , \; \omega_L = 2\pi f_C - \pi B, \omega_U = 2\pi f_C + \pi B \tag{2.19}$$

Solving the integral in (2.19) yields

$$-\frac{1}{2}\ln(1-T_0) > \frac{\pi^2 RC\left(4f_C^2 - B^2\right)}{2B} \tag{2.20}$$

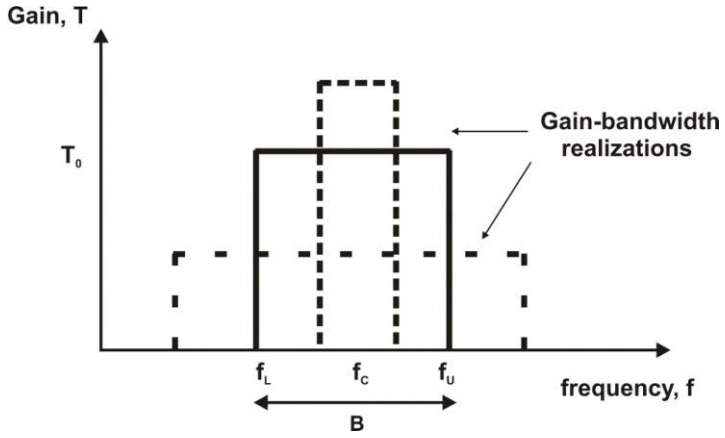

Fig. 2. 6. Illustration of different gain-bandwidth realizations and the corresponding matching areas under the ideal, constant reflection coefficient/constant transducer gain assumption.

Next, we assume the fractional bandwidth $\overline{B} = B / f_C$ to be small, i.e. $\overline{B} < 0.1$; we also assume that $T_0 << 1$. We then simplify the inequality in Eq. (2.20) by using the Taylor series expansion of the terms on the left hand side as follows

$$-\frac{1}{2}\ln(1-T_0) = -\frac{1}{2}\left[-T_0 - \frac{T_0^2}{2} + \ldots\right] \tag{2.21}$$

Ignoring the higher order terms and rewriting the resulting expression in terms of $\overline{B}$ as follows:

$$-\frac{1}{2}\ln(1-T_0) \approx \frac{T_0}{2} > \frac{2\pi^2 f_C RC}{\overline{B}}, \quad f_C RC \approx \frac{R(z)}{480\Omega}\frac{f_C}{f_{\text{res}}}\frac{1}{\left(\ln\frac{l_A}{2a} - 1\right)}, \quad z = \frac{\pi}{2}\frac{f_C}{f_{\text{res}}} \tag{2.22}$$

In Eq. (2.22), we have replaced the geometric mean of the upper and lower band frequencies by its center frequency, which is valid when i) $\overline{B} < 0.25$; ii) the half-wavelength approximation for dipole's resonant frequency is used; and iii) dipole's capacitance in the form $C^{-1} \approx 480\Omega \times f_{\text{res}}\left(\ln\frac{l_A}{2a} - 1\right)$ is chosen. The last approximation

follows from Eq. (2.15a) when z is at least less than one half. Thus, from Eq. (2.22) one obtains the upper estimate for the gain-bandwidth product in the form

$$T_0\overline{B} < 4\pi^2 \frac{R(z)}{480\Omega}\frac{f_C}{f_{\text{res}}}\frac{1}{\left(\ln\frac{l_A}{2a}-1\right)}, \quad z=\frac{\pi}{2}\frac{f_C}{f_{\text{res}}} \tag{2.22a}$$

The value of this simple equation is in the fact that the gain-bandwidth product is obtained and estimated explicitly. Unfortunately, Eq. (2.22a) is limited to small transducer gains.

2.8 The arbitrary fractional bandwidth and gain scenario

The only condition we will exploit here is $z = 0.5\pi\, f_C / f_{\text{res}} < 0.5$. In that case the dipole capacitance can still be approximately described by the formula from subsection 2.7. The analysis of subsection 2.7 also remains the same until Eq. (2.20). However, we now discard the assumption on small transducer gain. We define the fractional bandwidth $\overline{B} = B / f_C$ as before. After some manipulations Eq. (2.20) yields

$$\frac{\overline{B}}{\left(1-\overline{B}^2/4\right)}\ln\frac{1}{1-T_0} < 4\pi^2 \frac{R(z)}{480\Omega}\frac{f_C}{f_{\text{res}}}\frac{1}{\left(\ln\frac{l_A}{2a}-1\right)}, \quad z=\frac{\pi}{2}\frac{f_C}{f_{\text{res}}} \tag{2.22b}$$

This estimate does not contain the gain-bandwidth product $T_0\overline{B}$ explicitly, but rather individual contributions of T_0 and $\overline{B}$. It is valid below the first dipole resonance, and it is a function of two parameters: the dimensionless antenna geometry parameter $l_A/(2a)$ and the ratio of the matching frequency to the antenna's resonant frequency, f_C / f_{res}.

Frequently, the fractional bandwidth is given, and the maximum gain T_0 over this bandwidth is desired. In this case, Eq. (2.22b) can be transformed into

$$T_0 < 1 - \exp\left(-4\pi^2 \frac{R(z)}{480\Omega} \frac{f_C}{f_{\text{res}}} \frac{\left(1 - \overline{B}^2/4\right)}{\overline{B}\left(\ln\frac{l_A}{2a} - 1 \right)} \right), \quad z = \frac{\pi}{2}\frac{f_C}{f_{\text{res}}} \tag{2.22c}$$

We note that this result does not depend on particular value of the generator's resistance, R_g. Fig. 2.7 gives the maximum realizable gain according to Eq. (2.22c) obtained at different desired bandwidths as a function of matching frequency. In Fig. 2.7 a to c we have considered three different dipoles, with $l_A/2a = l_A/d = 5, 10, 50$, where $d = 2a$ is the dipole diameter. Also, we observe that the condition $\ln(l_A/2a) > 1.5$ is satisfied for every case in Fig. 2.7.

2.9 Dipole vs. monopole

As a first example we consider a short, thick dipole of total length l_A=23 cm and $l_A/t = 5$ that is designed to have a passband from 250 to 400 MHz, and a center frequency of 325 MHz. The resonant frequency of the corresponding infinitesimally thin dipole is found as $f_{\text{res}} = c_0/(2l_A) = 650$ MHz; thus, $f_C/f_{\text{res}} = 0.5$. The fractional bandwidth is approximately $\overline{B} \approx 0.5$. According to Fig. 2.7c, this leads to a significant generator gain of $T_0 \approx 0.8$ over the frequency band; it corresponds to the squared reflection coefficient $|\Gamma|^2 = 0.2$, and yields a return loss of 7dB ($\text{VSWR} = (1+|\Gamma|)/(1-|\Gamma|) = 2.6$) that is uniform over the operating frequency band.

Next, we consider a short thick monopole of total length l_A=11.5 cm and $l_A/d = 5$, over an infinite ground plane; it is designed to have the same passband from 250 to 400 MHz. The resonant frequency of the corresponding infinitesimally thin monopole is found to be

$f_{\text{res}} = c_0/(4l_A) = 650$ MHz so that again $f_C / f_{\text{res}} = 0.5$. The fractional bandwidth remains the same, i.e. $\overline{B} \approx 0.5$. However, the monopole's impedance is half of the dipole's impedance. At first glance, it might therefore appear that one should halve the argument of the exponent in Eq. (2.22c). This is not true because the argument contains the product *R*C. While the resistance *R* decreases by 0.5, the capacitance *C* increases by 0.5, and thus the total result remains unchanged. Consequently, the dipole consideration is always applicable to the monopole of half length, assuming an infinite ground plane. Unfortunately, the Bode-Fano theory does not answer the question of how to achieve the above limit, and how far this limit is from practically realizable matching circuits with reasonably small number of lumped elements.

2.10 Comparison with Chu's bandwidth limit

It is instructive to compare the above results with Chu's antenna bandwidth limit [33] conveniently rewritten in Refs.[34], [35]. in terms of tolerable output VSWR of the antenna and the antenna *ka*, where *a* is the radius of the enclosing sphere. For this dipole example with VSWR=2.6 and $ka = kl_A/2 = 0.78$, the Chu's bandwidth limit is found as [33] - [35],

$$Q_{chu} = \frac{1}{ka} + \frac{1}{(ka)^3} \tag{2.18}$$

$$BW_I = \frac{(ka)^3}{\left(1+(ka)^2\right)} \frac{S^2-1}{2S} \tag{2.19}$$

$$BW_{II} = \frac{\pi}{Q} \frac{1}{\ln\left(\frac{S+1}{S-1}\right)} \tag{2.20}$$

where S = VSWR. Substituting the values for *ka* and VSWR the bandwidth estimates are found to be 34 % and 79 % respectively. Note that while the first estimate is less optimistic, the second estimate suggests higher bandwidth achievability than the Bode-Fano model discussed above. The key issue is that it includes an uncertainty in relating the antenna *Q*-factor to the antenna's circuit parameters [34].

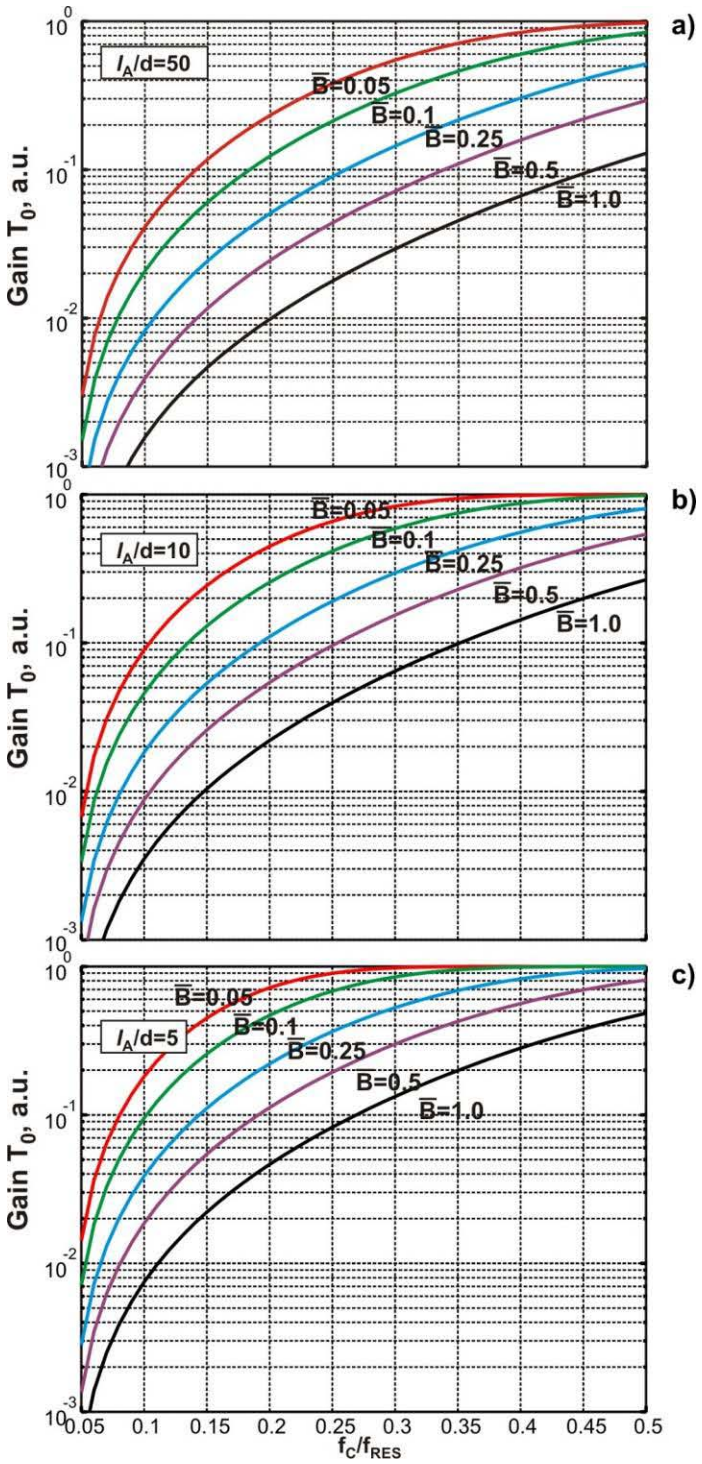

Fig.2. 7. Upper transducer gain limit for three dipoles (from a to c) of diameter *d* and length l_A as a function of matching frequency vs. resonant frequency of the infinitesimally thin dipole of the same length. The five curves correspond to five fractional bandwidth values 0.05, 0.1, 0.25, 0.5, and 1.0, as labeled in the figure, and have been generated by using Eq. (2.17c).

Chapter 3. Equalizer circuit development for the non-resonant dipole/monopole like antenna

The theoretical limit on wideband matching derived in chapter 2 is extremely useful to estimate the quality of the matching network in terms of the transducer gain. However, this is ultimately a limit and neither it nor the theoretical background suggests ways to achieve this limit (much like Shannon's limit in communication theory). Within the sections of this chapter we will develop a wideband matching network for the non-resonant dipole/monopole. In doing so, we first delve into the single and double tuning networks. The proposed wideband matching network will then be introduced and the investigation objectives will be stated.

3.1 Single and double tuning for the electrically short dipole

A small relatively-thin monopole (whip monopole) or a small dipole is frequently matched with a simple *L*-matching double-tuning section [30]. This section is shown in Fig. 3.1a. Ohmic losses of the matching circuit, R_o, are mostly due to losses in the series inductor, which may be the larger one for very short antennas. Namely, L_1 might be on the order of 0.1-1.0 mH for HF and VHF antennas. In this UHF-related study, we will neglect those losses. The single tuning circuit is also shown as another alternative in Fig 3.1b. In this circuit we get rid of the series inductor L_1. Naturally, the expectation here is that this approach will step up the impedance presented by the antenna.

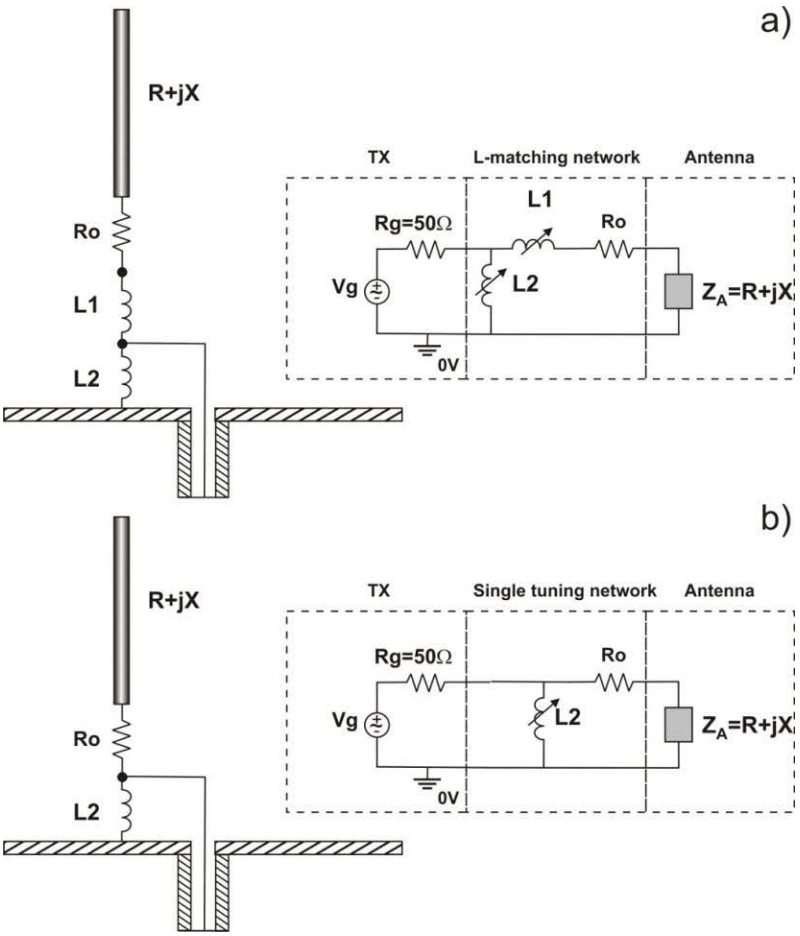

Fig. 3. 1. A whip-monopole with double tuning (L-tuning) [30] and the single tuning network. Ohmic resistance of the series inductor, R_o, will be neglected. The matching network does not show the DC blocking capacitor in series with L_2.

The goal is to tune the dipole antenna to 50 Ohm or to another real impedance at a desired frequency of interest, f_C. This frequency is the center band frequency of the antenna. For tuning, it does not really matter if the antenna is in the transmitting or in the receiving mode.

3.2 Analysis of double tuning circuit (L-section)

The tuning procedure is done with two inductors, the series inductor L_1 with the impedance Z_A and the parallel inductor L_2. Very roughly then, the series inductor essentially cancels the series capacitance whereas the parallel inductor increases the output resistance to 50 Ohm. The circuit analysis uses the standard impedance transformations known from the steady-state AC circuit theory. We need to find the equivalent impedance of the antenna Z_{out} with the tuner looking into the input terminals From Fig. 3.1a,

$$Z_{out} = Z_2 \,\|\, (Z_1 + jX + R) = \frac{Z_2(Z_1 + jX + R)}{Z_1 + jX + R + Z_2} = \frac{j\omega L_2\left(j\omega L_1 + jX + R\right)}{j\omega L_1 + j\omega L_2 + jX + R} =$$
$$Z_{out} = \frac{j\omega L_2\left(R + jB\right)}{R + jB + j\omega L_2}, \quad B = X + \omega L_1 \tag{3.1}$$

We need to have the real and imaginary part of Z_{out}. Multiplying both the numerator and the denominator by the complex conjugate of the denominator, we get,

$$Z_{out} = \frac{j\omega L_2\left(R + jB\right)\left(R - j\left[B + \omega L_2\right]\right)}{R^2 + \left[B + \omega L_2\right]^2}$$
$$Z_{out} = \frac{\omega^2 R L_2^2 + j\omega L_2\left(R^2 + B\left[B + \omega L_2\right]\right)}{R^2 + \left[B + \omega L_2\right]^2} \tag{3.2}$$

Therefore,

$$\mathrm{Re}(Z_{out}) = \frac{\omega^2 R L_2^2}{R^2 + \left[B + \omega L_2\right]^2}$$
$$\mathrm{Im}(Z_{out}) = \frac{\omega L_2\left(R^2 + B\left[B + \omega L_2\right]\right)}{R^2 + \left[B + \omega L_2\right]^2} \tag{3.3}$$

Clearly, $\mathrm{Re}(Z_{out}) > 0$. The condition of zero output reactance and 50 Ohm output resistance yield

$$\left(R^2 + B\left[B + \omega L_2\right]\right) = 0$$
$$\frac{\omega^2 R L_2^2}{R^2 + \left[B + \omega L_2\right]^2} = 50 \tag{3.4}$$

Two unknowns are B and L_2. We denote ωL_2 by X_1. Eqs. (3.4) are transformed to the form

$$R^2 + B^2 = -BX_1$$
$$\frac{RX_1^2}{R^2 + B^2 + 2X_1 B + X_1^2} = 50 \tag{3.5}$$

Further transformation gives

$$R^2 + B^2 = -BX_1$$
$$\frac{RX_1^2}{X_1^2 + X_1 B} = 50 \tag{3.6}$$

or, which is the same,

$$R^2 + B^2 = -BX_1$$
$$RX_1 = 50(X_1 + B) \tag{3.7}$$

Clearly,

$$X_1 = \frac{50B}{(R - 50)}$$
$$R^2 + B^2 = \mathrm{K}B^2 \quad \left(\because \mathrm{K} = \frac{50}{50 - R}\right) \tag{3.8}$$
$$\Rightarrow B = \pm\sqrt{\frac{R^2}{\mathrm{K} - 1}} = \pm\sqrt{R(50 - R)}$$

Inserting the negative solution for B into X_1 we get,

$$X_1 = \omega L_2 = 50\sqrt{\frac{R}{(50 - R)}} \tag{3.9}$$

Using the relation $B = X + \omega L_1$, we extract for the second component

$$\omega L_1 = -X - \sqrt{R(50 - R)} \tag{3.10}$$

Quantitatively from Eqs. 3.9 and 3.10, and referring to Fig. 3.1a, the analytical result for the tuning inductances has the form for $R_o = 0$, $R_g = 50\Omega$, and $\omega = \omega_C$, (also see Ref. [30])

$$L_2 = \frac{1}{\omega_C}\sqrt{\frac{R_g R}{1 - R/R_g}}, \quad L_1 = -\frac{X}{\omega_C} - \frac{L_2}{2} - \sqrt{\frac{L_2^2}{4} - \frac{R^2}{\omega_C^2}} \tag{3.11}$$

3.3 Sensitivity of the double tuning circuit

As noted in the prior section, the double tuning circuit for the electrically short dipole comprises two inductors arranged in a specific configuration as shown in Fig. 3.1 (a). The solution for the inductor values were derived in section 3.2 and shown in Eq. (3.11). Thus we can calculate the inductor values in a straightforward manner, if we know the dipole dimensions (see chapter 2, Eq. (2.10a)) and the generator resistance to be matched (typically 50 Ω). However, it is rarely the case that the inductor values predicted by theory can be found in the real world. In fact even the actual inductor value, if found, would have an associated tolerance specified.

It is worthwhile to investigate the effect of this variability on the tuning. This is done by observing the effective resistance and reactance at the input to the double tuning network due to the variations in inductor values. We consider a 150mm long thin dipole ($l_A/d = 60$), whose resonant frequency is 1 GHz. In Fig. 3.2, the reactance and resistance map is plotted as a function of variations from the nominal value of L_1 and L_2. Additionally, this map is shown for different choices of center frequency (f_C). The center frequencies satisfy the limiting condition $f_C / f_{\text{res}} \le 0.5$ for an antenna operated

below the first resonance. The nominal values for the inductors in the double tuning network are shown as a green circle in the plots.

The sensitivity maps clearly reveal the difficulty in maintaining a good impedance match at lower frequencies with the double tuning network. The reactance and resistance maps and the associated 3D surface plots in Figs. 3.2 and 3.3 show that the margin of error, for the double tuning network improves with increasing center frequency. In Fig. 3.3 for the f_C = 0.1 GHz case, the nominal values for inductance calculated by using Eq. 3.11 are precariously positioned over the dip in the reactance surface. On either side of this dip, the total reactance at the input to the network becomes large very quickly. Expectedly, it is the opposite behavior for the resistance wherein, the nominal values for inductance result in a sharp peak for the input resistance. In both cases, it is the sensitivity to L_1 that can cause more damage. At higher frequencies, the sensitivity function spreads out and the gradient close to the nominal values of the inductance becomes smoother in the case of the resistance. The reactance behavior is improved and shows some immunity to small variations in L_1.

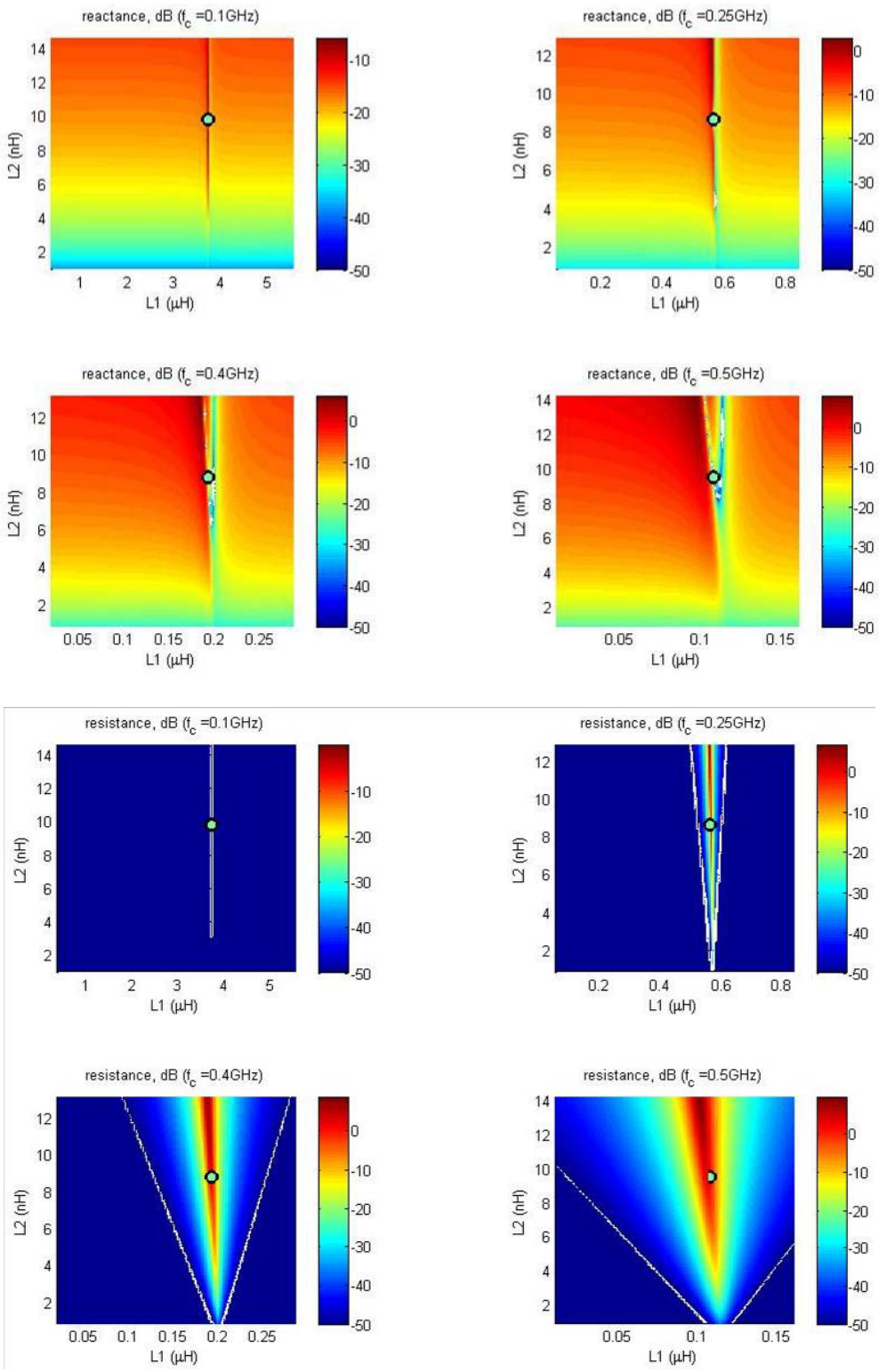

Fig. 3. 2. The reactance and resistance sensitivity maps for the double tuning network for an electrically short dipole (resonant at 1GHz). The values are plotted relative to R_g (50Ω) at four different frequencies, all within the small antenna criterion. The green circle indicates the nominal value for the inductors.

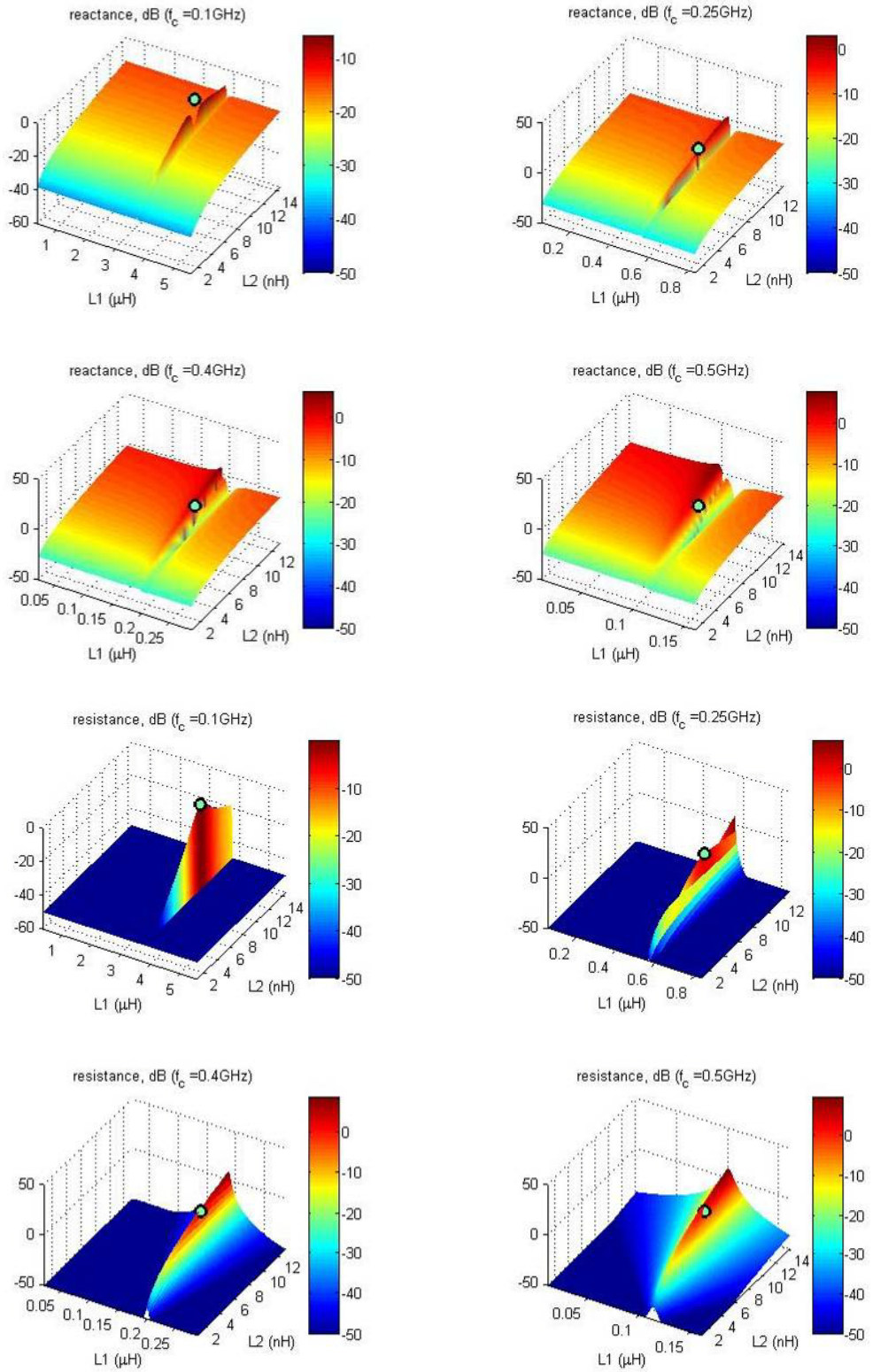

Fig. 3. 3. The three dimensional plot for reactance and resistance sensitivity of an electrically short dipole (resonant at 1GHz). The variation in the surface features of each function can be seen for four different frequencies. The green circle indicates the nominal value for the inductors.

In the case of different values of the generator resistance, the sensitivity plots in Fig. 3.4 and 3.5 clearly show that the underlying behavior is similar. At 0.1 GHz, the center frequency at which the double tuning network values are calculated, the reactance and resistance plots do not vary drastically due to changes in the generator resistance. It is to be noted that changes to the generator resistance affect only L_2, the shunt inductor. Therefore, we see that larger values of R_g, demand a bigger inductance. It is reasonable to expect that for higher center frequency of matching, the nominal inductance value will not be as large (owing to the larger antenna radiation resistance to begin with).

Changes to the thickness of the dipoles (or width in the case of the blade dipoles), does change the sensitivity maps for reactance and resistance. The Figs. 3.6 and 3.7 show plots of this variation at a center frequency of 0.5 GHz. The thinner dipoles (e.g. $l_A/d = 60$) are again the worse of the four cases considered. The reason is clear; the thicker dipoles have lesser capacitive reactance and this directly affects the series inductor L_1 in the double tuning network.

3.4 Analysis of single tuning circuit

The single tuning is made with the inductor L_2 in parallel. The inductance L_1 is exactly zero. From Eq. (3.3) one has

$$R^2 + X\left[X + \omega L_2\right] = 0 \Rightarrow L_2 = \frac{R^2 + X^2}{-X\omega} \tag{3.12}$$

and the resistance then becomes (B=X as long as L_1 is zero)

$$\mathrm{Re}(Z_{out}) = \frac{R\omega^2 L_2^2}{R^2 + \left[B + \omega L_2\right]^2} = \frac{R\omega^2 L_2^2}{R^2 + \left[X + \omega L_2\right]^2} = \frac{R(R^2 + X^2)^2}{(R^2 + R^4/X^2)X^2} = \frac{R^2 + X^2}{R} \tag{3.13}$$

The result implies that the available feed point resistance of the antenna is simply stepped up by the factor X, where

$$\mathrm{X} = \frac{R^2 + X^2}{R} \tag{3.14}$$

Thus, the single degree of freedom allows for achieving either a zero input reactance and an arbitrary resistance transformation as given by Eq. (3.14), or a possible $50\,\Omega$ input resistance with an non-zero transformed input reactance (a similar transformation can be derived by considering the alternative case of $Re\{Z_{in}\}=50\,\Omega$).

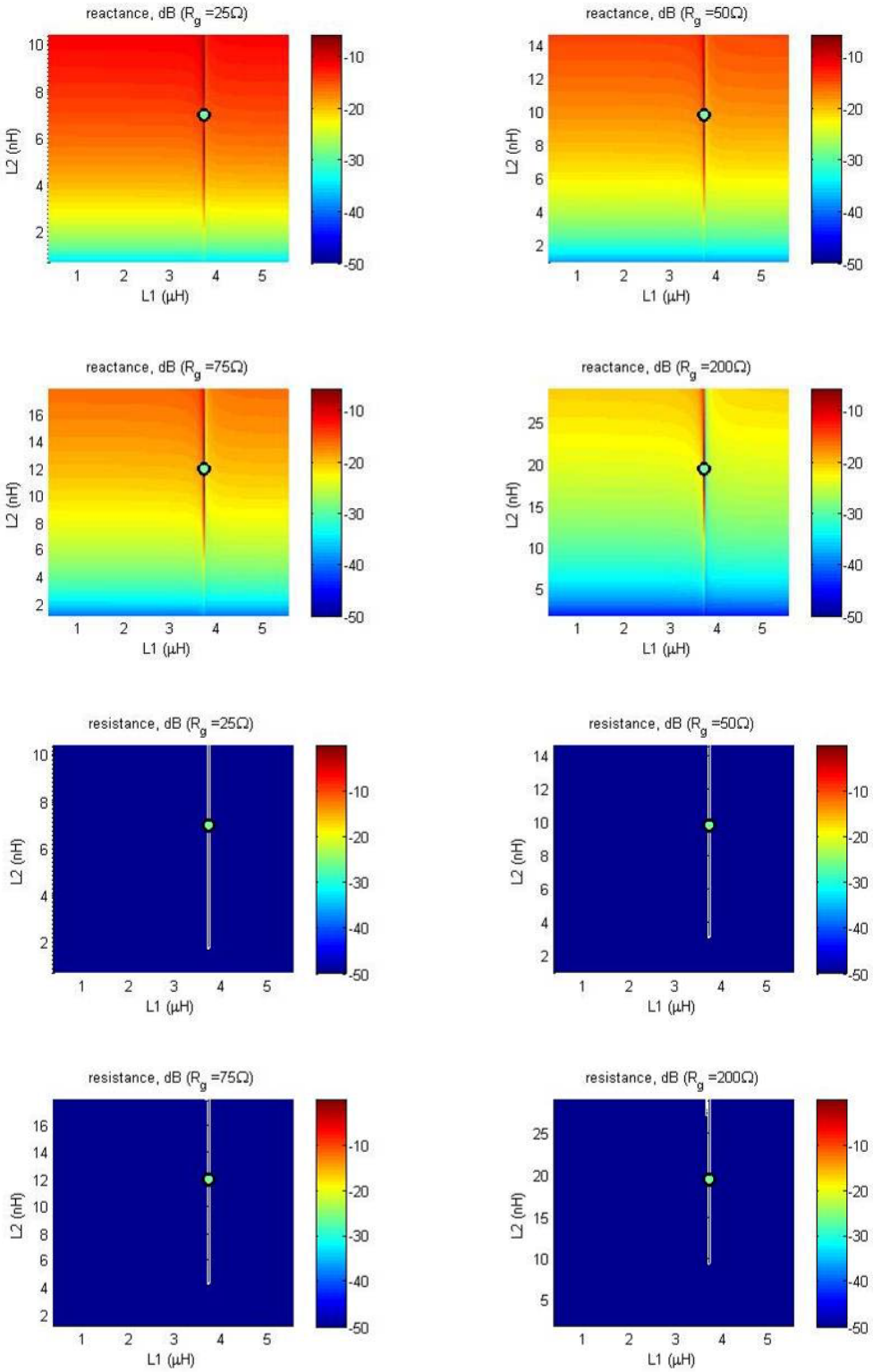

Fig. 3. 4. The reactance and resistance sensitivity maps for the double tuning network for an electrically short dipole (resonant at 1GHz). The values are plotted relative to four different values of R_g at f_C = 100 MHz. The green circle indicates the nominal value for the inductors.

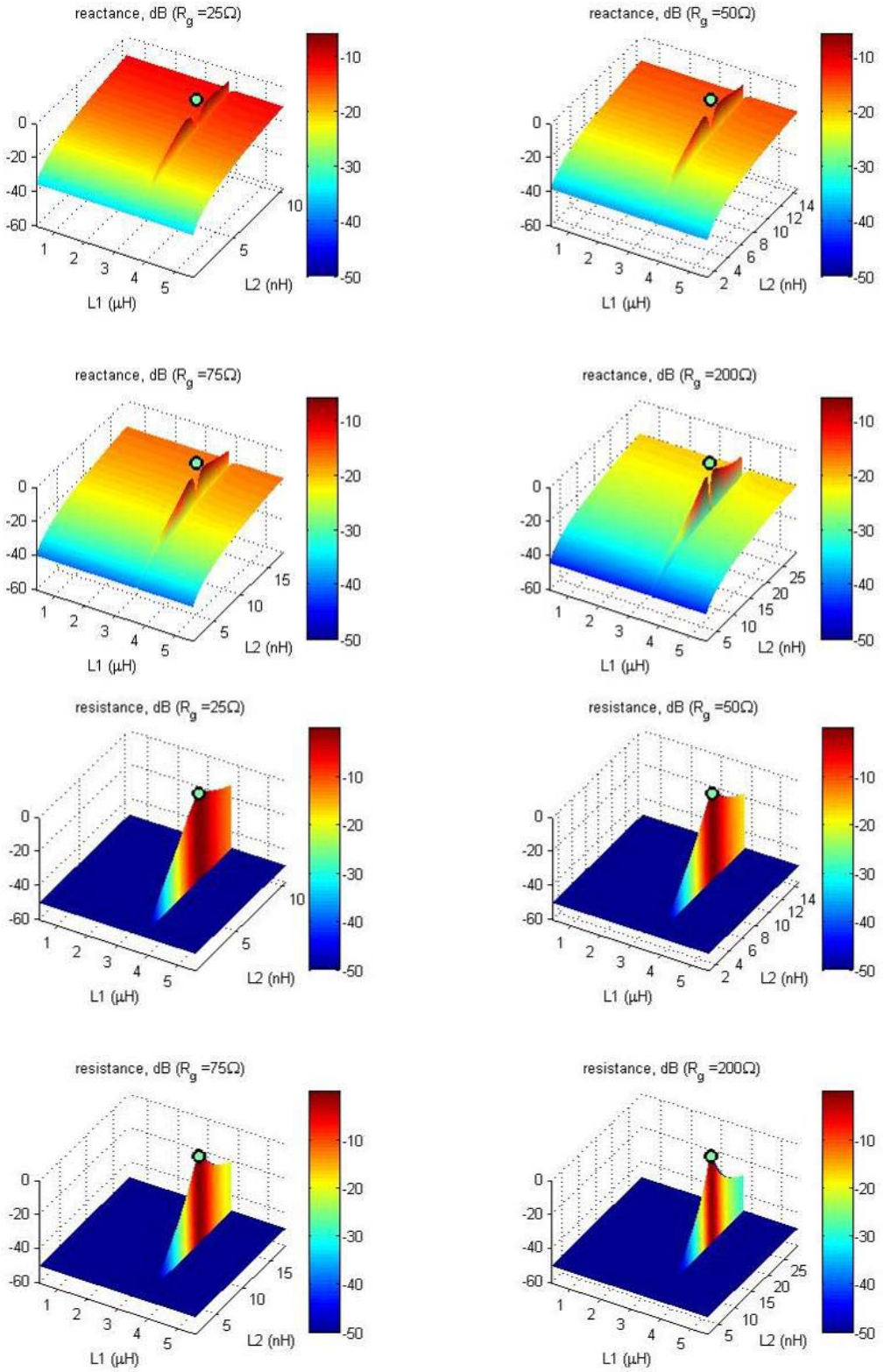

Fig. 3. 5. The three dimensional plot for reactance and resistance sensitivity of an electrically short dipole (resonant at 1GHz). The surface features of each function can be seen for four different values of generator resistance. The green circle indicates the nominal value for the inductors.

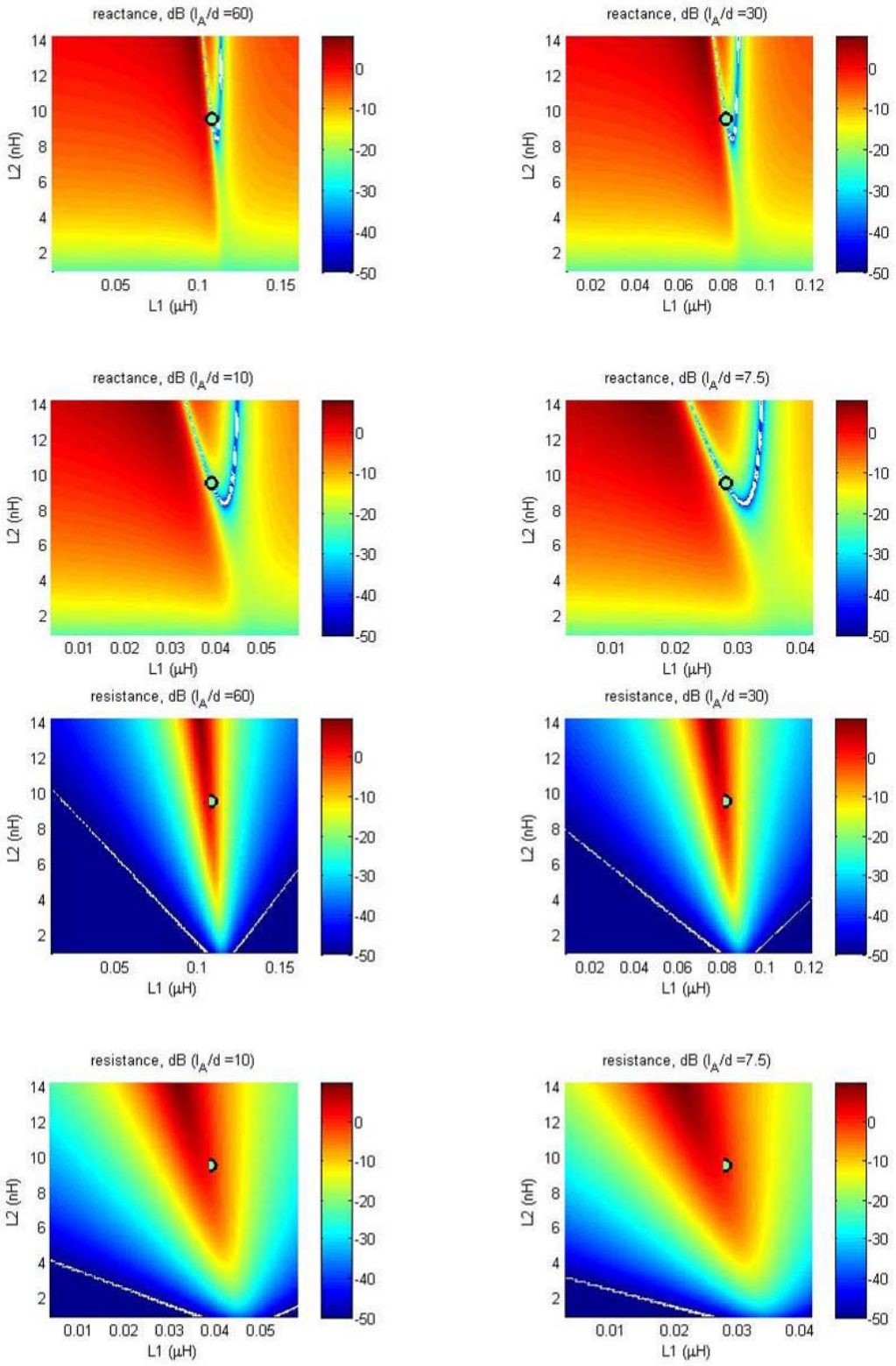

Fig. 3. 6. The reactance and resistance sensitivity maps for the double tuning network for an electrically short dipole (resonant at 1GHz). The values are plotted relative to four different values of $l_A/d = 60$ at f_C = 0.5 GHz. The green circle indicates the nominal value for the inductors.

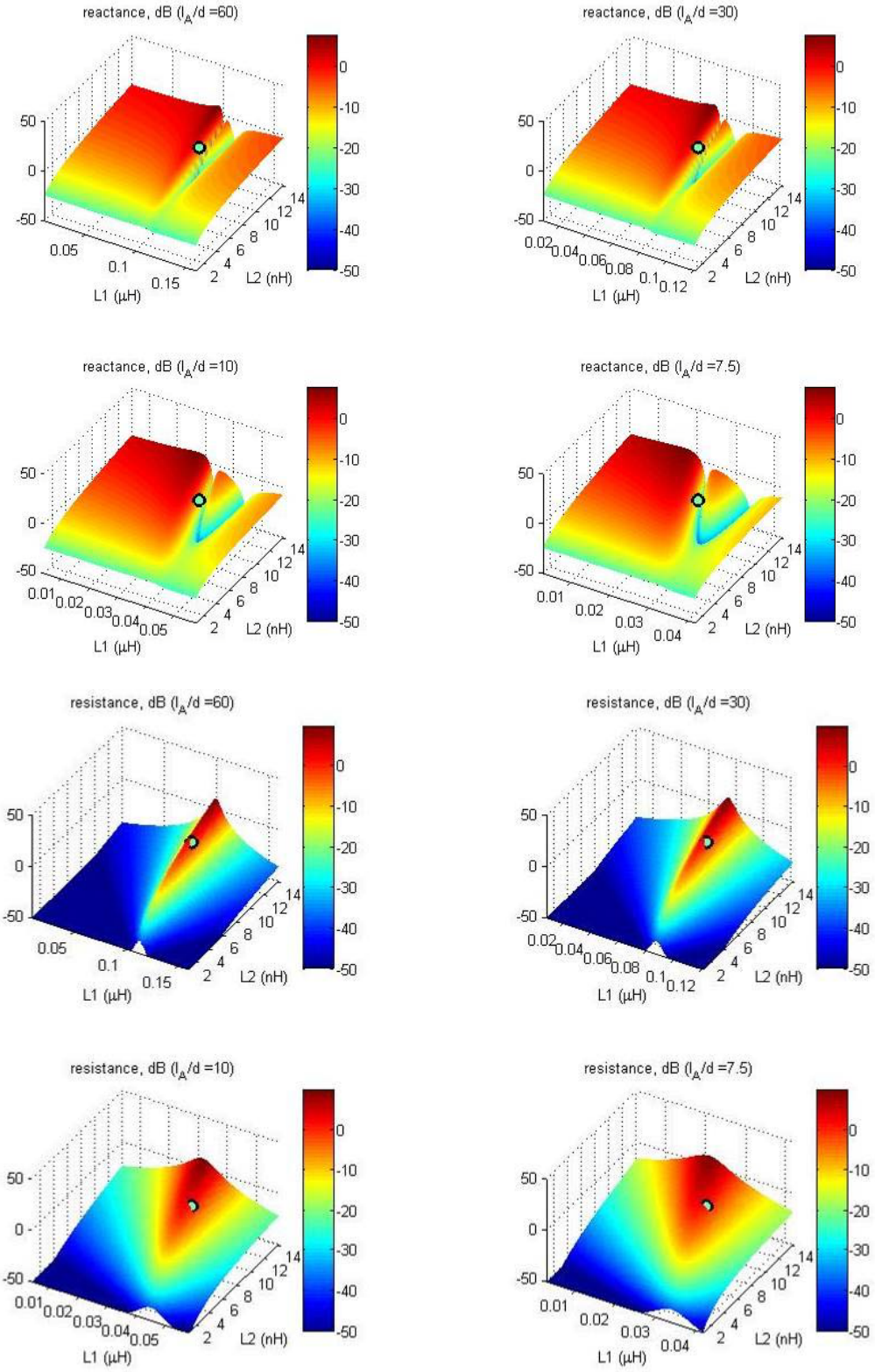

Fig. 3. 7. The three dimensional plot for reactance and resistance sensitivity of an electrically short dipole (resonant at 1GHz). The surface features of each function can be seen for four different values of generator resistance. The green circle indicates the nominal value for the inductors.

3.5 Extension of the L-section matching network

To increase the bandwidth of the *L*-tuning section at some fixed values of L_1, L_2, we suggest to consider the matching circuit shown in Fig. 3.8. It is seen from Fig. 3.8 that we can simply add a high-pass *T*-network with three lumped components (a shunt inductor and two series capacitors) to the *L*-section or, equivalently, use two sections of the high-pass *LC* ladder and investigate the bandwidth improvement. The Thévenin impedance of the equalizer, as seen from the antenna, is given by

$$Z_T = \frac{sL_2 Z_g}{sL_2 + Z_g} + sL_1, \quad \begin{cases} \text{case I} & Z_g = R_g \\ \text{case II} & Z_g = \dfrac{sL_4(R_g + 1/(sC_5))}{sL_4 + (R_g + 1/(sC_5))} + 1/(sC_3) \end{cases} \tag{3.15}$$

where $s = j\omega$. The default values of the circuit parameters for the sole *L*-tuning section read $C_3 = L_4 = C_5 = \infty$. Thus, we introduce three new lumped circuit elements, but avoid using transformers. Instead of using impedances, an ABCD matrix approach would be more beneficial when using transformers.

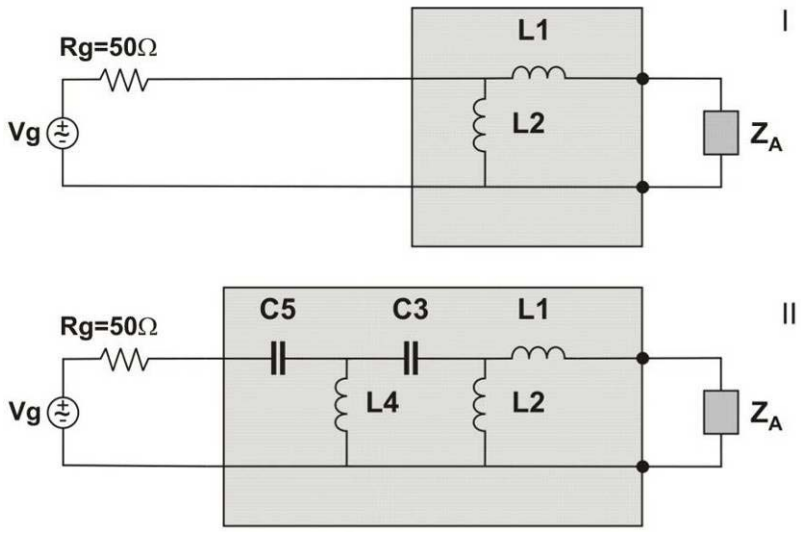

Fig. 3. 8. An extension of the *L*-tuning network for certain fixed values of L_1, L_2 by the *T*-match.

3.6 Objectives of the circuit optimization task

We assume that the antenna is to be matched over a certain band *B* centered at f_C, and that the gain variation in Eq. (2.16) does not exceed ±25% over the band. If, for this given equalizer circuit, we cannot achieve such small variations at any values of the circuit parameters, the equalizer is not considered capable of wideband impedance matching over the bandwidth *B*. We know that a low-order equalizer (the *L*-matching section) alone is not able to provide a nearly uniform gain over a wider band. However, increasing the circuit order helps. Thus, two practical questions need to be answered:

A. For a given center frequency f_C and bandwidth *B*, or for a given fractional bandwidth $\overline{B} = B / f_C$, what are the (normalized) circuit parameters that give the required bandwidth?

B. What is the gain-bandwidth product and how does it relate to the upper estimate given by Eq. (2.22c)?

Yet another important question is the phase linearity over the band; this question will not be considered in the present study.

3.7 Numerical method and the antenna parameters tested

To optimize the matching circuit with 5 lumped elements we employ a direct global numerical search in the space of circuit parameters. The grid in $\Re^5$ space includes up to 100^5 nodes. The vector implementation of the direct search is fast and simple, but it requires a large (64 Gbytes or higher) amount of RAM on a local machine.

For every set of circuit parameters, the minimum gain over the bandwidth is first calculated [23]. The results are converted into integer form and sorted in a linear array, in

descending order, using fast sorting routines on integer numbers. Then, starting with the first array element, every result is tested with regard to ±25% acceptable gain variation. Among those that pass the test, the result with the highest average gain is finally retained. After the global maximum position found on a coarse mesh, the process is repeated several times on finer meshes in the vicinity of the anticipated circuit solution.

We will consider the dipole case and assume monopole equivalency. The set of tested antenna parameters includes:

$$l_A / d = [50, 10, 5], \quad \overline{B} = [0.1, 0.5], \quad f_C / f_{\text{res}} = [0.05 : 0.05 : 0.50] \tag{3.16}$$

3.8 Alternative optimizers

A viable alternative to the direct global numerical search used in this study, which is also a derivative free and a global method, is the genetic algorithm [36]. The genetic algorithm (GA) belongs to a class of stochastic optimization algorithms that attempt to mimic some of the classical evolutionary processes that occur in the biological world. Processes such as reproduction, mutation and crossover, which are central to the evolution of a species in nature hold the same meaning when applied for the purpose of optimization. The striking feature of GA based optimization is that we begin with a *population* of possible candidates for the solution, thereby introducing an inherent parallelism into the process. The optimality of this population is tested by applying it to the fitness function (also known as the objective function to be optimized). Depending on the results, candidates are selected to populate the second generation by applying the three key processes mentioned earlier. This process repeats itself till either a good solution is found or a solution to the problem is deemed infeasible. GA's have been widely used in many fields including antenna array design [37] and electromagnetics

[38]. An interesting application of the GA was reported in ref. [39] wherein the authors have demonstrated its use in optimizing lumped component networks for an antenna synthesis application as well as the matching network.

The *MATLAB* © based Genetic Algorithm and Direct Search toolbox™ [40], provided us with an excellent platform to optimize the matching circuit under consideration in this study. This toolbox features a vast array of choices with which we were able to tailor the GA solver for our requirement. The results obtained from this GA are rather close to those achieved by the direct global numerical search and further work may be pursued in this direction. While the genetic algorithm by itself is a good candidate for a global optimizer, a direct search technique known as 'Pattern search' can be used with it to improve its performance. This is known as a hybrid GA [40] and it works by taking the best solution arrived at by the GA as the initial point and proceeds to refine the result by searching along a '*pattern*'. The pattern here refers to a set of vectors that define the parameter space (in our case the circuit parameters) for the current iteration over which the search is performed. Depending on the result from the objective function this set of vectors is expanded or contracted by specific amount and the process repeats. To use this method we first generated a population of random candidate solutions with a uniform distribution, for the circuit parameters. The GA solver then tests these candidate solutions based on a specified criterion, which in this particular case, is to maximize the minimum gain over the band. After assigning scores to the various candidate solutions, it then creates the next generation of solutions, referred to as the '*children'*, by pairing candidate solutions from the previous generation, referred to as the '*parents'*. To ensure diversity in the next generation, mutations, or random changes to one of the parents in a pair are

introduced. These new solutions replace the current population and the process repeats. Several options for stopping criterion can be used such as time limit, no. of successive generations or even simply the change in the value objective function between two generations. During this study, the results obtained with the GA toolbox were found to be in good agreement with the results obtained with the direct global numerical search. In the next section a comparison of the performance of our direct search routine with the algorithms from the GA toolbox will be presented.

Chapter 4. Numerical simulation and experimental results

In chapter 3 the wideband matching network was developed starting with the narrowband L-section. The circuit optimization task was identified and put forth. To solve for the network components a direct search based optimization scheme was used. A potential alternative to the direct search based approach was also proposed in the form of the Genetic algorithm. The results of the direct search based numerical simulations will be presented in this chapter. A variety of matching scenarios will be considered. The practicality of this network lies in whether the components can be procured easily. To investigate this, a comprehensive search across different antenna geometries and component sensitivities is made and tabulated. Also presented is a comparison between the performances of the network proposed in this thesis and a more advanced form of Carlin's equalizer [26]. This is done using both the direct search routine and the *MATLAB* © based Genetic Algorithm and Direct Search toolbox™ [40]. Finally experimental results are presented together with a discussion on the same.

4.1 Realized gain – wideband matching for $\overline{B} = 0.5$

Fig. 4.1 shows the realized average generator gain over the passband based on the ±25% gain variation rule at different matching center frequencies. Three dipole geometries with $l_A / d = 50, 10, 5$ are considered. The bandwidth is fixed at $\overline{B} = 0.5$; we again consider three dipoles of different radii/widths. The realized values are shown by circles; the ideal upper estimate from Fig. 2.7 is given by solid curves. One can see that the 5-element equalizer performs rather closely to the upper theoretical limit T_0 when the average gain

over the band, $\overline{T}$, is substituted instead. For the majority of cases, the difference between T_0 and $\overline{T}$ is within 30% of T_0. The sole *L*-section was not able to satisfy the ±25% gain variation rule in all cases except the very last center frequency for the thickest dipole.

4.2 Gain and circuit parameters – wideband matching for $\overline{B} = 0.5,\ f_C / f_{\text{res}} = 0.5$

Table 1a reports circuit parameters of the equalizer for three dipoles with $l_A / d = 50, 10, 5$. In every case, matching is done for $f_C / f_{\text{res}} = 0.5$, $\overline{B} \approx 0.5$. Fig. 4.2 shows the corresponding gain variation with frequency within the passband. In Table 1, we have presented all circuit parameters for a 23 cm long dipole. To scale parameters to other antenna lengths one needs to multiply them by the factor $l_A / 0.23\,\text{m}$. Table 1 also shows the anticipated gain tolerance error. Whilst the average gain itself does not significantly change when changing capacitor/inductor values, the gain uniformity may require extra attention for a thin dipole (second row in Table 1). For thicker dipoles (third and fourth row of the table) one solution to the potential tolerance problem is to slightly overestimate the circuit parameters for a better tolerance. Generally, the usual uncertainty in low-cost chip capacitors and chip inductors seems to be acceptable. Table 1 also indicates that the equalizer for a wideband matching of the dipole does not involve very large inductors (and large capacitors) and is thus potentially low-loss.

Table 4. 1. Circuit parameters and gain tolerance for a short dipole with the total length l_A=23 cm. Matching is done for $f_C / f_{\text{res}} = 0.5$, $\overline{B} \approx 0.5$ based on the ±25% gain variation rule.

Antenna geometry l_A / d	Circuit parameters	Gain/Variance over the band	Gain/Variance over the band at +5% parameter variation	Gain/Variance over the band at -5% parameter variation
50	$L_1 = 176$ nH $L_2 = 70$ nH $C_3 = 4.9$ pF $L_4 = 80$ nH $C_5 = 15.3$ pF	$\overline{T} = 0.20$ $\lvert\Delta T / \overline{T}\rvert < 25\%$	$\overline{T} = 0.19$ $\lvert\Delta T / \overline{T}\rvert < 27\%$	$\overline{T} = 0.20$ $\lvert\Delta T / \overline{T}\rvert < 38\%$
10	$L_1 = 72.4$ nH $L_2 = 48.7$ nH $C_3 = 39.6$ pF $L_4 = 102$ nH $C_5 = 10.2$ pF	$\overline{T} = 0.36$ $\lvert\Delta T / \overline{T}\rvert < 24\%$	$\overline{T} = 0.35$ $\lvert\Delta T / \overline{T}\rvert < 19\%$	$\overline{T} = 0.38$ $\lvert\Delta T / \overline{T}\rvert < 35\%$
5	$L_1 = 21.5$ nH $L_2 = 24.6$ nH $C_3 = 61.9$ pF $L_4 = 537$ nH $C_5 = 15.3$ pF	$\overline{T} = 0.60$ $\lvert\Delta T / \overline{T}\rvert < 25\%$	$\overline{T} = 0.59$ $\lvert\Delta T / \overline{T}\rvert < 19\%$	$\overline{T} = 0.61$ $\lvert\Delta T / \overline{T}\rvert < 34\%$

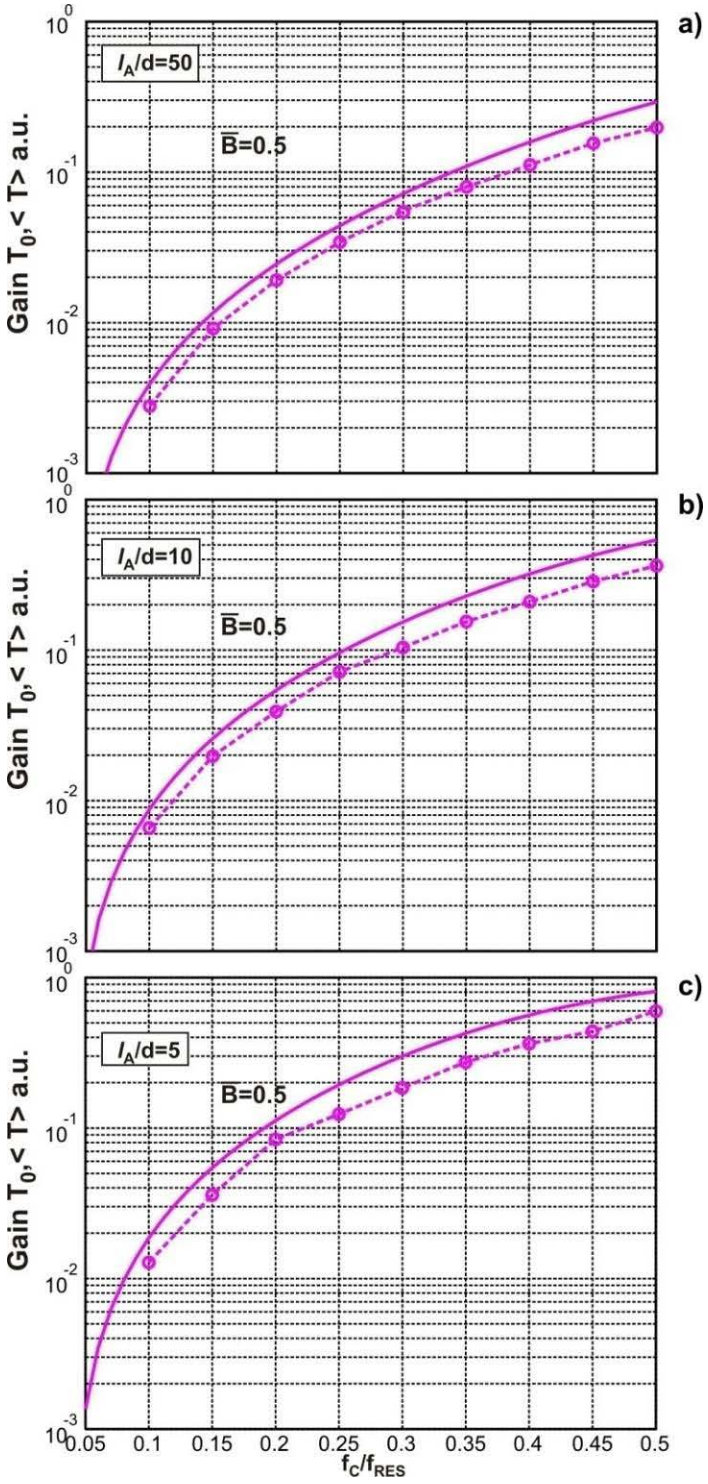

Fig. 4. 1. Realized average generator gain $\overline{T}$ over the band (circles) based on the ±25% gain variation rule at different matching center frequencies and $\overline{B} = 0.5$ for three different dipoles, obtained through numerical simulation. The realized values are shown by circles; the ideal upper estimates of T_0 from Fig. 2.7 are given by solid curves, which are realized by using eqn. (2.22c).

4.3 Gain and circuit parameters – narrowband matching for $\overline{B} = 0.1$

It is not the subject of this study to discuss the narrowband matching results; however, they have been obtained and may be discussed briefly. When the two-element *L*-section network is able to provide us with the required match, its performance is not really distinguishable from that of the full 5-element equalizer. However, it does not always happen that the reduced *L*-section equalizer is able to do so. The full equalizer is the only solution at smaller resonant frequencies and for thinner dipoles.

Unfortunately, the deviation from the Bode-Fano maximum gain may be higher for narrowband matching than for the wideband matching; in certain cases it reaches 100%. It is not clear whether this high degree of deviation is due to the numerical method or if it has a physical nature.

4.4 Gain and circuit parameters – wideband matching for $\overline{B} = 0.5,\ f_C / f_{\text{res}} = 0.15$

A more challenging case is a smaller wideband dipole; we consider here the case when $f_C / f_{\text{res}} = 0.15$ and refer to the corresponding theoretical curves presented in Fig. 2.7. Fig. 4.3 shows the transducer gain variation with frequency within the passband, after the equalizer has been applied based on the ±25% gain variation rule. The circuit parameters indicate a higher value of $L_1 = 2.46\mu\text{H}$ for $l_A / d = 50$ and $L_1 = 1.06\mu\text{H}$ for $l_A / d = 10$. For $l_A / d = 5$, inductance L_4 attains a larger value of $1.40\mu\text{H}$.

4.5 Comparison with the results of Ref. [26]

In Ref. [26] a similar matching problem was solved for a thin dipole of length $l_A = 0.5$ m and the radius a of 0.001m. Matching is carried out for $f_C / f_{\text{res}} = 0.416$, $\overline{B} = 0.4$. A Carlin's equalizer with an extra LC section has been considered. Fig. 4.4 reports the performance of our equalizer for this problem (dashed curve). The thick solid curve within the passband is the corresponding result of Ref. [26] (and copied from Fig. 6). In our case, the optimization was done based on the ±25% gain variation rule. The difference between the two average band gains was found to be 5%. The circuit components for our circuit are 1.06μH, 0.21 μH, 20 pF, 0.95μH, and 17 pF. Note that without the extra LC section, the Carlin's equalizer may lead to a considerably lower passband gain than the gain shown in Fig. 4.4 [26]. Without any equalizer, the performance is expectedly far worse. The plot indicates that a 20 dB improvement is achieved at the lower edge of the band and approximately 10 dB at the upper band edge, when the equalizer is used.

In Fig. 4.5 we show the performance of the *MATLAB* © based Genetic Algorithm and Direct Search toolbox™ [40] in comparison with the direct global numerical search for the same matching problem as in [26]. The Genetic algorithm is used in conjunction with the patternsearch algorithm and yields a solution with an average band gain variation of 24.67 %. It is noted that the performance is very close to the direct global numerical search. The component values produced by the GADS toolbox are (in order L_1 – C_5): 1.09 μH, 0.18 μH, 95.3 pF, 0.99 μH, 11.34 pF. Note, that all component values but for C_3 are very similar to that produced by the direct global numerical search.

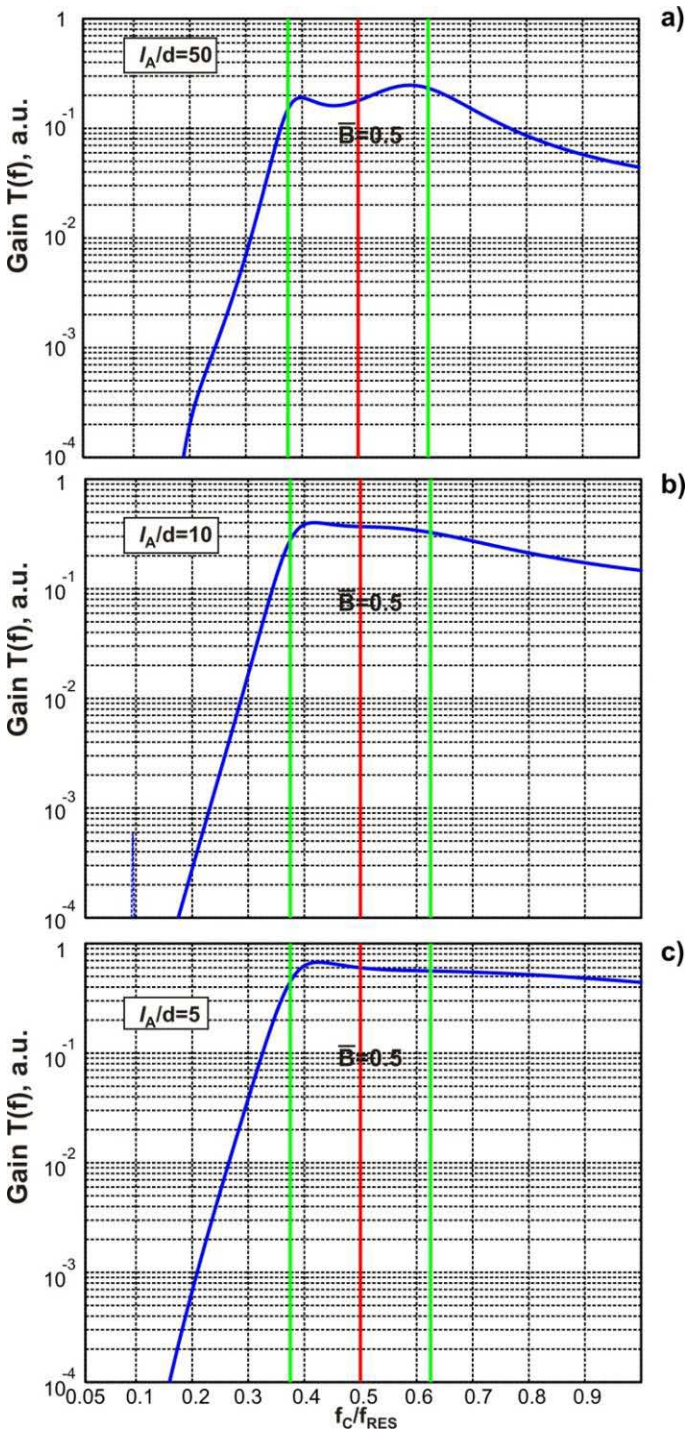

Fig. 4. 2. Gain variation with frequency for a short dipole or for an equivalent monopole at different thicknesses/widths obtained by numerical simulation which uses Eq. (2.16). Matching is done for $f_C / f_{\text{res}} = 0.5$, $\overline{B} \approx 0.5$ based on the ±25% gain variation rule. Vertical lines show the center frequency and the passband.

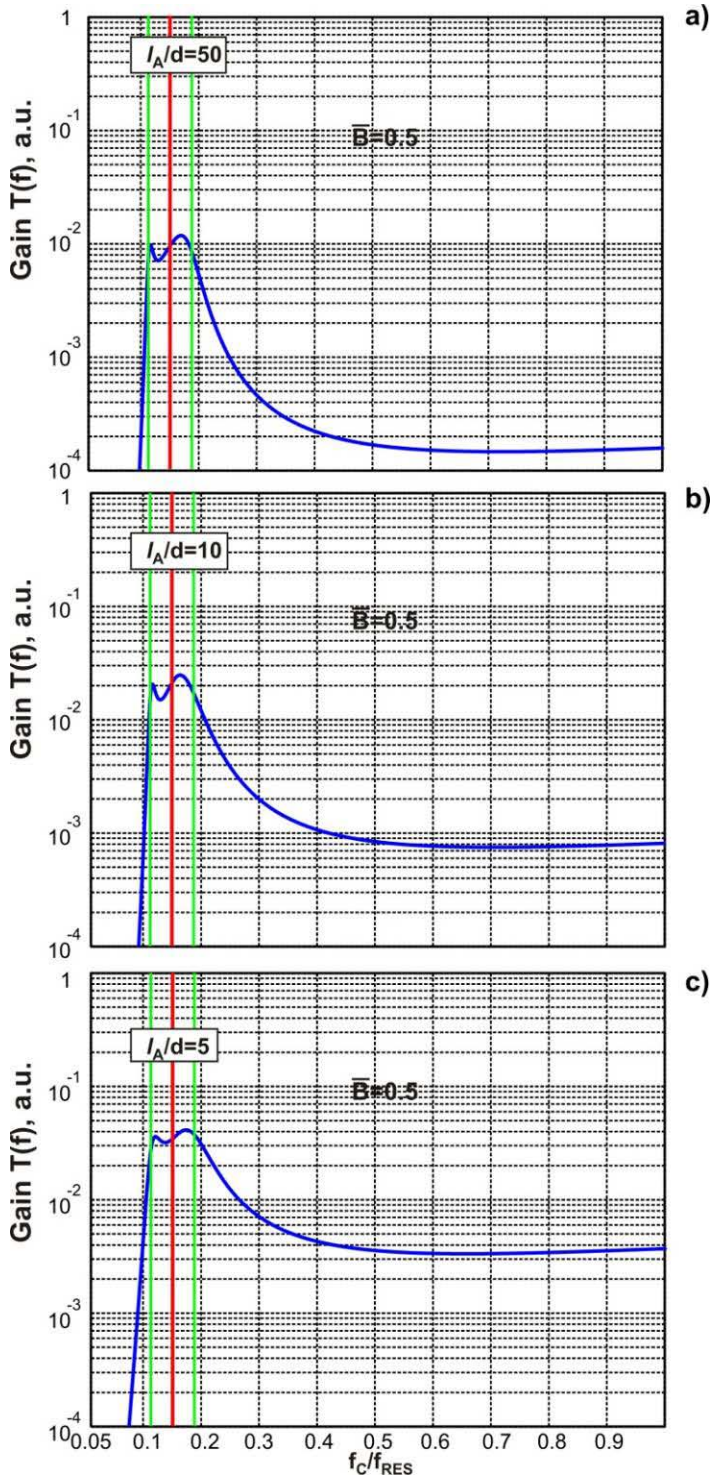

Fig. 4. 3. Gain variation with frequency for a short dipole or for an equivalent monopole at different thicknesses/widths obtained by numerical simulation which uses Eq. (2.16). Matching is done for $f_C / f_{\text{res}} = 0.15$, $\overline{B} \approx 0.5$ based on the ±25% gain variation rule. Vertical lines show the center frequency and the passband.

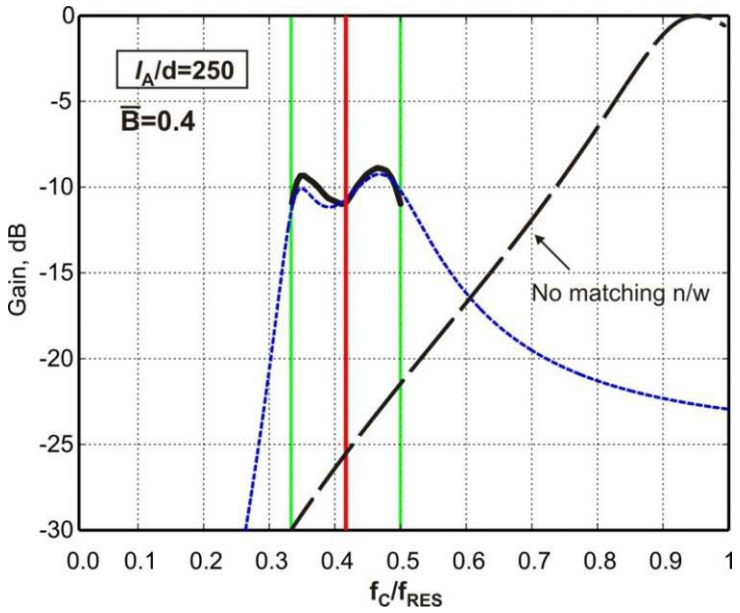

Fig. 4. 4. Gain variation with frequency for a short dipole or for an equivalent monopole of length 0.5 m and radius of 0.001m, by numerical simulation of associated matching network. Matching is done for $f_C / f_{\text{res}} = 0.416$, $\overline{B} = 0.4$ based on the ±25% gain variation rule (dashed curve). The thick solid curve is the result of Ref. [25] with the modified Carlin's equalizer, which was optimized over the same passband for the same dipole. Vertical lines show the center frequency and the passband. Transducer gain, in the absence of a matching network, is also shown by a dashed curve following Eq. (2.16).

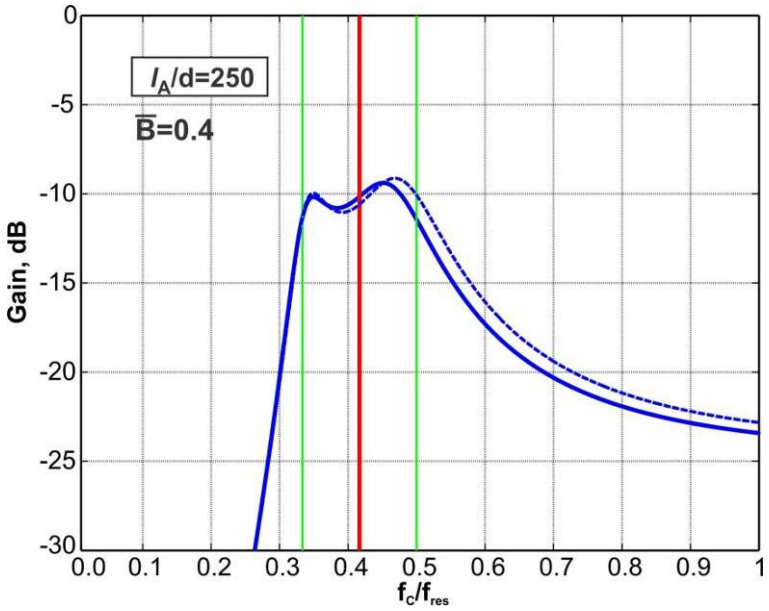

Fig. 4. 5. Comparison between the results from the genetic algorithm (solid blue curve), and the direct global numerical search algorithm (dashed blue curve) for an equivalent monopole of length 0.5 m and radius of 0.001m, by numerical simulation of associated matching network.

4.6 Effect of impedance transformer

A set of numerical simulations for the same dipoles with a 4:1 ideal transformer has shown that the wideband matching results (achievable gain) are hardly affected by the presence of a transformer, even though the parameters of the matching circuit change considerably. For example, in the case of $\overline{B} = 0.5$, $f_C / f_{\text{res}} = 0.15$ and discussed above, the average gain without and with transformer is 0.0092/0.0092, 0.020/0.020, and 0.036/0.040 for the three dipoles with $l_A / d = 50, 10, 5$.

4.7 Experiment - Short blade monopole

We have designed, constructed, and tested a number of short blade monopole test antennas and the corresponding matching networks. The antenna's first resonant frequency is in the range 550-650 MHz. The matching is to be done over a wide, lower frequency band of 250-400 MHz, with the center frequency of 325 MHz. For every monopole, the ratio, l_A / d, equal to 20 has been used in the experiment. Fig. 4.6 shows the generic monopole setup.

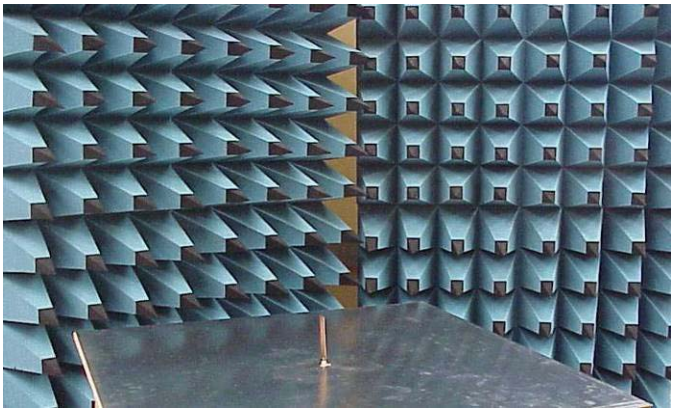

Fig. 4. 6. A 10.1cm long and 2.3cm wide blade monopole over a 1×1 m ground plane used as a test antenna for wideband impedance matching.

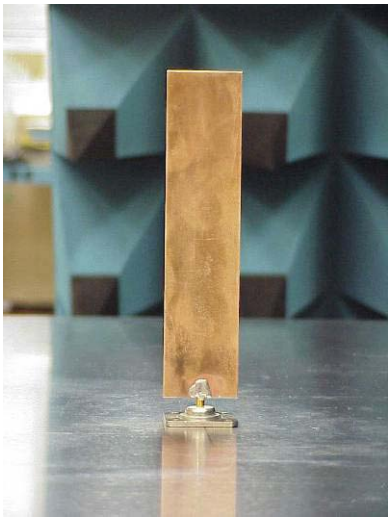

Fig. 4. 7. A closer view of the test monopole over the ground plane.

The brass monopole antennas have been centered in the middle of the 1×1 m aluminum ground plane. We then investigated the matching performance for two specific cases: i) the monopole is resonant at 650 MHz and; ii) monopole is resonant at a slightly lower frequency of 600 MHz. The results for both cases are reported in this section.

4.8 Experiment - Wideband equalizer

The ubiquitous FR-4 substrate has been used for the equalizer. We have chosen two tunable high-*Q* components among the five to compensate for parasitic effects due to the board assembly, the finite *Q* of the discrete components and the manufacturing uncertainties. These tunable components were L_1 and C_5, respectively. L_1 is a tunable RF inductor from Coilcraft's series 148 with a tuning range of 56nH - 86nH, and a nominal value of 73nH. This inductor has a *Q* of 106 at 50MHz. C_5 is a Voltronics series JR ceramic chip trimmer capacitor with a tuning range of 4.5pF - 20pF within a half turn. This capacitor has a minimum Q of 1500 at 1MHz. Apart from L_1 which is a leaded component, all the other components are the high-*Q* surface mount devices.

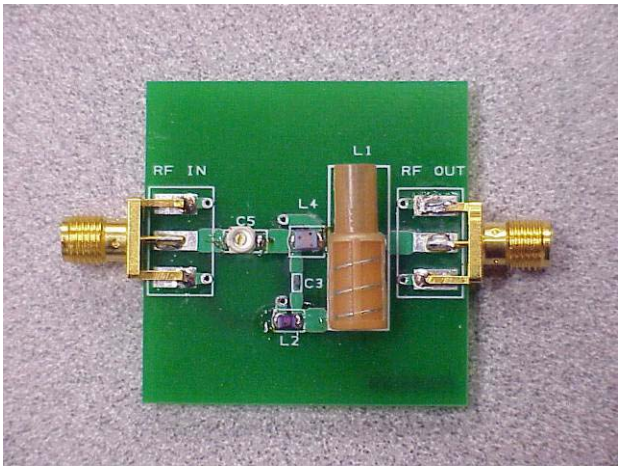

Fig. 4. 8. Practical realization of the wideband equalizer for the blade monopole antenna following Table 2.

Table 4.2 lists the parameter values. The designed wideband equalizer is shown in Fig. 4.8.

Table 4. 2. Practical component values used in the monopole equalizer for l_A / d =20 and t = 2.3 cm.

Component	Value
L_1	56 nH - 86 nH
L_2	48 nH
C_3	39.1 pF
L_4	100 nH
C_5	4.5 pF - 20 pF

4.9 Gain comparison – 1×1 m ground plane

We compare the gain performance for two different modifications of the blade monopole dimensions in Fig. 4.9. The first modification involves a 10.1 cm long an 2.3 cm wide blade monopole, which is resonant at 650 MHz. In Fig. 4.9a the gain achieved by the unmatched monopole antenna (thin solid curve) and the gain of the monopole antenna

with the designed wideband equalizer (thick dotted curve), respectively are shown. The average transducer gain achieved in experiment is 0.262 over the bandwidth 250MHz - 400MHz with a gain variation of 40 %. The L_1 and C_5 values for this particular result are 86 nH and 7.63 pF respectively.

Next, we consider a blade monopole antenna of length 10.8 cm and width 2.3 cm. This blade monopole resonates at 600MHz. Fig. 4.9b shows the matching performance with (thick dotted curve) and without (thin solid curve) the wideband equalizer. We see that the equalizer performs rather well even under this scenario and achieves a gain of 0.259 within the bandwidth of interest. The gain variation over the band is 28.8 %. In this case the value of L_1 is changed to 73nH while the capacitance C_5 is unchanged.

Here, we also notice an approximate 10dB improvement over the unmatched antenna, provided by the equalizer at the lower edge of the band. During the experiments we have noticed that a resonance may appear at lower frequencies below 200 MHz. The theoretically predicted gain is shown by thick solid curves in Fig. 4.9a and 4.9b. Generally the experiment follows the theory. In the case of Fig. 4.9a, the average experimental gain over the band is 0.262 and is slightly higher than the corresponding theoretical value of 0.245. In the case of Fig. 4.9b, the average experimental gain over the band is 0.259 versus the theoretical value of 0.245. We believe that the average gain difference is within the experimental uncertainty. This statement can be further confirmed by the results from the fourth and fifth column of Table 4.1, where we observe the quite similar variation when the component values of the matching circuit are varied by ±5%.

However, for the local gain behavior, we observe somewhat larger variations. The experimental gain is higher in the middle of the band, but is lowered at the band edges.

We explain these variations by the associated tuning procedure and by the inability to exactly follow the requested values of inductance L_1 and capacitance C_5. An additional important mechanism is lumped-element losses at the higher band end. Yet one more uncertainty factor is due to a relatively small size of the measurement chamber. This effect becomes apparent at low frequencies as Fig. 4.9 indicates. The present results are preliminary and have a very significant room for improvement.

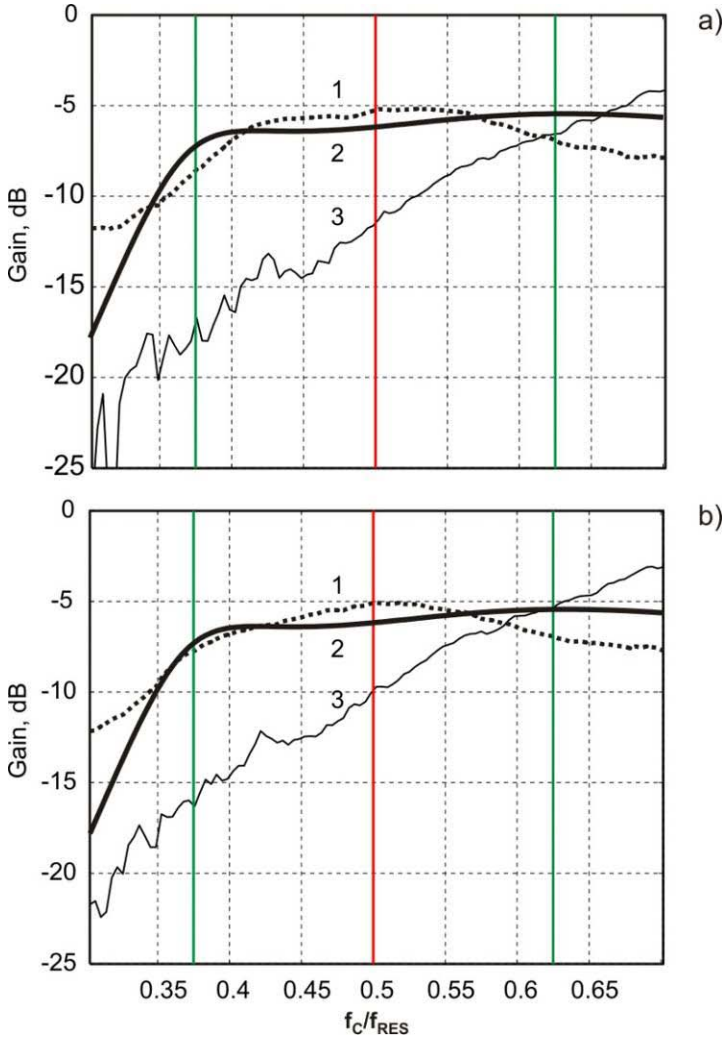

Fig. 4. 9. The experimental gain data (dotted curve 1) in comparison with the theoretical result (thick curve 2) for two blade monopoles with the matching network from Table 2: a) - the blade length is 10.1 cm and the width is 2.3 cm; b) - the blade length is 10.8 cm and the width is 2.3 cm. The thin solid curve 2 in this graph corresponds to the antenna gain (based on the measured return loss) without the matching network.

4.10 Gain comparison – 75×75 cm ground plane

The effect of ground plane size on the matching performance is considered. The size of the ground plane for this experiment was reduced to 75×75 cm. The length of the blade monopole was retained to be 11.5 cm since the first resonance observed with this setup is approximately 650 MHz. The width of the blade monopole is 2.3 cm. The gain performance for this setup is shown in Fig. 4.10. The component values are the same except for the L_1 and C_5 values which are 60 nH and 12pF respectively. The average transducer gain achieved in this experiment is 0.2854 over the bandwidth 250MHz - 400MHz with a gain variation of 37 %.

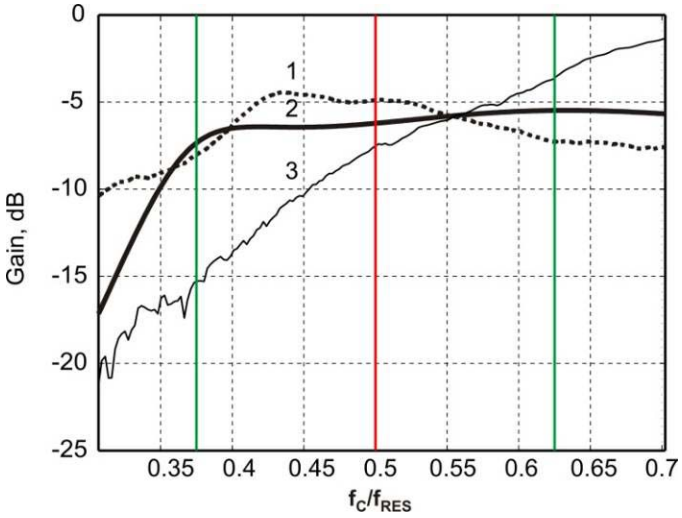

Fig. 4. 10. The experimental gain data (dotted curve 1) in comparison with the theoretical result (thick curve 2) for a blade monopole of length 11.5cm and width 2.3cm over a reduced ground plane size with the equalizer network from Table 2: The thin solid curve 3 in this graph corresponds to the gain (based on the measured S_{11}) without the equalizer network.

Even though the overall gain variation over the band is greater than 25%, the average gain is slightly higher as compared to the experiments with the larger ground plane. Again the inability to exactly follow the suggested tuning values is the reason for this large gain variation. In Fig. 4.11 the S_{11} for this antenna is plotted in dB scale. The tuning

procedure results in better S_{11} in the middle of the band as compared to the edges thus resulting in higher transducer gain in that region as observed in Fig. 4.10.

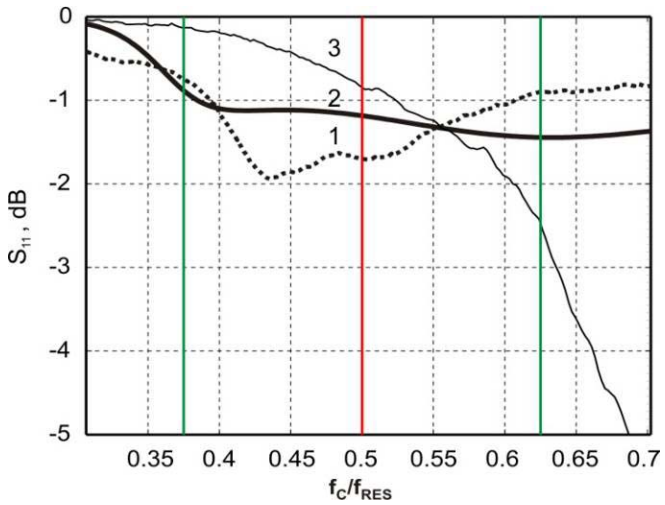

Fig. 4. 11. The experimental S_{11} data (dotted curve 1) in comparison with the theoretical result (thick curve 2) for a blade monopole of length 11.5cm and width 2.3cm over a reduced ground plane size with the equalizer network from Table 2. The thin solid curve 3 in this graph corresponds to the measured S_{11} without the equalizer network.

4.11 Discussion on S_{11}

The results shown in Figs. 4.9-4.11 about the transducer gain and the S_{11}, indicate that if the generator can tolerate an input VSWR in the range 7:1, then using the reflective equalizer approach can improve the transducer power gain for an electrically short antenna. However, if the input VSWR requirement needs to be restricted to lie below 4:1 then as discussed in section 2.9 and later in Table 4.1, the l_A / d ratio for the antenna needs to be reduced, which would result in a thicker cylindrical dipole (or monopole) or alternatively a wider blade dipole (or monopole). Specifically, using an $l_A / d = 5$ for a similar antenna as considered in the experiments resulted in a higher theoretical transducer gain and a minimum theoretical VSWR of 2.6:1. By theoretical we imply the upper limit predicted by using the Eq. 2.22c. In section 4.2, Table 4.1 provides the component values and the realized transducer gain for our 5 element equalizer. Based on

the experimental results for the blade monopoles with $l_A / d = 20$ we can safely predict that a lower VSWR can be expected for smaller l_A / d ratios as well, by using the reflective equalizer.

Chapter 5. Introduction to Modular arrays

The demand for higher bandwidths and gain from antenna systems for communication and positioning/navigation purpose is on the rise [41]-[44]. With the advent of software defined radios and cognitive radios, much more will be demanded from the antenna systems of the future [45]-[47]. While single antenna systems do achieve bandwidths far greater than an octave, there is a degree of complexity in their design and construction**.** Some of the common examples of such antennas are the spiral [48], [49]and the log-periodic antennas [50]. Antennas like the dipoles, monopoles and patches are relatively simpler to design and fabricate. The dipoles and monopole antennas have figured prominently in wide bandwidth designs [51]. Expectedly the directive gain of such antennas is lower than what can be achieved by using an array.

The design of arrays comprising small number of elements requires a different approach as compared to the large arrays (so called infinite arrays). Antenna array design with large number of elements wherein the total number of elements can range anywhere from 100-10000 and higher involves a good choice of the individual element and then proceeds to an infinite array based simulation. An example of such large arrays is the Cobra Dane phased array system located in Alaska shown in Fig. 5.1. This system was developed for tracking the threat of an InterContinental Ballistic Missile (ICBM) attack on the United States.

Fig. 5. 1. The Cobra Dane phased array system a) and the array face b) [52].

In this approach, the individual element is considered to be part of an infinitely large array. The Floquet theory of periodicity is invoked and the relevant array parameters such as impedance bandwidth, pattern gain etc. are derived. The mutual coupling among individual elements is taken into account through this approach. An important characteristic of such arrays is that the edge elements are far smaller in number than the number of elements they surround. As a result, the accuracy of analysis using the infinite

array approach, for finite large size arrays increases with the number of elements. One can expect that the accuracy for a 5000 element array would be higher than one for a 100 element array. This approach is widely used and is well documented [53], [54].

The arrays of smaller sizes such as 2x1, 4x1, 2x2, 4x2, and 4x4 present an interesting set of challenges. In fact, for these arrays, the edge elements outnumber those bounded by them (in planar arrays 2x2 is an exception in that all elements are indeed edge elements!). Thus, these edge elements play a significant role in the overall performance. An infinite array simulation cannot be expected to accurately represent the performance of such small arrays. Instead, a finite array based analysis can be employed as suggested in [54]-[59]. In [60] - [67] , various approaches for the modular design of arrays are suggested. These approaches however are still oriented towards large size finite arrays.

The contribution of this thesis is to investigate the distributed impedance matching approach in the design of modular arrays. In doing so, the canonic planar resonant dipole is used to design the square unit cell (planar dipole over ground plane) such that, the 2x1, 2x2 and 4x1 arrays attain a VSWR of at least 2:1 over a bandwidth of at least 2:1, and stable gain (directive gain variation ≤ 3dB) over the entire band. The bandwidth definition used is shown below,

$$B = \frac{f_U}{f_L} \tag{5.1}$$

where, f_U and f_L represent the upper and lower frequencies which satisfy the S_{11} < -10 dB criterion. Furthermore, gain behavior at the lower frequencies in the band is of interest and it will be compared to the prediction by the array area rule [68]. It is the attempt of this thesis to show that through careful design we can exploit mutual coupling between

the unit cells to enhance the impedance bandwidth and provide for a stable broadside gain. The modular design approach is an attractive one for the following reasons:

- It is easy to build arrays of a specific configuration, once the individual radiator has been optimized.
- Individual elements in the array can be easily replaced if a problem develops in them.
- Since the individual radiator satisfies multiple array configurations, it allows for flexibility in the deployment of different arrays without loss of performance

The present modular approach may be used for low-cost larger-volume small broadside array design. The effect of scanning on such arrays has not been investigated.

5.1 Unit Cell Geometry

The unit cell serves as the basic building block for all the arrays and is shown in Fig. 5.2. It comprises of a resonant dipole of total length *2L*, and width *W* placed over a finite ground plane of dimensions $S_x \times S_y$ at a height *h*. The x-axis is along the horizontal in the Fig. 5.2. A wide blade dipole is chosen since it is easier to impedance match to such dipoles (thick dipoles if considering cylindrical) [69], [70]. If needed a conical impedance matching structure could be incorporated within the dipole, providing a smoother transition from the feed to the wing of the blade dipole. However, this unit cell does not have such a structure and therefore makes it easier to build. The blade dipole as well as ground plane need the mechanical support. For this reason, two substrates are provided for the dipole element and the ground plane respectively. In addition, 4 supporting posts are located at the corners of the unit cell in between the dipole and the ground plane.

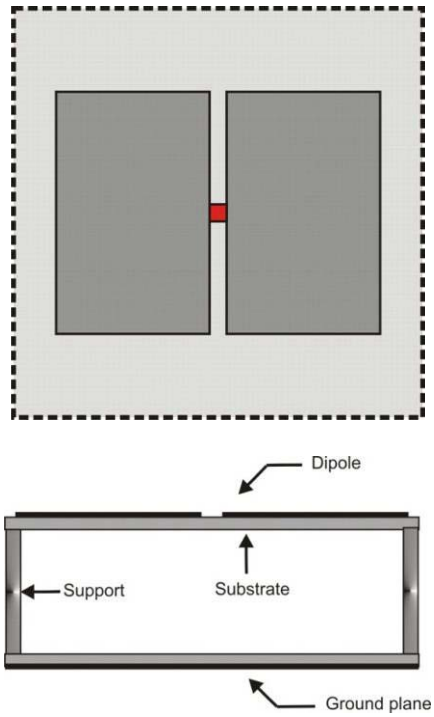

Fig. 5. 2. The unit cell geometry in plan and elevation. The feed is shown in red, and the ground plane is indicated with the dotted outline in the plan view.

5.2 Analysis for 2x1 array active impedance with power combiner

As stated previously this thesis suggests to build modular arrays of different configurations starting with the simplest 2x1 array to the 4x4 array. However, even the simplest 2x1 array consists of unit cell, the connecting RF cables (coaxial) and a 2 way power combiner/divider. The goal is to at least achieve a bandwidth of 2:1 with a VSWR of 2:1 measured at the input to the power combiner. This implies that the active array impedance and hence the active array reflection coefficient are well matched to the source impedance, typically 50Ω.

The active array impedance/reflection coefficient is defined as the impedance/reflection coefficient measured when all the elements of the array are excited, and thus includes the effects of mutual coupling. The 2x1 array is shown in Fig. 5.3, along with the port

numbering scheme. The antennas are excited uniformly and are not intended to have scanning capability.

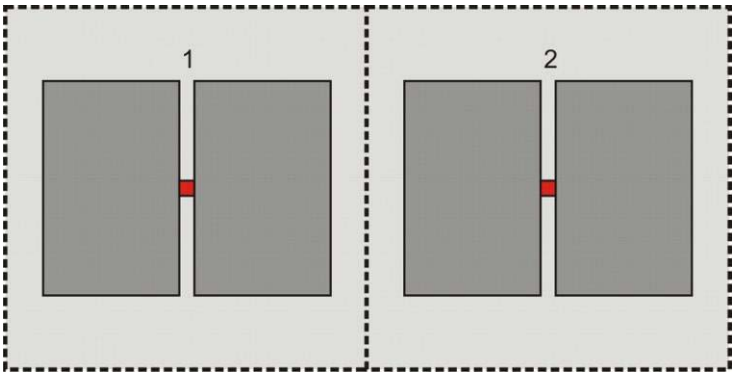

Fig. 5. 3. The 2x1 array of planar dipoles located over a ground plane. The feed region is shown as the square in between the dipole wings.

5.2.1 Active Scattering Parameters

The array reflection coefficient behavior can be determined by firstly calculating the active scattering parameters (S-parameters) whereby all the array elements are radiating and as mentioned before are fed uniformly with the same amount of power. Thus for the 2x1 configuration as shown in Fig. 5.3, the S-parameter equations can be written as,

$$\begin{aligned} V_1^- &= S_{11}V_1^+ + S_{12}V_2^+ \\ V_2^- &= S_{21}V_1^+ + S_{22}V_2^+ \end{aligned} \tag{5.2}$$

V_1^+, V_2^+ are the forward traveling voltage waves, and V_1^-, V_2^- are the reflected voltage waves at the port 1 and port 2 respectively. Note that S-parameters indicated in Eq. (5.2) are derived under standard conditions by terminating all ports except the port under consideration into 50 ohms. Since both elements are fed uniformly, we can assume $V_1^+ = V_2^+$. Thus the pair of equations in Eq. (5.2) can be reduced to

$$\begin{aligned} S_{11}^{active} &= V_1^- / V_1^+ = S_{11} + S_{12} \\ S_{22}^{active} &= V_2^- / V_1^+ = S_{21} + S_{22} \end{aligned} \tag{5.3}$$

This approach can be extended in a similar way to obtain the active reflection scattering parameters for larger array, i.e. the 2x2, 4x1, 4x2, 4x4 arrays and so on.

5.2.2 Model for Power Combiner with Cables

Arrays inherently require a power combining/dividing network to function. Typically such power combining networks are based on the common Wilkinson power divider [72]. However, since the antenna impedance is frequency dependant, we expect to see impedances at the output ports of the Wilkinson that are not exactly 50Ω. Therefore, we have to optimize the array performance by including the impedance transformation through the power combiner/divider. Additionally, there are cables connecting the array feed to the power divider and hence the active array feed point impedance is transformed over the length of the cable.

The expectation is that for a well matched array, the active impedances will remain close to 50Ω and therefore the array performance will not degrade after the power combiner. Nevertheless, we carry out the analysis to confirm this aspect of the design. The analysis is performed for the 2x1 array configuration only.

Consider the active impedance parameters for each array element within the 2x1 array to be defined as

$$Z_{11}^{active} = Z_0\left(\frac{1+S_{11}^{active}}{1-S_{11}^{active}}\right)$$
$$Z_{22}^{active} = Z_0\left(\frac{1+S_{22}^{active}}{1-S_{22}^{active}}\right) \quad (5.4)$$

The characteristic impedance Z_0 is 50Ω and the coaxial cables of length L are connected to the elements, the transformed input impedance is given by

$$Z_{11\_t}^{active} = Z_0\left(\frac{Z_{11}^{active} + jZ_0\tan(\beta L)}{Z_0 + jZ_{11}^{active}\tan(\beta L)}\right)$$
$$Z_{22\_t}^{active} = Z_0\left(\frac{Z_{22}^{active} + jZ_0\tan(\beta L)}{Z_0 + jZ_{22}^{active}\tan(\beta L)}\right). \quad (5.5)$$

The losses in the coaxial cable are ignored and the propagation constant is defined as $\beta = 2\pi/\lambda$. These transformed active array impedances appear at the output ports of the 2-way Wilkinson power divider. An equivalent circuit for the 2-way Wilkinson power combiner is shown in Fig. 5.4. The voltages at specific nodes have been identified together with currents through the different branches. The source voltage and current phasors are V and I respectively. The combiner has load impedances $Z_1 = Z_{11\_t}^{active}$ and $Z_2 = Z_{22\_t}^{active}$. The resistor R_d connected in shunt ensures that any reflected power due to imbalances in the two arms is dissipated before reaching the input. The value of this resistor is set to $2Z_0$ [72].

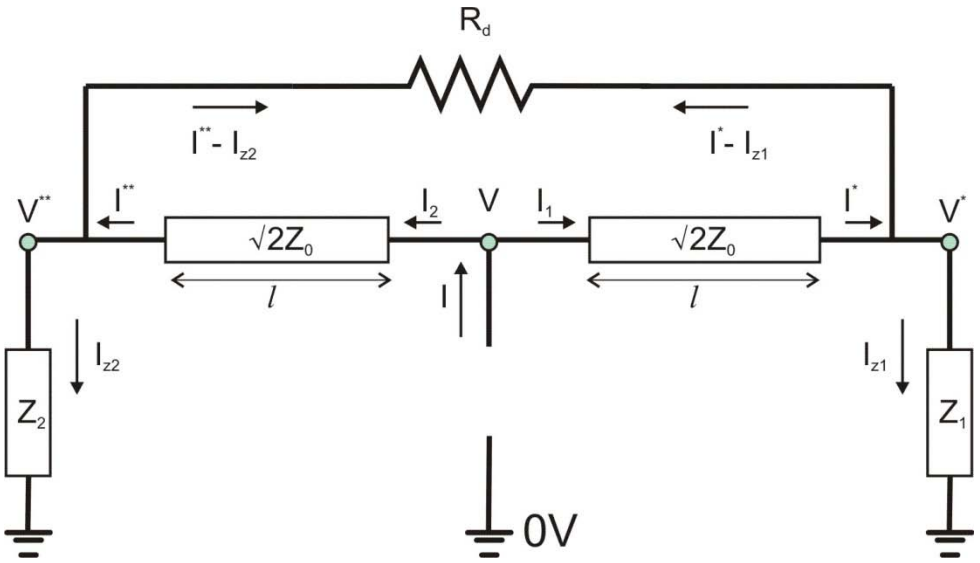

Fig. 5. 4. An equivalent circuit for the 2-way Wilkinson power combiner.

The two transmission lines connected between the input and output ports are identical and have a characteristic impedance of $Z_{TL}=\sqrt{2}Z_0$. They have a length l << L. The active input impedance can then be defined as,

$$Z_{in}^{active} = \frac{V}{I} = \frac{V}{I_1 + I_2} \tag{5.6}$$

From Fig. 5. 4, we can write down the following three equations,

$$\begin{aligned} &I = I_1 + I_2 \\ &V^{**} = V^{*} - \left(I^{*} - I_{z1}\right)R_d \\ &I^{*} - I_{z1} = I_{z2} - I^{**}. \end{aligned} \tag{5.7}$$

Here, $I_{z1} = V^{*}/Z_1$, and $I_{z2} = V^{**}/Z_2$ are the currents flowing through the two loads at the output ports respectively. Using the ABCD matrix approach we can solve for V and I_1 as follows

$$\begin{bmatrix} V \\ I_1 \end{bmatrix} = \begin{bmatrix} A & B \\ C & D \end{bmatrix} \begin{bmatrix} V^{*} \\ I^{*} \end{bmatrix} = \begin{bmatrix} V^{*}\cos(\beta l) + jI^{*}Z_{TL}\sin(\beta l) \\ jY_{TL}V^{*}\cos(\beta l) + I^{*}\cos(\beta l) \end{bmatrix}. \tag{5.8}$$

Similarly we can also write the equations for V and I_2 as follows

$$\begin{bmatrix} V \\ I_2 \end{bmatrix} = \begin{bmatrix} A & B \\ C & D \end{bmatrix} \begin{bmatrix} V^{**} \\ I^{**} \end{bmatrix} = \begin{bmatrix} V^{**}\cos(\beta l) + jI^{**}Z_{TL}\sin(\beta l) \\ jY_{TL}V^{**}\cos(\beta l) + I^{**}\cos(\beta l) \end{bmatrix}. \tag{5.9}$$

By using the fact that since $l = \lambda/4$, $\beta l = \pi/2$, from Eqs. (5.8) and (5.9) we get

$$\begin{aligned} &V = jZ_{TL}I^{*} = jZ_{TL}I^{**} \\ &I_1 = jY_{TL}V^{*} \\ &I_2 = jY_{TL}V^{**} \end{aligned} \tag{5.10}$$

Assuming that the excitation is 1V, we can express the branch currents and node voltages as,

$$I^{*} = I^{**} = \frac{-j}{Z_{TL}}$$
$$V^{*} = \frac{-jI_1}{Y_{TL}} \tag{5.11}$$
$$V^{**} = \frac{-jI_2}{Y_{TL}}$$

Thus using Eq. (5.7) and (5.11) we get

$$\frac{1}{Z_{TL}} - \frac{I_1}{Z_1 Y_{TL}} = \frac{I_2}{Y_{TL} Z_2} - \frac{1}{Z_{TL}}$$
$$\frac{I_1}{Y_{TL}} - \frac{R}{Z_{TL}} - \frac{RI_1}{Y_{TL} Z_1} = \frac{I_2}{Y_{TL}} \tag{5.12}$$

Using the definition for the input impedance expressed in Eq. (5.6)

$$Z_{in}^{active} = \frac{1}{I_2 + i_1} = \frac{Z_{TL}(Z_1 + R + Z_2)}{Y_{TL} Z_1 (2Z_2 + R) + Y_{TL} Z_2 (2Z_1 + R)} \tag{5.13}$$

In addition, by using the fact that $Z_1 = Z_{11\_t}^{active}$ as well as $Z_2 = Z_{22\_t}^{active}$ we arrive at the active impedance at the input to the power combiner as

$$Z_{in}^{active} = \frac{2Z_0^{\,2}\left(Z_{11\_t}^{active} + R_d + Z_{22\_t}^{active}\right)}{\left(Z_{11\_t}^{active} R_d + 4Z_{11\_t}^{active} Z_{22\_t}^{active} + Z_{22\_t}^{active} R_d\right)}. \tag{5.14}$$

Under matched conditions $Z_{11\_t}^{active} = Z_{22\_t}^{active} = 50\Omega$, we get the input impedance $Z_{in}^{active} = 50\Omega$. Using the active array impedance at the input to the power combiner we calculate the input reflection coefficient for the 2x1 array as

$$\Gamma_{in}^{active} = \left(\frac{Z_{in}^{active} - Z_0}{Z_{in}^{active} + Z_0}\right). \tag{5.15}$$

We can extend this to the 2x2, and 4x1 arrays, which use a 4 - way power divider, by translating the active impedances at the output ports of the power divider twice by using Eqs. (5.14) and obtain the input reflection coefficient as in (5.15).

5.3 Peak Broadside Gain

Consider a large array located on the *xy*-plane as shown in Fig. 5.5.

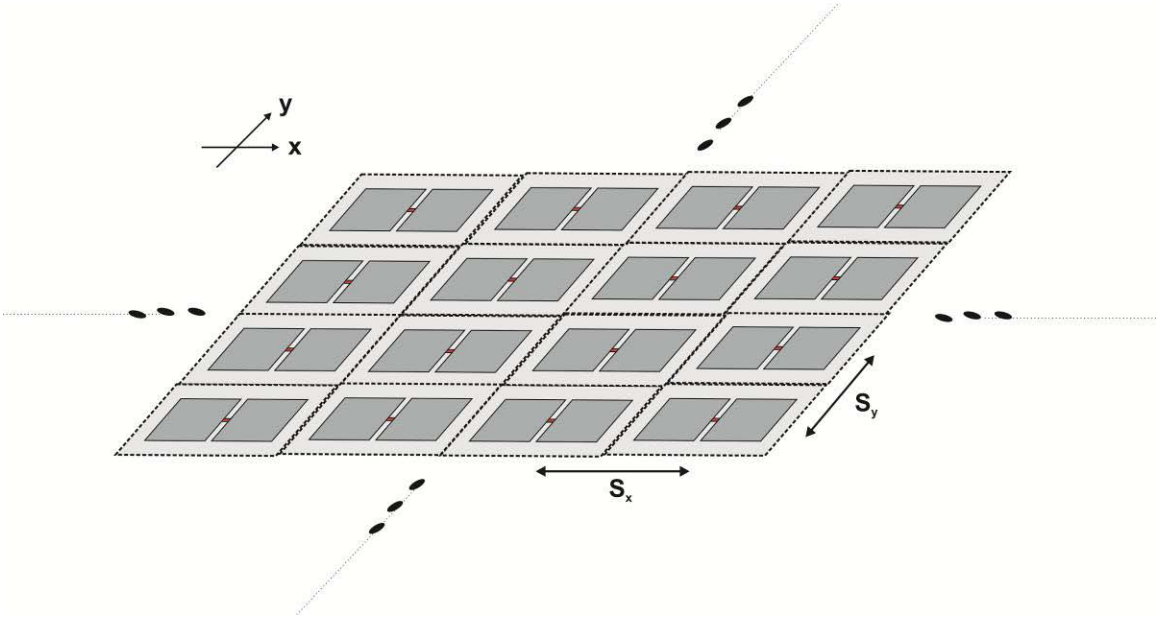

Fig. 5. 5. A large uniformly excited array located on the *xy* – plane. While the individual radiator in this figure is a dipole, the actual element itself is irrelevant since the array area rule is purely a function of the physical area and the wavelength.

Under the uniformly excited case, and possesses no grating lobes, the peak directive gain is given in [53], [68] , and [71] as follows:

$$G_d = \frac{4\pi NA}{\lambda^2} = \frac{4\pi N_x N_y S_x S_y}{\lambda^2} \tag{5.16}$$

where G_d is the peak directive gain of the array, N is the total no. of elements in the array (with N_x elements along the x direction, N_y elements along the y direction), A represents the array area, S_x and S_y are the inter element separation within the array. The directive gain does not take into account the mismatch loss and the ohmic losses. For small arrays such as the ones being considered in this paper the peak broadside directive gain will be

compared against the theoretical limit given in Eq. (5.16). Of particular interest is the performance at the lower frequencies within the band of interest.

Chapter 6. Full wave modeling, simulation and experimental results

In this chapter, the optimization based modular array design will be explained. This design approach will attempt to satisfy two criterions namely:

i. The $\left|\Gamma_{in}^{active}\right| \leq$ -10 dB over at least a 2:1 bandwidth

ii. A maximum variation in directive gain of 3 dB over the 2:1 bandwidth

The optimization procedure will be based on exploiting distributed reactance's within the structure. The simulation results for the active reflection coefficient at the input to the power combiner and the directive gain will be presented for three modular array configurations; the 2x1, 4x1 and the 2x2 arrays. Additionally, the directive gain results from the optimized modular arrays will be compared with the prediction from the array are rule. The optimized unit cell performance in an infinite array scenario will be provided in the form of the active reflection coefficient and discussed. The construction of the experimental arrays will be described and followed by a discussion on the results for their active reflection coefficient.

6.1 Optimization procedure and full wave modeling

The design of modular arrays as described in chapter 5 is based on a simple premise: a single optimized unit cell should be able to achieve the two criterions mentioned earlier. To investigate whether this is indeed achievable, we adopt an optimization procedure that uses the variables within the unit cell itself. This is the distributed approach to impedance matching. In fact, apart from impedance matching we will also attempt to achieve gain-

bandwidth, wherein the gain refers to the directive gain of the array. Consider the Fig. 6.1 where we have identified 6 variables which could be potentially used for optimization. These are,

- Length L and width W of the unit cell – which becomes the dimensions of the ground plane
- Length L_D and width W_D of the dipole
- Feed spacing s
- Height above the ground plane h

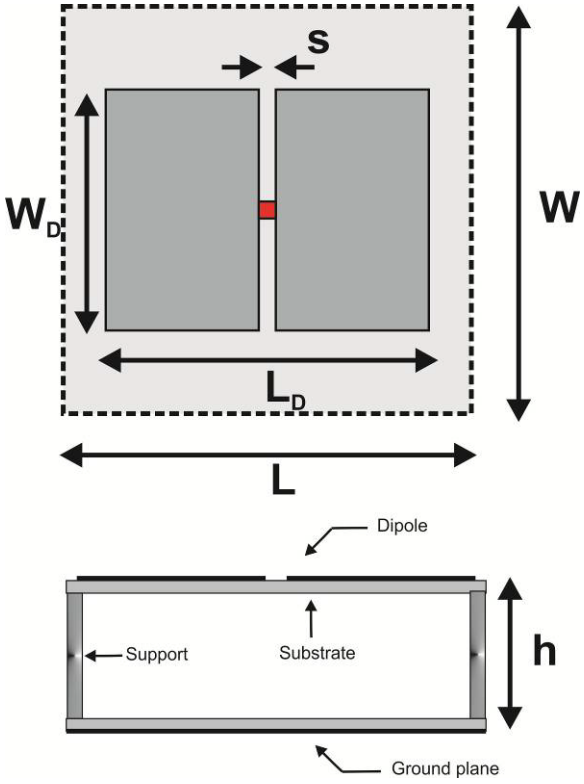

Fig. 6. 1. Optimization variables for the unit cell radiator.

By modeling the three array configurations as shown in Fig. 6.2 and optimizing each of them subject to the variables, the optimum unit cell solution should be found.

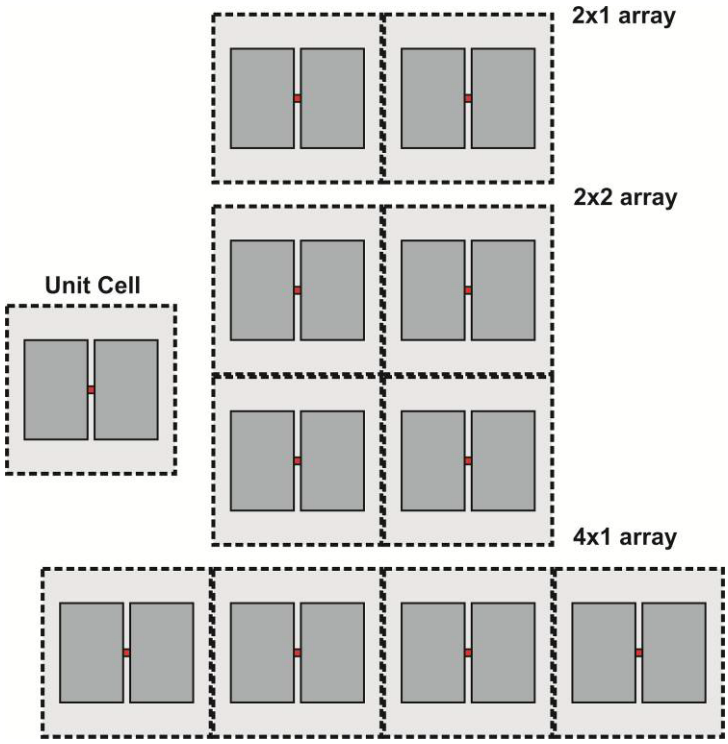

Fig. 6. 2. Unit cell and the three array configurations to be optimized.

6.2 Simulation setup

Three configurations namely, the 2x1, 2x2 and the 4x1 arrays were chosen for simulation and experimental investigations. Ansys/Ansoft HFSS ver.12.0 was used for modeling and simulation of these arrays.. All the metal portions were assigned a boundary condition of Perfect electric conductor (PEC). A lossless substrate of relative permittivity (ε_r) 2.9 is provided for both the dipole and the ground plane. The feed was modeled as a lumped port with impedance 50Ω. It is expected that for a first pass design we will be using a coaxial cable to connect the feed to the power combiner and not use a balun transformer. The dipole is rarely used without a balun transformer. However, to make it easier to design, implement as well as from an investigative point of view it was decided that the balun transformer would be excluded in this initial design. For similar reasons a conical impedance matching section between the feed point and the dipole wings has been

excluded. In fact during simulations it was noted that the extra section did not change the impedance behavior significantly

The computational domain was surrounded with a perfectly matched layer (PML) in order to minimize reflections and ensure good solution accuracy. A discrete frequency sweep was chosen from 0.6 – 1.8 GHz. Our design frequency range is from 0.8 GHz to 1.6 GHz. All the elements in the arrays are uniformly excited with 1 Watt of power. The full wave modeling yielded a final mesh size of 30000 tetrahedra with good solution convergence. The optimized unit cell dimensions are shown in Fig. 6.3.

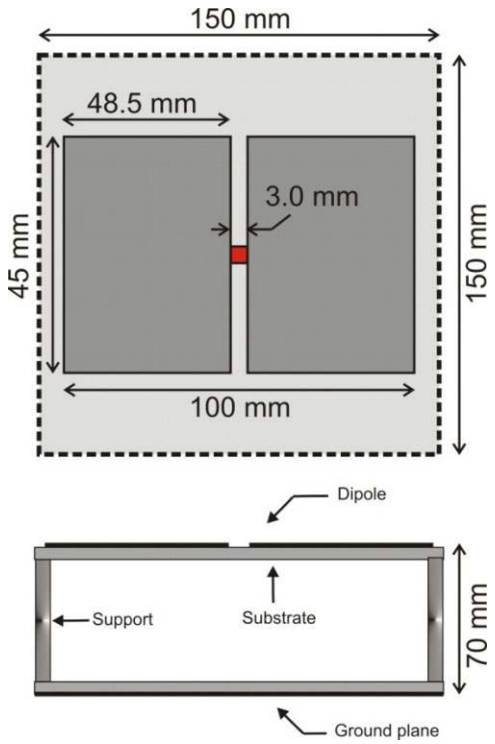

Fig. 6. 3. Optimized unit cell dimensions obtained through full-wave modeling in Ansoft HFSS ver 12.0.

6.3 Input reflection coefficient – Unit cell, 2x1, 4x1 and 2x2 arrays

The optimized unit cell radiator is indeed wideband and is well matched from 0.9 GHz – 1.8 GHz with a well defined resonance at 1 GHz. This is shown in Fig. 6.4. The

simulation results, for the active input reflection coefficient for the different modular array configurations as calculated using Eq. (5.15) are shown in Fig. 6.5. The results for the active reflection coefficient suggest that the 2x1, 4x1, and the 2x2 arrays are well matched from 0.8 GHz to 1.6 GHz. All the three arrays show good impedance matching even above 1.6 GHz and upto 1.8GHz which would correspond to 2.25:1 impedance bandwidth as per the definition in Eq. (5.1). However, we would expect the broadside gain to drop drastically at the high frequency end, primarily due to the distance of separation from the ground plane.

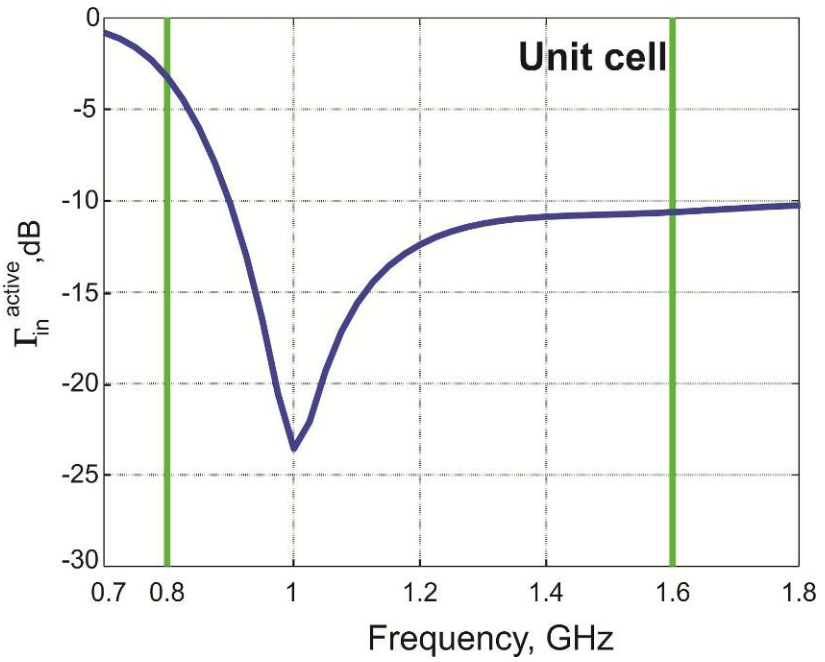

Fig. 6. 4. The input reflection coefficient for the optimized modular array unit cell. The solid green vertical lines indicate the bandwidth of interest.

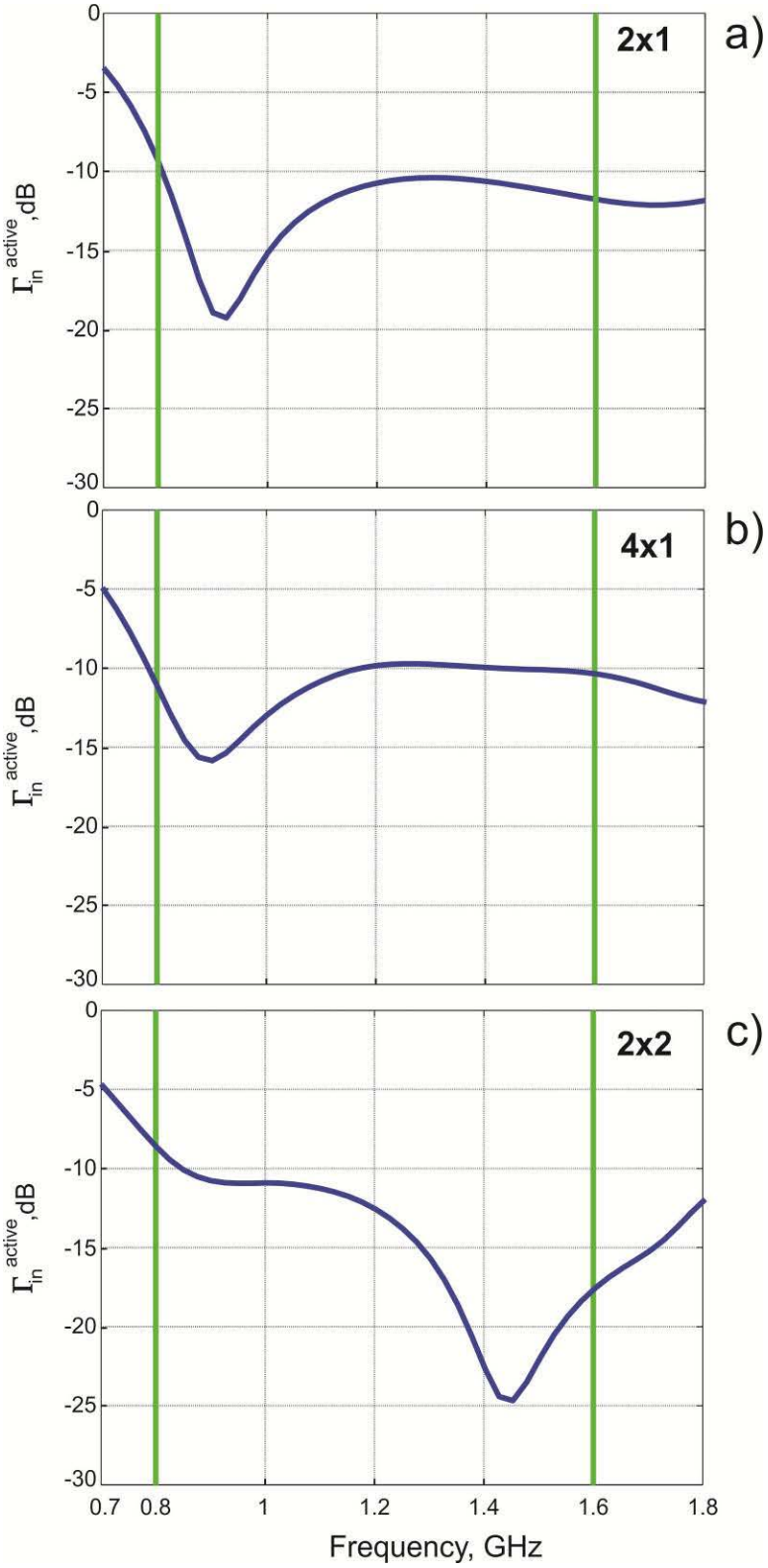

Fig. 6. 5. The active input reflection coefficient obtained from the simulation of 2x1, 4x1 and 2x2 arrays. The solid green vertical lines indicate the bandwidth of interest

6.4 Broadside gain as a function of frequency

Although the impedance bandwidth over the desired frequency band of 0.8GHz - 1.6GHz has been established, it is the peak directive gain at broadside (θ=0 deg., φ=0 deg.) which will be crucial in determining the overall gain as well as the usable gain-bandwidth of the arrays. In Fig. 6.6 the peak directive gain at broadside is plotted as a function of frequency. The dashed curves are the simulation results from the HFSS models. Clearly over the band of interest the gain achieved is significantly higher than that possible by a single dipole over a ground plane (maximum of 7.2 dB at 0.8GHz), which is the unit cell radiator. To understand the behavior of such modular arrays of small sizes, it is helpful to compare the performance against the well established theoretical estimate for the peak directive array gain as expressed in Eq. (5.16). For all three arrays considered, this theoretical estimate is plotted as a function of frequency in Fig. 6.6(a) - (c). Clearly, the peak gain is higher for the three arrays as compared to the theoretical estimate, at the lower frequencies. In the case of the 2x1 array, the gain is relatively stable over the band of interest. However, beyond 1 GHz, the gain is lower than that predicted by Eq. (5.16). The 2x2 array follows the theoretical prediction remarkably well over the range 1 GHz - 1.4 GHz, before dropping off to 10dB at 1.8 GHz. In fact the behavior of the 2x2 array gain from simulation can be traced to the 4x1 case. Similar to the other cases the theoretical estimate is lesser at the low frequencies. However, at frequencies between 1 - 1.2 GHz. the array gain is approximately equal to the theoretical value. From 1.2 - 1.8GHz, there is a gradual drop in the gain value. Beyond 1.8 GHz, a broadside gain null would be present. The frequency of occurrence of this minimum can be modified by adjusting the height of the dipole over the ground plane.

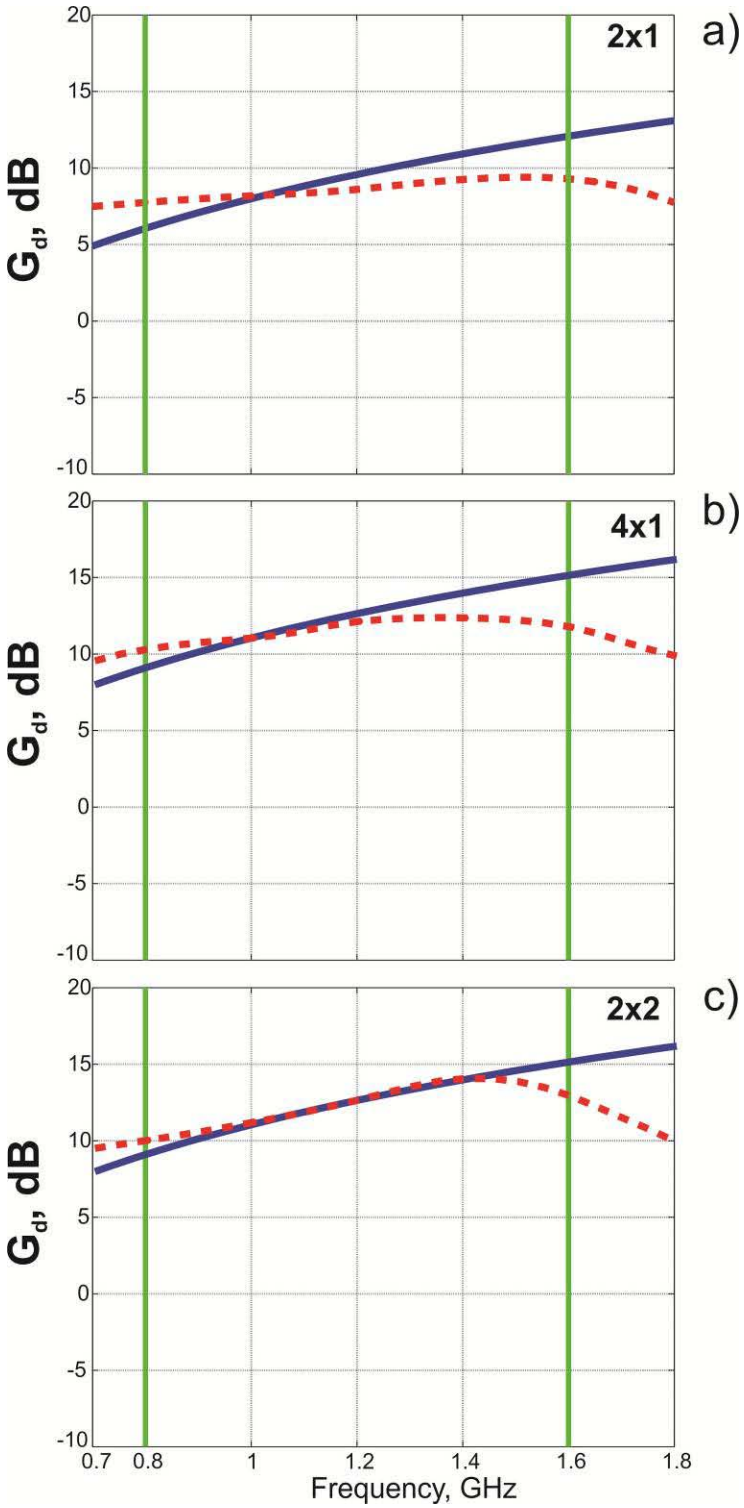

Fig. 6. 6. The peak directive gain at broadside plotted as a function of frequency for the a) 2x1 array, b) 4x1 array and c) 2x2 arrays. The theoretical estimate (solid curve) is compared with the simulation results (dotted red curve) over the bandwidth of interest (solid green vertical lines).

A larger height will reduce this minimum gain frequency while simultaneously improving the impedance matching performance. Depending on the design requirements, this parameter represents an important tradeoff between array gain and bandwidth.

6.5 Optimized unit cell in an infinite array

It is worth investigating the performance of the optimized unit cell in an infinite array environment. The design of small modular arrays cannot be accomplished by using the Floquet theory based infinite array modeling and this experiment will suitably confirm our hypothesis. In Fig. 6.7 we plot the active reflection coefficient of the infinite array, which uses the optimized radiator of the modular array as the active element. Clearly, the impedance bandwidth is significantly degraded. Instead of at least an octave bandwidth design we now have a narrowband (relative) array with less than 25% fractional bandwidth.

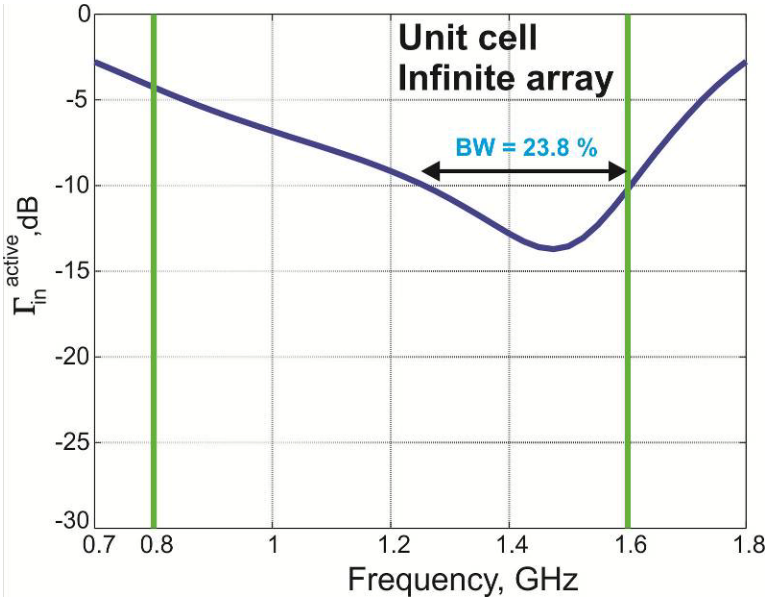

Fig. 6. 7. The active reflection coefficient for an infinite array using the optimized modular array unit cell as the active element. The solid green vertical lines indicate the bandwidth of interest.

6.6 Experimental Unit cell, 2x1, 4x1 and 2x2 arrays

The square unit cell radiator, used to build the 2x1, 2x2 and the 4x1 arrays, comprised of a 150 mm x 150 mm ground plane and a 100mm long dipole (inclusive of feed gap) positioned 70 mm over it. Since the planar dipoles are to be positioned at a fixed distance above the ground plane, we had to provide for a mechanical support to both the dipole and the ground plane. For this purpose we have chosen Polymethyl methacrylate (PMMA), also commonly known as Plexiglass, to be the substrate material. Plexiglass has a relative permittivity of 3.0, is low loss and easily available. The Plexiglass substrate for the dipole and the ground plane has a thickness of 5mm (approximately). Supporting posts as shown in Fig. 6.1 made of Delrin® are provided at the four corners of the unit cell. Two threaded holes have been provided in orthogonal directions on each supporting post so as to facilitate array expansion in either linear or planar configurations. For the planar dipole and the ground plane, Copper foils of 10 mil thickness were glued onto the substrates. A hole was drilled in the center of both substrates to allow for a coaxial cable to be inserted and soldered to the blade dipoles. As noted earlier in this chapter, no balun transformer has been used for this initial design. However, subsequent designs would use a balun transformer. A 2-way and 4-way power divider from Mini-circuits was used as the power combiner of the 2x1, 4x1 and 2x2 arrays which are shown in Fig. 6.8..

The active reflection coefficient of the unit cell is plotted in Fig. 6.9. The unit cell is broadband and possesses greater than 2:1 impedance bandwidth. The well defined resonance close to 1 GHz, as predicted from simulation and shown in Fig. 6.5, is also observed during measurements. Significantly, the unit cell displays a much better impedance match over the frequency band of interest (0.8 GHz- 1.6GHz) and beyond.

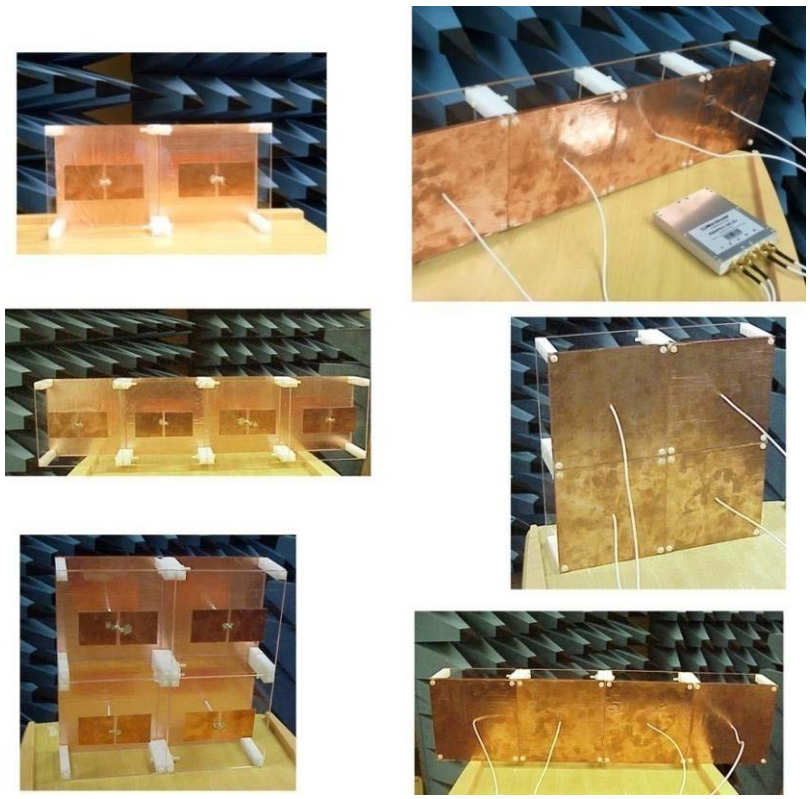

Fig. 6. 8. The three experimental modular arrays.

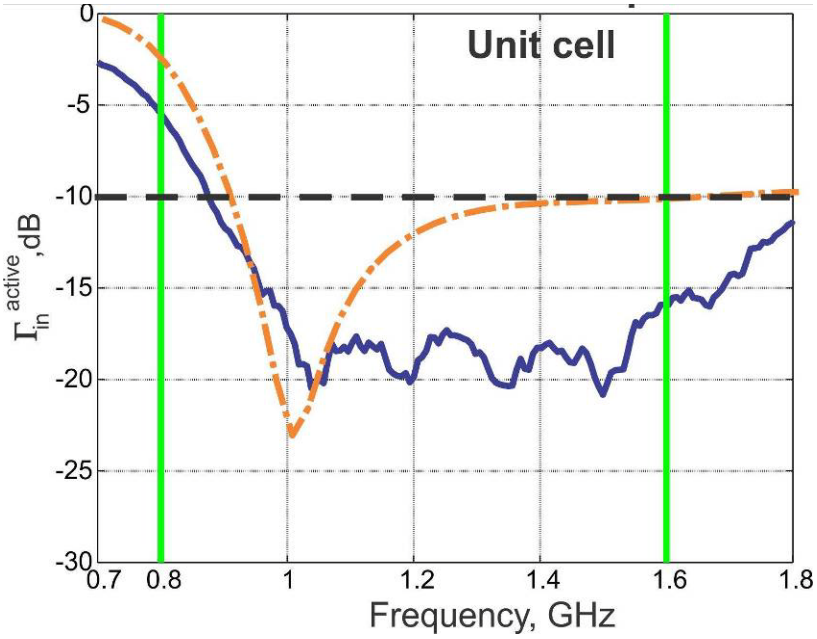

Fig. 6. 9. The input reflection coefficient for the experimental unit cell radiator. The solid green vertical lines indicate the bandwidth of interest.

There could be two reasons for this:

i. The losses within the structure at such high frequencies which includes Copper foils, Plexiglass substrates and 4 Delrin® posts could be significant enough to improve the reflection coefficient.

ii. The absence of a balun implies that there will be a non-zero current flowing on the outer conductor of the coaxial cable. Given the length of this cable is larger than the smallest wavelength in the band of interest, there could be a traveling wave leaking energy via radiation and hence improving the reflection characteristics. If true, then the radiation pattern would be severely degraded and an adverse impact in the form of a larger back lobe will result.

The effect of the cables and connectors originating from the network analyzer has been calibrated out.

In Fig. 6.10 the active input reflection coefficient measurements for the 2x1, 4x1 and 2x2 arrays is shown. All three arrays satisfy the $\left|\Gamma_{in}^{active}\right| \leq$ -10 dB requirement. However, unlike the simulation results shown in Fig. 6.5, there exist multiple resonances in the reflection curve. A possible reason for this behavior could be the power combiner/divider. Further investigation is required to confirm this fact. In Fig. 6.11, radiation pattern in the H-plane, at 1GHz, has been plotted for one of the modular arrays, the 2x2 array. The solid curve is the result from the Ansoft HFSS simulation, while the dashed curve is the measurement result from the experimental array. Overall, there is good agreement between simulation and measurement. We note the presence of a dip at boresight (0 degrees) as well as a slightly higher backlobe level (180 degrees). The gain measurements were performed outdoors using standard Horn antennas at the receiving end.

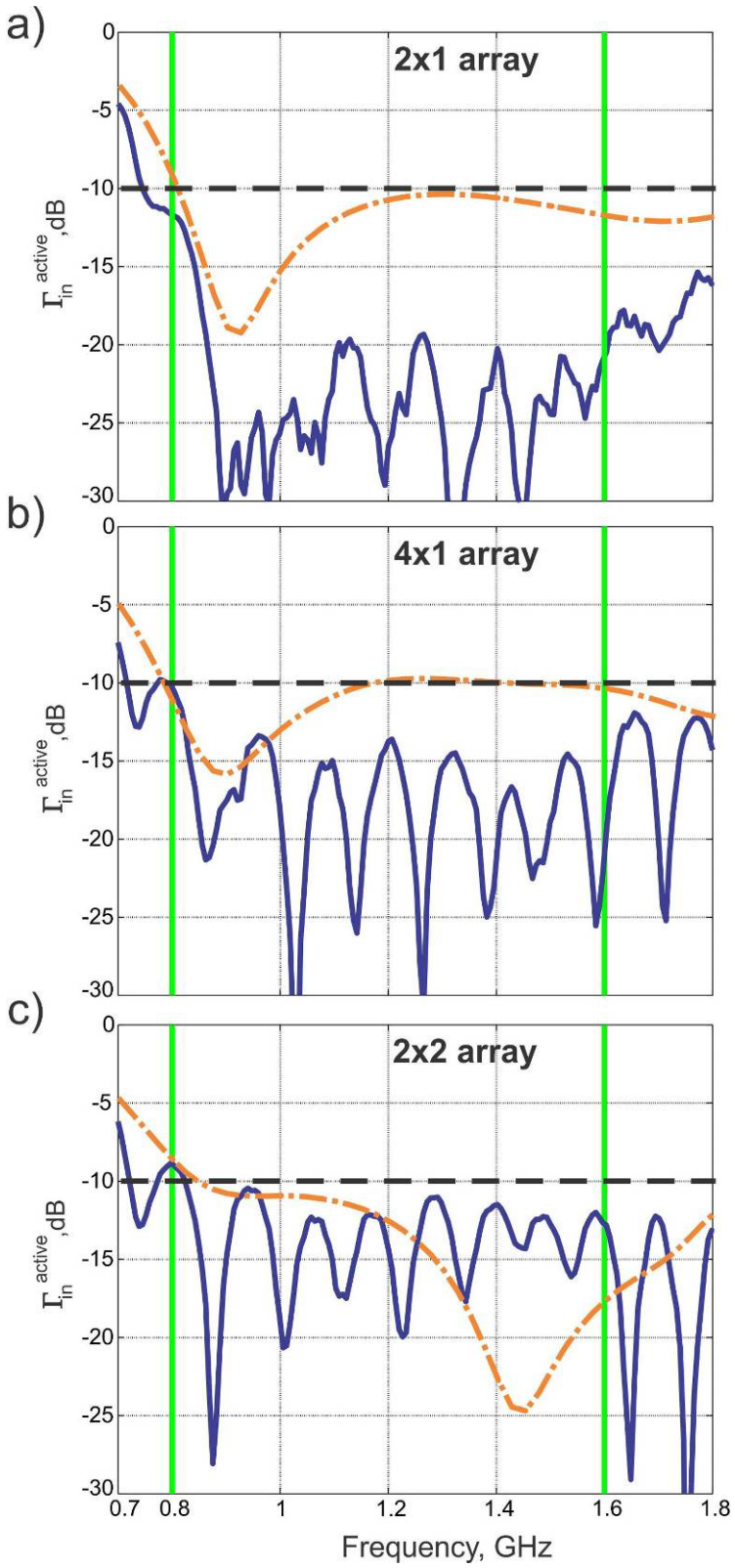

Fig. 6. 10. The active input reflection coefficient obtained from the experimental 2x1, 4x1 and 2x2 arrays. The solid green vertical lines indicate the bandwidth of interest.

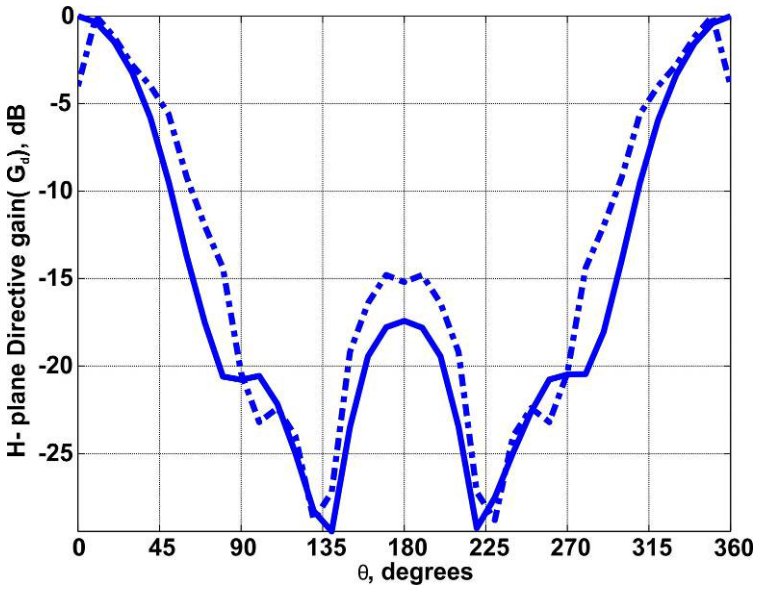

Fig. 6. 11. H-plane radiation pattern for 2 x 2 modular array at 1 GHz. The solid blue curve is the simulation result from HFSS, while the dashed blue curve is the experimental result.

Chapter 7. Conclusion

This thesis addressed the topic of impedance matching of antenna radiators and in particular the problem of broadband impedance matching. The two approaches to impedance matching were identified, namely the distributed impedance matching techniques and the lumped element approach. The work described in this thesis has made original contributions to both approaches in the form of:

I. Wideband impedance matching of non-resonant dipole/monopole antennas using the lumped element techniques

II. Modular array design of small arrays of resonant dipoles using the distributed impedance matching techniques.

The specific contributions to each will now be outlined in the next two sections.

7.1 Thesis contributions using lumped element techniques

1) The thesis proposes a new technique for impedance matching of short non-resonant dipole-like antennas. Instead of constructing network topology from the particular antenna impedance data, we propose to use a simple network of one *fixed* topology for all dipole-like antennas. This network is the narrowband L-section cascaded with the high-pass T-section.
2) Matching with the network proposed in this thesis results in a performance close to the theoretical limit on impedance matching confirmed by Bode-Fano theory.
3) Matching with the network proposed in this thesis results in a near identical performance compared to advanced matching techniques such as the Carlin's

equalizer. More importantly, the network proposed in this thesis is simpler to design and would occupy lesser area on a PCB since there are no transformers.

4) An upper bound on the maximum achievable theoretical transducer gain as a function of dipole/monopole geometry, center frequency and bandwidth sought has been derived.
5) Experimentally validated the theoretical and numerical simulation predictions for a blade monopole on a 1 m x 1 m and a 75 cm x 75 cm ground plane.
6) A direct global numerical search routine for finding the optimum reflective equalizer components written in MATLAB ©.

7.2 Thesis contributions using distributed matching techniques

1) This thesis introduces the concept of modular array design using the canonic planar resonant dipole. The unique aspect of this approach is we seek a single optimum unit cell radiator which will satisfy different array configurations and yet maintain good impedance bandwidth as well as possess stable gain variation over the bandwidth of interest.
2) We establish the need to eschew infinite array simulation models in the design of modular arrays, by showing that the identical optimized unit cell for a 2x1, 4x1 and 2x2 array with at least an octave bandwidth, yields less than 25 % fractional bandwidth in an infinite array.
3) Using a optimization approach and full wave modeling technique, we have found a solution for the unit cell radiator that satisfies the VSWR of 2:1 over a bandwidth of 2:1 and upto 3dB local directive gain variation in the band of interest, for three array configurations 2x1, 4x1, and 2x2 arrays.

4) Experimentally verified the impedance bandwidth performance of the three modular array configurations mentioned in 2, and 3.

7.3 Future research directions

The scope for further research in each area will be now outlined

Lumped element techniques for wideband matching of non-resonant antenna radiators –

1) Investigate the phase characteristics of the proposed 5 element equalizer
2) Digital tuning could pave the way for adaptive reflective equalizers. Dynamic equalization would allow for antenna response reconfigurability.
3) Optimize the noise performance of such networks

Distributed matching techniques for Modular arrays –

1) Gain measurements have to be done to confirm the broadside array gain behavior.
2) Extend the search for the optimum unit cell radiator to other configurations such as 3x1, 4x2, and 4x4 arrays.
3) Related to 2, answer the fundamental question of whether a solution exists for larger configurations and what is the limit on size beyond which no solution exists.
4) Arrays of small sizes such as the ones proposed in this thesis suffer from the finite ground plane size edge effects. Novel ground plane shaping strategies could be investigated to negate such effects.
5) Explore modular array design for different unit cell radiators such as the microstrip patches.

Appendix A – Impedance Matching of Small Dipole and Loop Antennas for Wideband RFID Operation

I. Introduction

The shrinking size of radio equipment coupled with increasingly complex signal structures has resulted in the need for reduction in antenna size and the demand for wider bandwidths. In RFID based systems, we typically encounter electrically small antennas. While the scope of RFID technology has been well defined in the realm of supply chain management, yet more novel applications are being researched in areas such as mobile healthcare services and surveillance [73], [74], near-field communication among wireless mobile devices [75], and distributed sensor networks[76], [77]. Several practical approaches are provided in [73], [78]-[80], for the design of RFID antennas while in [81] the efficiency of such small antennas is discussed. However, these designs provide fractional bandwidths of lesser than 20%.

To achieve wideband operation, impedance matching of the antenna to the source/load has to be done. Impedance matching techniques such as the standard L, T, and Π networks which comprise of either reactive lumped elements or sections of transmission lines using stubs, belong in the narrowband matching category [27],[28].

In this investigation we have attempted to do wideband impedance matching i.e., higher than 20% fractional bandwidth, of electrically small dipole, and loop antennas using lumped components. The method we have used bypasses both the pure analytical [16]-[19], and the RFT numerical approach [23]-[26], [82]-[84]. Instead, we introduce the equalizer topology upfront and subsequently employ a direct numerical optimization

technique to find the component values. In order to get an idea regarding the maximum achievable gain for the matching network the Bode-Fano criterion will be used and this analysis will be presented in section II. Section III describes the two equalizer circuits to be used for the dipole and the loop respectively. An upper bound on the system efficiency for will be discussed in Section IV. Section V will present the simulation results. Finally, section VI provides the conclusions.

II. Theoretical Limit On Wideband Impedance Matching Of Small Dipole And Loop

A. Antenna Impedance Model – Small Dipole, Small Circular Loop

The input impedance, of a small dipole, Z_{dp} can be expressed as $Z_{dp} = R_{dp} + jX_{dp}$ [32], where, the radiation resistance is given by

$$R_{dp} = 20\pi^2 \left(l_A/\lambda\right)^2 \forall \quad \lambda/50 \le l_A \le \lambda/10 \tag{1}$$

and, the input reactance

$$X_{dp} = -120\frac{\left[\ln\left(l_A/2a\right)-1\right]}{\tan\left(kl_A/2\right)} \; . \tag{2}$$

In (1), (2), l_A is the dipole length, *a,* is the dipole radius, and $k = 2\pi/\lambda$ is the wavenumber. The small dipole condition can be expressed in the frequency domain as $0.04 < f_c / f_{res} \le 0.2$, where, $f_{res} \equiv c_0/2l_A$ is the resonant frequency of a half wave resonant ideal dipole, c_0 is the speed of light and f_c is the center frequency. The input impedance is predominantly capacitive. In the case of a monopole over an infinite ground plane the impedance Z_{dp} is halved.

For the small circular loop, the impedance, Z_{lp} can be expressed as $Z_{lp} = R_{lp} + jX_{lp}$ [32], where, the loop radiation resistance can be expressed as,

$$R_{lp} = 20\pi^2 (C/\lambda)^4 \forall\ C < \lambda/10 \tag{3}$$

and the loop inductance is,

$$L = \mu_0 r[\ln(8r/b) - 2] \tag{4}$$

In (3), (4) r is the radius of the loop, b the radius of the conductor and $C = 2\pi r$, is the circumference of the loop. The internal reactance of the loop conductor has been ignored. The thickness of the conductor is chosen by using $\rho = 2\ln(2\pi r/b)$, such that $\rho < 9$ represents moderately thick loops [32]. Since we consider the small circular loop, in the frequency domain the condition to be met is, $f_c / f_{res} < 0.1$, where $f_{res} \equiv c_0 / C$, is the resonant frequency of the electrically large loop, and f_c is the center frequency. The input impedance for the small circular loop is predominantly inductive.

B. Wideband Impedance Matching - The Reflective Equalizer

The reactive matching network and the Thévenin equivalent circuit when viewed from the antenna is shown in Fig. A.1a and A.1b, respectively [23]. This network can be considered to be a reflective equalizer which always reflects a portion of the power back to the generator over the bandwidth of interest. The transducer gain is [23],

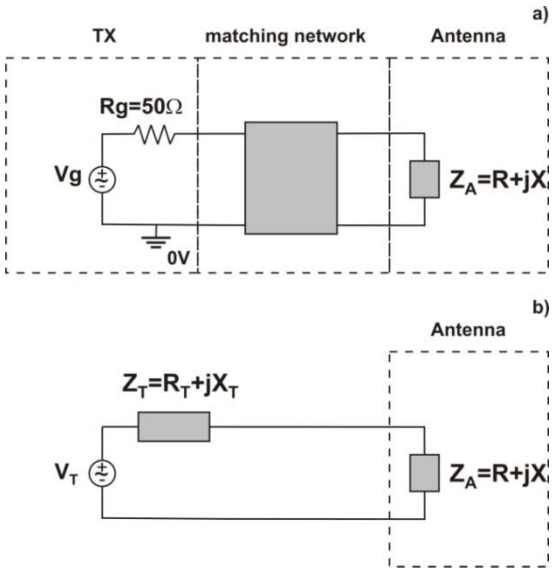

Fig. A. 1. Matching network: a) reactive matching network representation. b) Thévenin-equivalent circuit.

$$T(\omega^2)=\frac{4R_T(\omega)R(\omega)}{\left|Z_A(\omega)+Z_T(\omega)\right|^2}=1-\left|\Gamma(\omega)\right|^2. \tag{5}$$

The problem can therefore be summarized as one of maximizing the minimum gain over a specified wide bandwidth *B* [23], [26].

C. Bode-Fano Bandwidth Limit

We can approximate the antenna model for these two antennas as series RC and RL networks respectively. The Bode-Fano relations pertaining to the small dipole and the small loop in terms of the reflection coefficient $\left|\Gamma(\omega)\right|$ at the input to the matching network is expressed as [28],

$$\begin{aligned} &Small\ Dipole \Rightarrow \int_0^\infty \frac{1}{\omega^2}\ln\left[\frac{1}{\left|\Gamma(\omega)\right|}\right]d\omega < \pi RC \\ &Small\ Loop \ \Rightarrow \int_0^\infty \ln\left[\frac{1}{\left|\Gamma(\omega)\right|}\right]d\omega < \frac{\pi R}{L}. \end{aligned} \tag{6}$$

These integral relations will be solved over a rectangular band-pass frequency window of bandwidth *B* and centered at f_c. The transducer gain within this window is $T = T_0$ and $T = 0$ outside of it.

D. Arbitrary Fractional Bandwidth and Transducer Gain

The first case we will consider is the small dipole. To reference Fig. 1, Z_A=Z_{dp} is the load impedance under consideration. From (2), we extract the capacitance of the small dipole. Let us define, $z = kl_A/2$, which is restricted to $\pi/50 < z \le \pi/10$. Therefore, we can rewrite (2) as,

$$X_{dp} = -120\frac{\left[\ln\left(l_A/2a\right)-1\right]}{z}\ . \tag{7}$$

The capacitance, *C* is then found to be from (7),

$$C = \left(480\, f_{res}\left[\ln\left(l_A/2a\right)-1\right]\right)^{-1}. \tag{8}$$

Solving the Bode-Fano integral for the small dipole from (6) by using (8), and by defining the fractional bandwidth as $\overline{B} = B/f_c$, we arrive at,

$$T_0^{(dp)} < 1-\exp\left(-\frac{\pi^4 f_c^3\left(1-\left(\overline{B}^2/4\right)\right.}{24\overline{B}\, f_{res}^3 \ln\left(\left(l_A/2a\right)-1\right)}\right) \qquad . \tag{9}$$

Hence, given the desired fractional bandwidth from a small dipole, the maximum achievable transducer gain $T_0^{(dp)}$ over this bandwidth can be predicted by (9).

In a similar approach, solving the integral relation for the small circular loop with Z_A=Z_{lp} and using (3) and (4) in (6), we get,

$$T_0^{(lp)} < 1 - \exp\left(- \frac{20\pi^2 f_C^3}{\overline{B} f_{res}^4 \mu_0 r\left(\ln\left(8r/b\right) - 2\right)} \right). \tag{10}$$

which represents the upper limit on transducer gain for the small circular loop, over a desired fractional bandwidth.

III. MATCHING CIRCUITS

Conventional impedance matching technique such as the 2 element L or C-section match for a given load is narrowband since the match occurs exactly only at a single frequency. To increase the bandwidths of these sections we suggest a high-pass network be cascaded to the 2-element matching sections as shown in Fig. A.2 and A.3. The Thévenin impedance for the equalizer as seen from the antenna for both, the small dipole and loop circuits is given as,

$$Z_T^{dp} = \frac{sL_2 Z_g}{sL_2 + Z_g} + sL_1, Z_g = \frac{sL_4\left(R_g + 1/sC_5\right)}{sL_4 + \left(R_g + 1/sC_5\right)} + \frac{1}{sC_3} \tag{11}$$

$$Z_T^{lp} = \frac{\left(1/sC_2\right)Z_g}{\left(1/sC_2\right) + Z_g} + \frac{1}{sC_1}, Z_g = \frac{\left(R_g sL_4\right)}{\left(R_g + sL_4\right)} + \frac{1}{sC_3} \tag{12}$$

where $s=j\omega$. The upper limit in (9), (10) will be used for the sake of comparison.

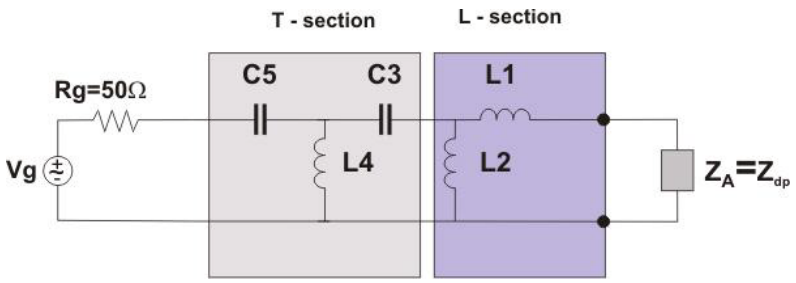

Fig. A. 2. Extension of the *L*-tuning network for certain fixed values of L_1, L_2 by the T-section for small dipole.

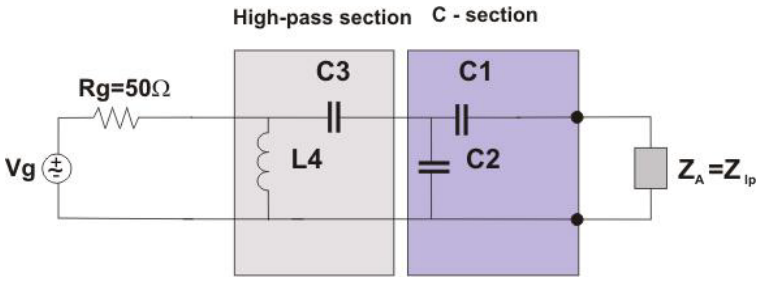

Fig. A. 3. Extension of the L-tuning network for certain fixed values of C1, C2 by a high pass section for small loop.

IV. UPPER BOUND ON SYSTEM EFFICIENCY

The upper bound on efficiency for a system comprising an electrically small antenna with a corresponding impedance matching network, as shown in Fig. A.2 and Fig. A.3, is sought. Let $R_{in}(\omega)$, be the input resistance at the antenna feed point. The input resistance can be expressed in terms of the radiation resistance, $R_r(\omega)$, and the loss resistance, $R_{loss}(\omega)$, as,

$$R_{in}(\omega) = R_r(\omega) + R_{loss}(\omega). \tag{13}$$

In [85] it is suggested that the system efficiency of the antenna-matching network combination would be maximum if the network has no storage elements that store energy of the same form as the antenna. Thus, the system efficiency η_s, has been defined as,

$$\eta_s(\omega) = \eta_a(\omega)\eta_m(\omega) = \frac{\eta_a(\omega)}{1 + \frac{Q_a(\omega)}{Q'}} \tag{14}$$

where, η_m, is the efficiency of the matching network, η_a is the efficiency of the antenna, Q' is the Quality factor of the network elements that store energy in the form opposite to that of the antenna, and Q_a is the antenna quality factor. We can therefore deduce that the

simple L - section or the C - section matching network comprising of only inductors or capacitors, as shown in Fig. A.2 and Fig. A.3, for a dipole or loop antenna respectively, would achieve the highest possible system efficiency. The antenna Quality factor, Q_a is approximated as,

$$Q_a(\omega=\omega_C)=\frac{|X(\omega=\omega_c)|}{R_{in}(\omega=\omega_c)}. \tag{15}$$

Using (13) we can rewrite (15) as,

$$Q_a(\omega=\omega_C)=\frac{|X(\omega=\omega_c)|}{R_r(\omega=\omega_c)+R_{loss}(\omega=\omega_c)}. \tag{16}$$

We can use this approximation since we are clearly below the first resonance of the antenna. Since, losses in antenna structure have been assumed to be small, we set the term $R_{loss}(\omega) \approx 0$ to obtain,

$$Q_a(\omega=\omega_C)=\frac{|X(\omega=\omega_c)|}{R_r(\omega=\omega_c)}. \tag{17}$$

The efficiency of the antenna is defined in the standard way as follows,

$$\eta_a = \frac{R_r(\omega)}{R_r(\omega)+R_{loss}(\omega)} \tag{18}$$

Since the loss resistance is assumed to be negligible in the antenna structure, the efficiency of the antenna $\eta_a \approx 1$. Therefore, a simple expression for the upper bound on system efficiency for the case of an electrically small antenna in combination with a matching network is obtained from (14) as

$$\eta_s(\omega) = \frac{1}{1 + \frac{Q_a(\omega)}{Q'}} \tag{19}$$

V. NUMERICAL SIMULATION AND RESULTS

A. Simulation Setup

The set of tested antenna parameters for small dipole and loop are shown in Table A.1. The resonant frequency of both the small dipole and circular loop was chosen as 1 GHz. For the small dipole, *d* refers to the diameter. The matching network components are obtained through optimization. This is done by using a direct global numerical search in the space of circuit parameters. The minimum gain achieved over the band is calculated [23] for every circuit parameter set and only the ones that satisfy the ±25% gain variation criterion are retained.

Table A. 1. SIMULATION PARAMETERS

Parameter	*Small Dipole*	*Small Loop*
Geometry	$l_A/d = 10$	$\rho = 10$
$\overline{B}$	0.5	0.5
f_C / f_{res}	[0.05:0.2]	[0.05:0.1]

B. Realized Gain – Small Dipole, $l_A/d = 10, \overline{B} = 0.5$

Fig. A. 4 shows the realized average generator gain for the small dipole. The solid line is the upper limit derived from Bode-Fano theory in Eq. (9) and the realized values are shown by squares. The network performs rather closely to the upper limit T_0 if we

consider the average gain over the band. The deviation from the upper limit is 33%. The component values for f_c / f_{res} = 0.15 are, [L1, L2, C3, L4, C5] = [762.8nH, 175.8nH, 49.6pF, 837.4nH, 10.5pF].

C. Realized Gain – Small Circular Loop, ρ=10, $\overline{B} = 0.5$

In Fig. A.5 the realized average generator gains for a small circular loop are plotted for different center frequencies. As before the solid line corresponds to the theoretical upper limit derived from the Bode-Fano criterion in Eq. (10). The small loop requires one less component in the matching network as compared to the small dipole. The generator gain approaches this upper limit, with the average deviation between the two being 34%. The component values for f_c / f_{res} = 0.0875 are, [C1, C2, C3, L4] = [23.1pF, 94.08pF, 571.5pF, 40.7nH].

D. System Efficiency – Small Dipole and Small Loop

The upper bound on system efficiency for the small dipole and loop has been calculated at various center frequencies using Eq. (19). For the case of the small dipole, the L-section matching network uses two inductors, L1 and L2. The Q factor for these components is assumed to be 55. Similarly the C-section matching network for the small loop uses two capacitors C1 and C2 with Q-factor of 1000. Fig. A.6. shows the upper bound on system efficiency for the small dipole.

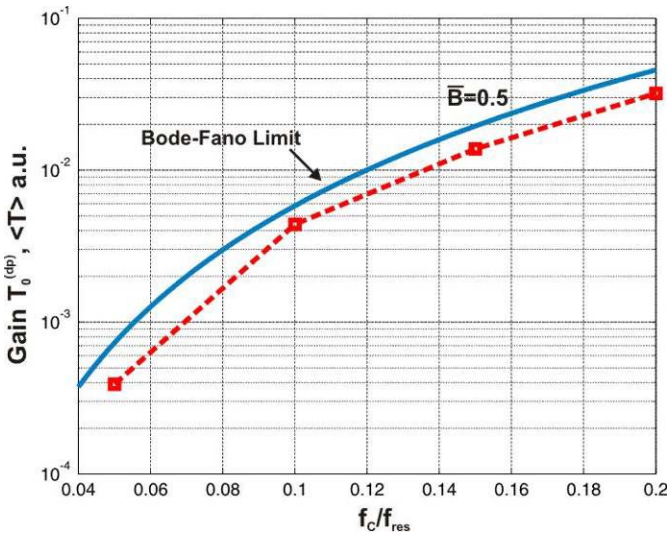

Fig. A. 4. Realized average generator gain $T_0^{(dp)}$(squares) for a small dipole with $l_A/d = 10$.

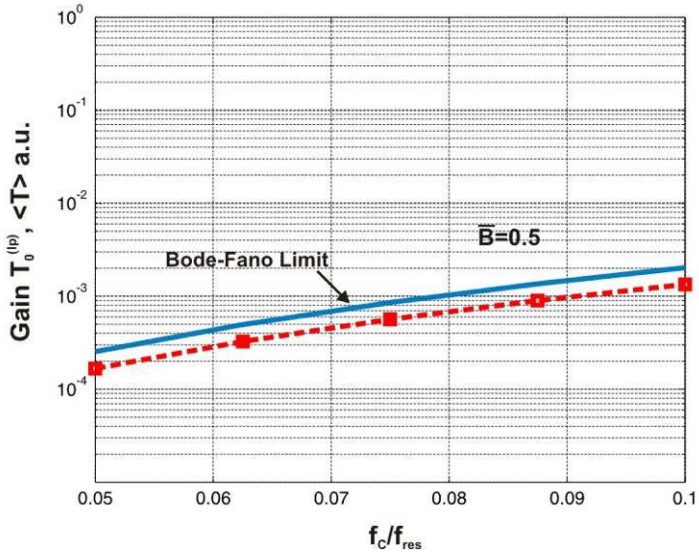

Fig. A. 5. Realized average generator gain $T_0^{(lp)}$ (squares) for a loop with ρ=10.

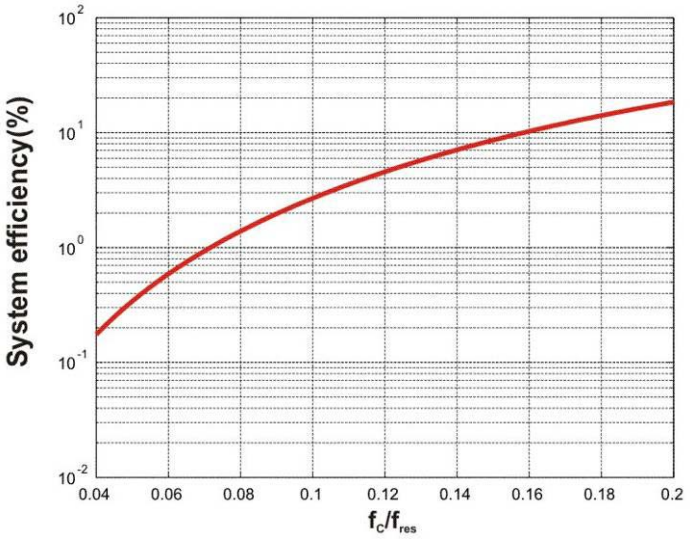

Fig. A. 6. Upper bound on system efficiency for the small dipole with l_A/d=10.

Similarly, Fig. A.7 shows the upper bound on system efficiency for a small loop.

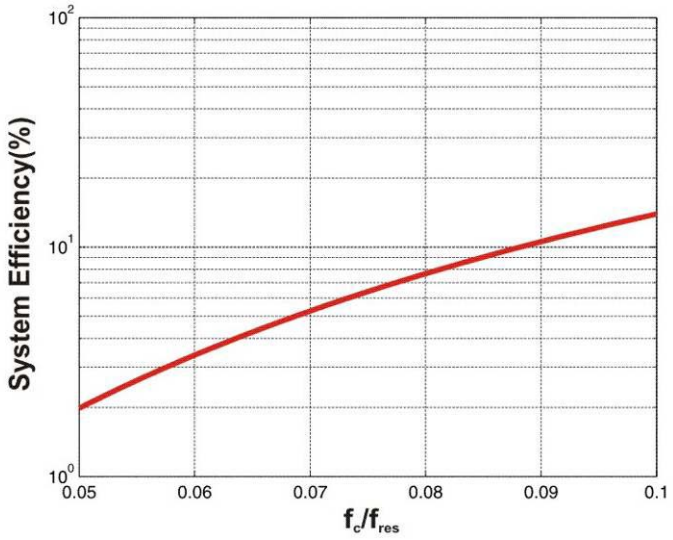

Fig. A. 7. Upper bound on system efficiency for the small loop with ρ=10

VI. CONCLUSION

In this study we have presented a wideband impedance matching approach for the electrically small dipole and loop antennas. The Bode-Fano theoretical limit for maximum transducer gain has been derived and used for comparison of the proposed

networks. It has been shown that the average deviation between the realized gain and the theoretical upper limit is approximately 33% for both types of antennas. In doing so a gain variation criterion of ±25% over the band of interest has been applied while calculating the transducer gain. The system efficiency for the small antenna in combination with the matching network was discussed; an upper bound was derived and plotted at different center frequencies.

It is observed that the realized generator gain and the efficiencies are low. This is primarily because of the low value of radiation resistance of the small antenna. Even so, the small loop is capable of higher efficiency than the small dipole. Modifying the antenna structure to increase the radiation resistance would potentially alleviate this issue and increase generator gain. Of course, it is then possible that the antenna efficiency might decrease.

Appendix B – ADS analysis of a monopole with reflective equalizer

I. MODELING THE WIDEBAND IMPEDANCE MATCHING OF MONOPOLE ANTENNA IN AGILENT - ADS

Goal: To analyze the behavior of the lumped component based equalizer, designed to do wideband impedance matching for a 11.5 cm monopole antenna over ground plane, by simulating it in Agilent ADS.

Solution:

Our goal is to build a model of the system comprising of the wideband matching network and the monopole antenna to effectively mirror the real system.

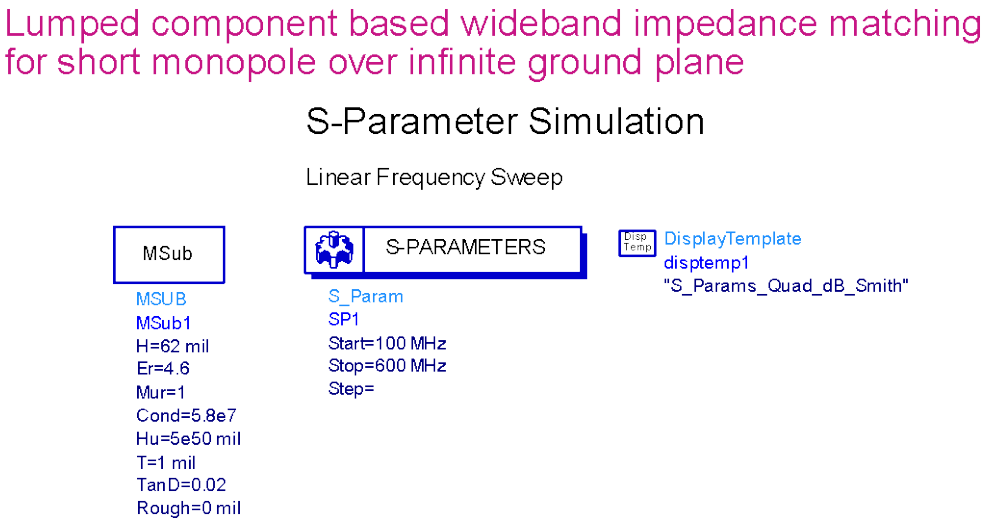

Fig. B. 1. ADS simulation set up.

In Fig. B.1 and Fig. B.2, the S-parameter simulation set up is shown in ADS along with the substrate parameters corresponding to the FR-4 board that was used as substrate for the wideband matching network PCB. The results of this simulation are seen in Fig. B.3.

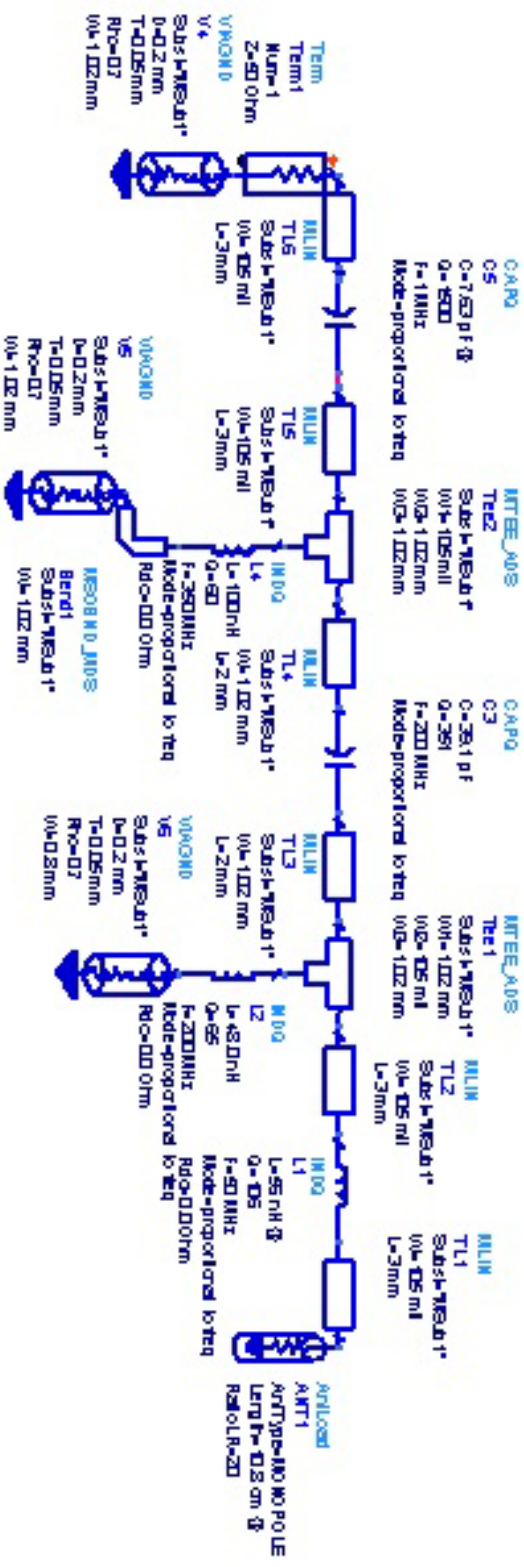

Fig. B. 2. ADS simulation set up of the wideband reflective equalizer.

Results

Case I : - L = 11.5 cm, W = 2.3 cm

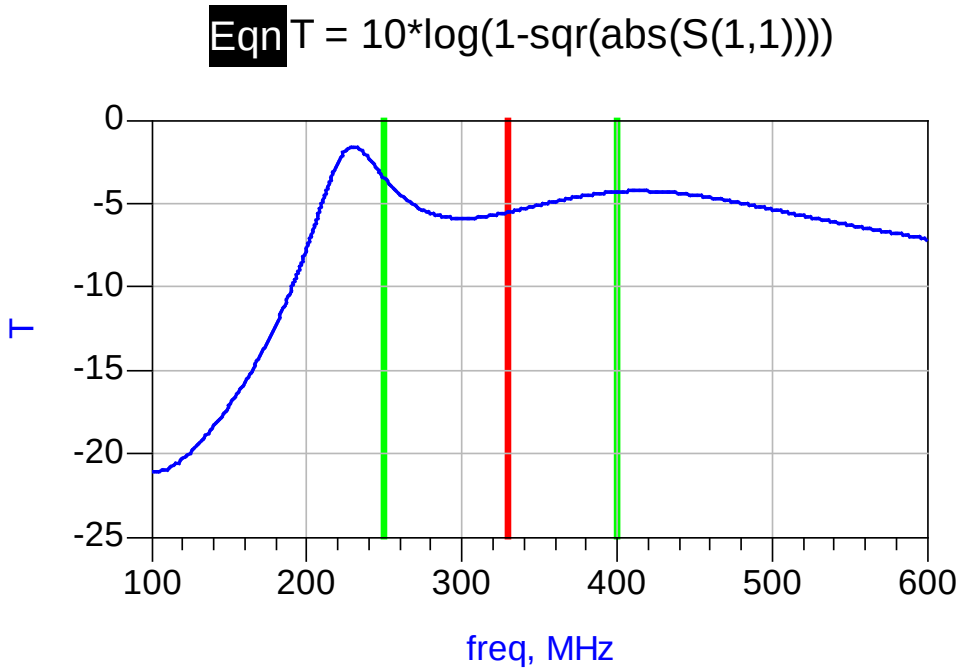

Fig. B. 3. Simulation result, for L1 = 56nH, C5 = 7.63pF.

Appendix C – Comparison of input impedance of the electrically small dipole and loop antennas using analytical, Method of Moments (MoM) and Ansoft HFSS solutions

The input resistance R of an *electrically small* (this means small compared to the wavelength at the center frequency) dipole antenna has the form

$$R = \frac{2\pi\eta_0}{3}\frac{\tilde{l}_A^{\,2}}{\lambda^2} = \frac{\pi\eta_0}{6}\frac{l_A^{\,2}}{\lambda^2} \tag{1}$$

where $\tilde{l}_A$ is the antenna **half** length and $\lambda = c_0 / f$ is the wavelength.

The blade dipole antenna has total length l_A=150mm and the width of 5 mm, 15mm respectively

Table C. 1. Input resistance of a small dipole antenna $(\Omega), l/t = 30$.

Frequency	20 MHz $\lambda/100$	40 MHz $\lambda/50$	100 MHz $\lambda/20$	200 MHz $\lambda/10$	400 MHz $\lambda/5$
R- Analytical	1.97 e-2	7.9 e-2	4.94 e-1	1.97	7.90
R-MoM, *t* = 5mm	1.449 e-2	5.8 e-2	3.65e-1	1.497	6.63
R-FEM, *t* = 5mm PML, 1000x1000x1000mm 15 passes, 1GHz	4.15 e-2	7.8 e-2	3.9 e-1	1.56	6.94

Table C. 2. Input resistance of a small dipole antenna (Ω), $l/t = 10$

Frequency	20 MHz $\lambda/100$	40 MHz $\lambda/50$	100 MHz $\lambda/20$	200 MHz $\lambda/10$	400 MHz $\lambda/5$
R- Analytical	1.97 e-2	7.9 e-2	4.94 e-1	1.97	7.90
R-MoM, *t* = 15mm	1.122 e-2	4.49 e-2	2.84 e-1	1.175	5.42
R-FEM, *t* = 15mm PML, 1000x1000x1000mm 15 passes, 1GHz	2.64 e-2	5.9 e-2	3.1 e-1	1.27	5.88

The input reactance X of an *electrically small* (this means small compared to the wavelength at the center frequency) dipole antenna has the form

$$X = -\left[\frac{\eta_0}{\pi^2}\left(\ln\frac{l_A}{2a} - 1\right)\frac{\lambda}{l_A}\right] \tag{2}$$

$a = t/4$ where a is the (equivalent) wire radius and t is the (equivalent) blade width.

Table C. 3. Input reactance of a small dipole antenna (Ω), $l/t = 30$.

Frequency	20 MHz $\lambda/100$	40 MHz $\lambda/50$	100 MHz $\lambda/20$	200 MHz $\lambda/10$	400 MHz $\lambda/5$
X- Analytical	-11807.45	-5897.89	-2342.78	-1141.96	-510.61
X-MoM, t = 5 mm	-10811.13	-5400.21	-2145.05	-1045.33	-465.36
X-FEM, t = 5 mm PML 1000x1000x1000mm 15 passes, 1 GHz	-10717.6	-5353.37	-2126.02	-1035.27	-459.33

Table C. 4. Input reactance of a small dipole antenna (Ω), l/t = 10.

Frequency	20 MHz $\lambda/100$	40 MHz $\lambda/50$	100 MHz $\lambda/20$	200 MHz $\lambda/10$	400 MHz $\lambda/5$
X- Analytical	-7615.35	-3803.9	-1511.00	-736.52	-329.32
X-MoM, *t* = 15 mm	-6395.01	-3194.55	-1269.52	-619.66	-277.38
X-FEM, *t* = 15 mm PML 1000x1000x1000mm 15 passes, 1 GHz	-6541.54	-3267.60	-1298.12	-632.84	-281.74

The input resistance R of an *electrically small* (this means small compared to the wavelength at the center frequency) loop antenna has the form (Balanis, p. 238)

$$R = \frac{2\pi\eta_0}{3}\frac{(kS_A)^2}{\lambda^2} \tag{3}$$

where $S_A = \pi r_A^2 = \frac{C_A^2}{4\pi}$ is the loop area; C_A is the loop circumference; $k = 2\pi/\lambda$ is the wavenumber. In other words (see Balanis, p. 238),

$$R = \frac{2\pi\eta_0}{3}\frac{(C_A^2/(2\lambda))^2}{\lambda^2} = \frac{\pi\eta_0}{6}\frac{C_A^4}{\lambda^4} \tag{4}$$

For the blade loop antenna of the total circumference (drawn through the center of the blade) C_A=150mm and the width of 5 mm, 15mm respectively.

Table C. 5. Input resistance of a small loop antenna (Ω) $C/t = 30$.

Frequency	20 MHz $\lambda/100$	40 MHz $\lambda/50$	100 MHz $\lambda/20$	200 MHz $\lambda/10$	400 MHz $\lambda/5$
R- Analytical	1.97 e-6	3.167 e-5	1.23 e-3	1.97 e-2	3.167 e-1
R-MoM, *t* = 5mm	1.90 e-6	3.05 e-5	1.2 e-3	2.18 e-2	5.58 e-1
R-FEM, *t* = 5mm PML, 1000x1000x1000mm 12 passes, 1 GHz	2 e-6	3 e-5	1.198 e-3	2.13 e-2	5.3 e-1

Table C. 6. Input resistance of a small loop antenna $(\Omega)\, C/t = 10$.

Frequency	20 MHz $\lambda/100$	40 MHz $\lambda/50$	100 MHz $\lambda/20$	200 MHz $\lambda/10$	400 MHz $\lambda/5$
R- Analytical	1.97 e-6	3.167 e-5	1.23 e-3	1.97 e-2	3.167 e-1
R-MoM, *t* = 15mm	1.46 e-6	2.35 e-5	9.49 e-4	1.72 e-2	4.7 e-1
R-FEM, *t* = 15mm PML, 1000x1000x1000mm 12 passes, 1 GHz	1.37 e-6	2.26 e-5	9.1 e-4	1.65 e-2	4.3 e-1

The input reactance X of an *electrically small* (this means small compared to the wavelength at the center frequency) loop antenna has the form (Balanis, p. 245)

$$X_A \approx \omega L = 2\pi fL, \quad L = \mu_0 R_A \left(\ln\left(\frac{8R_A}{a} \right) - 2 \right) \tag{5}$$

where R_A is the loop radius; $a = t/4$ where a is the (equivalent) wire radius and t is the (equivalent) blade width.

Table C. 7. Input reactance of a small loop antenna (Ω) $C/t = 30$.

Frequency	20 MHz $\lambda/100$	40 MHz $\lambda/50$	100 MHz $\lambda/20$	200 MHz $\lambda/10$	400 MHz $\lambda/5$
X- Analytical	11.42	22.83	57.09	141.92	228.38
X-MoM, t = 5mm	11.59	23.22	58.69	122.15	292.37
X-FEM, t = 5mm PML 1000x1000x1000mm 12 passes, 1 GHz	11.21	22.46	56.72	117.73	278.05

Table C. 8. Input reactance of a small loop antenna $(\Omega)\, C/t = 10$.

Frequency	20 MHz $\lambda/100$	40 MHz $\lambda/50$	100 MHz $\lambda/20$	200 MHz $\lambda/10$	400 MHz $\lambda/5$
X- Analytical	7.27	14.55	36.38	72.77	145.55
X-MoM, *t* = 15mm	6.8	13.63	34.51	72.31	179.12
X-FEM, *t* = 15mm PML 1000x1000x1000mm 12 passes, 1 GHz	6.63	13.29	33.62	70.10	169.47

Appendix D – Example design of single and dual band matching networks

I. LLNL – HANDSET MATCHING NETWORK SPECIFICATIONS

Handset Specifications: -

Dimensions: - W X D X H = 7cm X 5cm X 15cm

Frequency: - 250MHz – 400MHz

Bandwidth: - 150MHz

Antenna specifications: -

Type: - Blade

Length: - 11.5cm

Width: - 2.3cm

Thickness: - 0.25mm

II. FULL WAVE MODELING

These specifications were used to model the structure in ANSOFT – HFSS. The entire structure consisting of the blade and the handset is considered to be the antenna. A lumped port feed with a feed gap of 1mm was used for the excitation source. The radiation boundary was located at 0.325λ from the structure on all sides. Fig. D.1 shows the final model built using HFSS. The blade and the handset are modeled as Perfect electric conductors (PEC). The blade and the corresponding feed are located off of the edge of the top surface on the handset. A total of 15 passes were used for mesh generation which resulted in about 16,500 tetrahedra being generated.

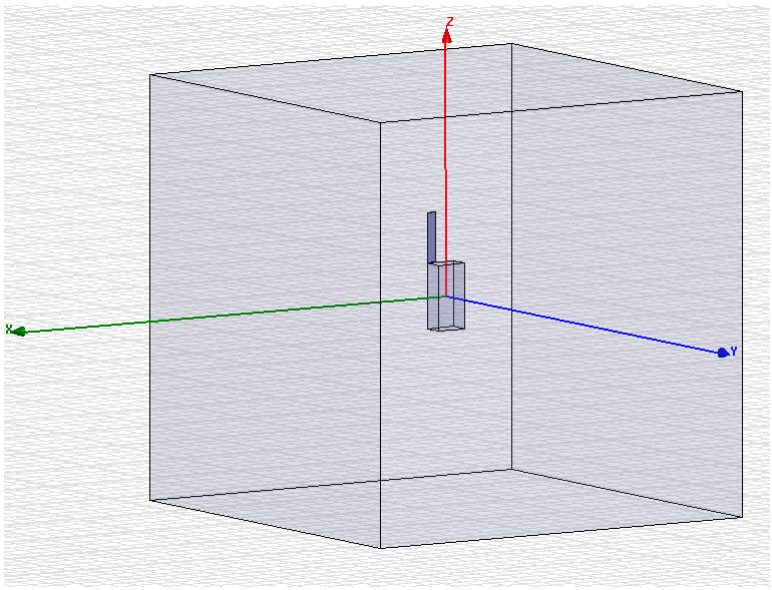

Fig. D. 1. Handset model in ANSOFT- HFSS.

III. MATCHING NETWORK

The device is being operated below the first resonance of the blade-handset structure. The input impedance of this structure is shown in Fig. D.2 over the operating bandwidth of 150MHz.

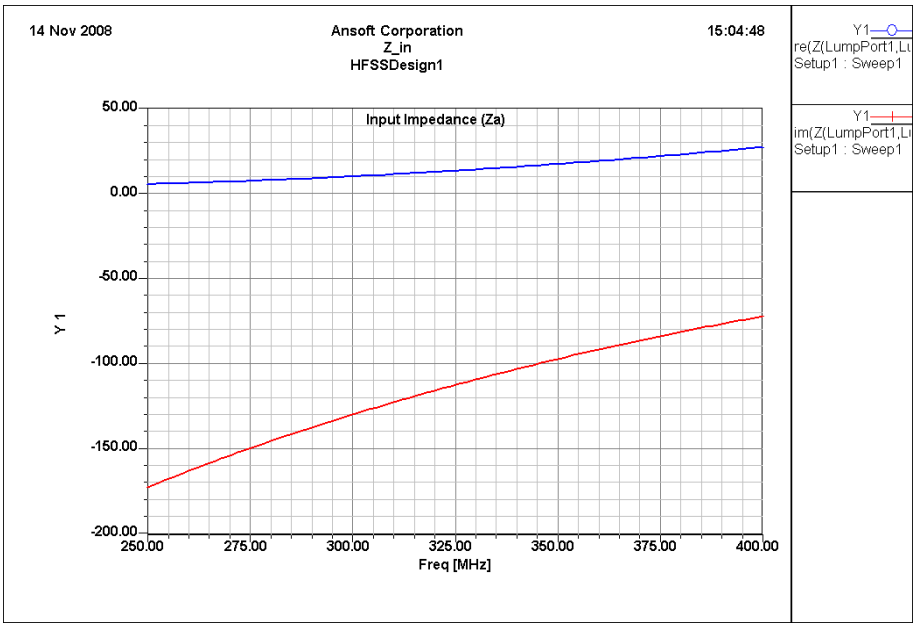

Fig. D. 2. Input impedance of blade-handset antenna.

As observed, the antenna impedance is predominantly capacitive with a resistive part that varies from approximately 5 - 25Ω across 250MHz – 400MHz. The maximum directivity of this antenna is close to that of an ideal dipole in free space (~2.2dB) and is shown in Fig. D.3. There is a slight tilt observed in the pattern wherein the null is no longer exactly at zenith. This structure is essentially an offset center fed dipole, wherein the the handset body is also contributing to the radiation. Since, the gain is the important parameter of interest, we must attempt to make this antenna efficient as well as reduce the mismatch loss. Assuming a highly efficient structure, we focus on reducing the mismatch losses that would occur due to this antenna being driven by a purely resistive 50Ω source.

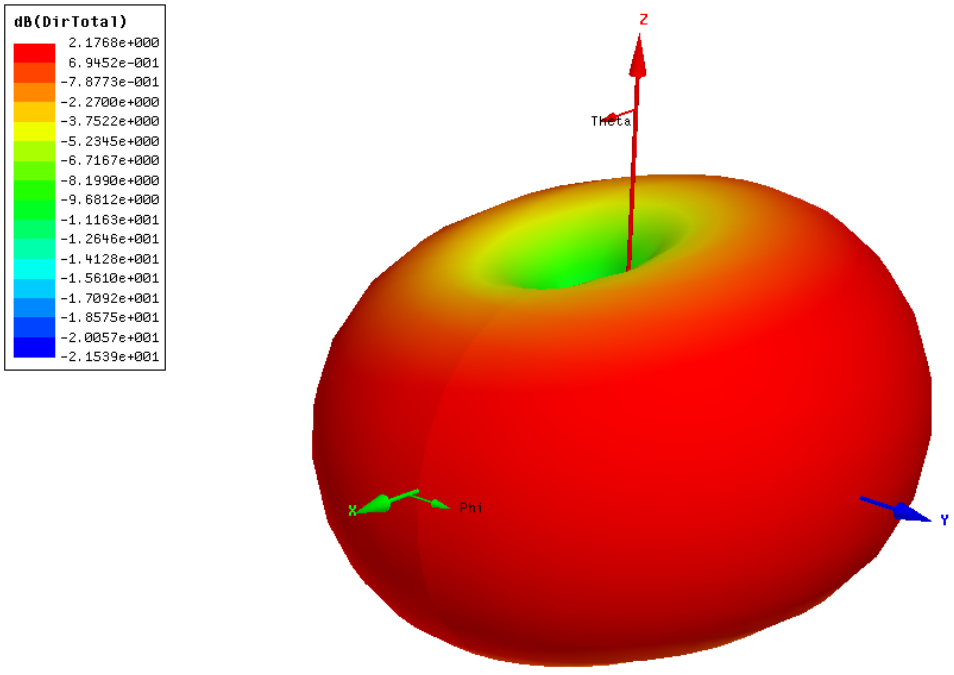

Fig. D. 3. Directivity of the blade-handset antenna.

Our approach is to design a 5 element matching network built entirely out of reactive components. We extend the traditional L-section matching used for narrowband impedance matching and cascade a highpass T-section comprising of two series

capacitors and a shunt inductor as shown in Fig. D.4. A direct search based technique is used to obtain the component values in the matching network.

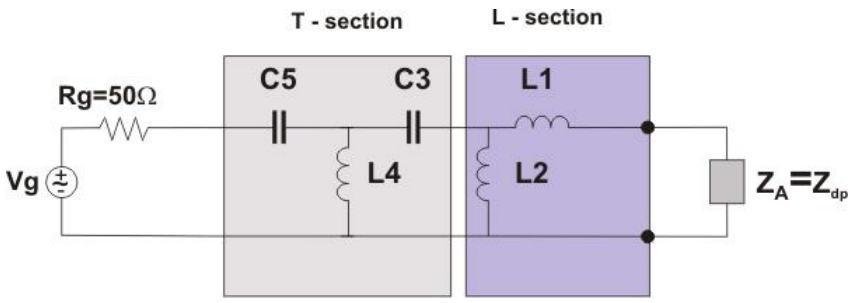

Fig. D. 4. Extension of the L-tuning section for fixed values of L_1, L_2 by the T-section.

Results

A 5 element matching network was obtained from the optimization procedure and the component values are shown in Table D.1.

Table D. 1. Circuit parameters for the matching network used to match the blade-handset antenna to resistive 50Ω source.

COMPONENT	VALUE (nH/pF)
L1	47.24
L2	31.49
C3	16.12
L4	466.66
C5	13.33

The transducer gain obtained across the operating bandwidth due to the matching network is shown in Fig. D.5. The average transducer gain can be translated to an average return loss as follows, $T(\omega^2) = 1 - |\Gamma(\omega)|^2$ where T is the transducer gain and Γ is the reflection coefficient. Thus, the avg. gain of 0.42871 translates to approximately 2.43dB average return loss across the 150MHz bandwidth. This is an improvement and we can compare it to the return loss of the blade-handset antenna without the matching network

which is shown in Fig. D.6. As seen in this plot, the S_{11} varies from about 0dB to roughly -3dB at the higher end of the frequency range.

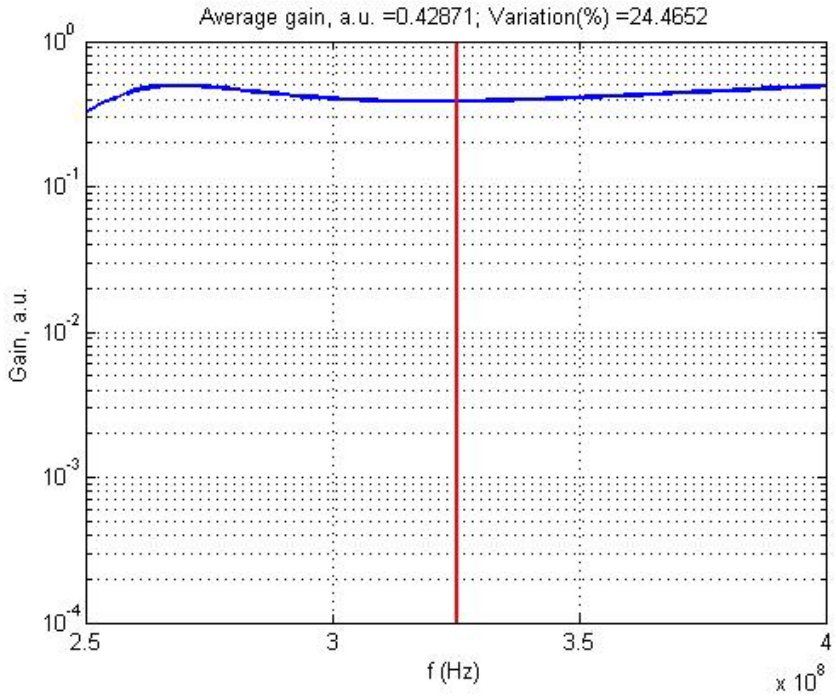

Fig. D. 5. Average transducer gain.

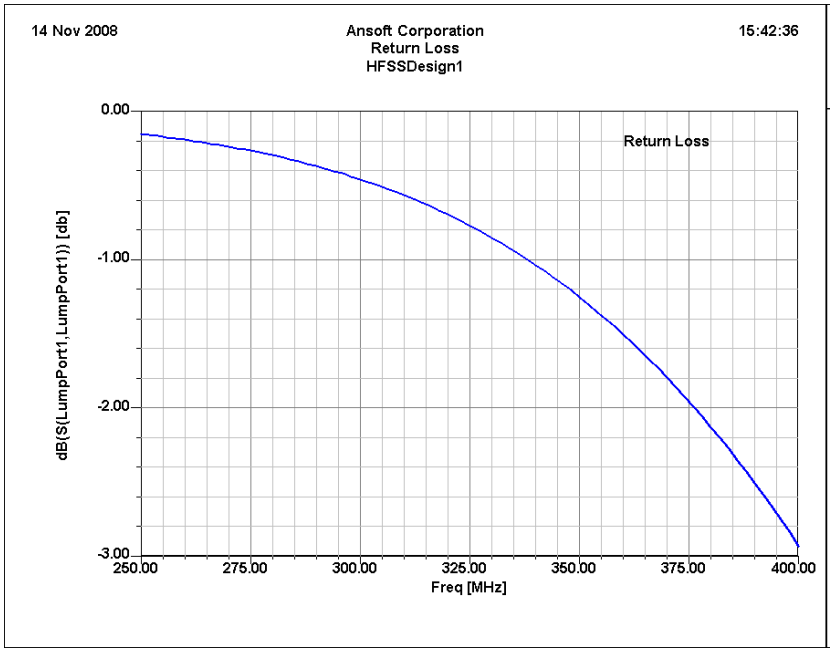

Fig. D. 6. S_{11} of blade-handset antenna without matching network.

The antenna resistance should be increased in order to improve this return loss across the required operating frequency range.

II. COMPONENT VALUES FOR REFLECTIVE EQUALIZERS IN HF-VHF BAND

Antenna - Dipole

Length - 2m

Resonant frequency - 75 MHz

Bandwidth - 50 %

Band 1 - 14.625 MHz - 24.375 MHz

Band 2 - 22.5 MHz - 37.5 MHz

The antenna geometry chosen is l_A / d =10, l_A is the total dipole length and d is the diameter of the dipole

Table D. 2. Component values for a 5 element reflective equalizer in two different bands along with the average theoretical transducer gain.

Band	**Component value**	**Gain**
f_c = 19.5 MHz 14.625 MHz - 24.375 MHz	$L_1 = 2.92$ µH $L_2 = 1.09$ µH $C_3 = 3.54$ nF $L_4 = 5.43$ µH $C_5 = 94.8$ pF	$\overline{T} = 0.072$
f_c = 30.0 MHz 22.5 MHz - 37.5 MHz	$L_1 = 1.05$ µH $L_2 = 634.9$ nH $C_3 = 344.1$ pF $L_4 = 1.77$ µH $C_5 = 88.9$ pF	$\overline{T} = 0.2094$

Appendix E – Upper Limit on System Efficiency for Electrically Small Dipole and Loop Antennas with Matching Networks

The efficiency of a system comprising of an electrically small antenna with a corresponding impedance matching network is considered in this study. This system is connected to generator whose internal impedance is $Z_G = R_G$ and thus no energy is stored. Fig E.1 shows this setup

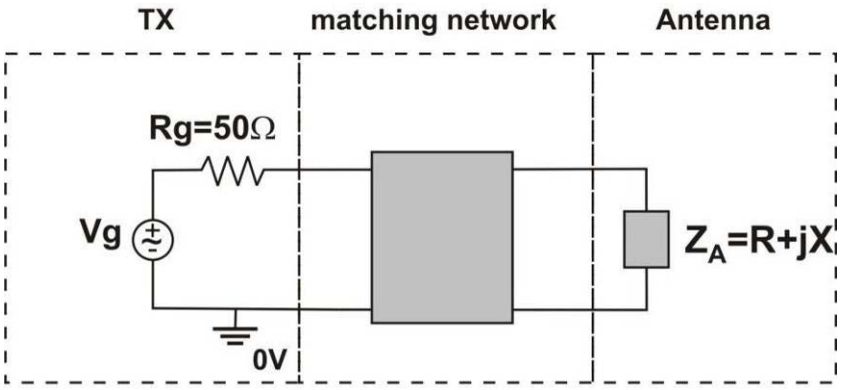

Fig. E. 1. Reactive matching network representation

The impedance of electrically small antennas such as the dipole and the loop comprises of a very small radiation resistance and a large reactance, either capacitive or inductive respectively. The overall resistance at the antenna feed can be therefore expressed as,

$$R(\omega) = R_r(\omega) + R_{Loss}(\omega) \tag{1}$$

Let us assume that the loss resistance in the antenna is very small and therefore can be approximated such that $R_{Loss}(\omega) \approx 0$. The efficiency for this antenna $\eta_a(\omega)$ is,

$$\eta_a(\omega) = \frac{R_r(\omega)}{R_r(\omega) + R_{Loss}(\omega)} = 1 \tag{2}$$

In [85] it is suggested that the system efficiency of the antenna-matching network combination would be maximum if the network has no storage elements that store energy of the same form as the antenna. Thus, the system efficiency $\eta_s(\omega)$, has been defined as,

$$\eta_s(\omega) = \eta_a \eta_m = \frac{\eta_a(\omega)}{1 + \frac{Q_a(\omega)}{Q'}} \tag{3}$$

where, η_m, is the efficiency of the matching network, Q' is the Quality factor of the network elements that store energy in the form opposite to that of the antenna, and Q_a is the antenna Quality factor. We can therefore deduce that the L section matching network comprising of all inductors or all capacitors, as shown in Fig. E.2 for a dipole or loop antenna respectively would achieve the highest possible system efficiency.

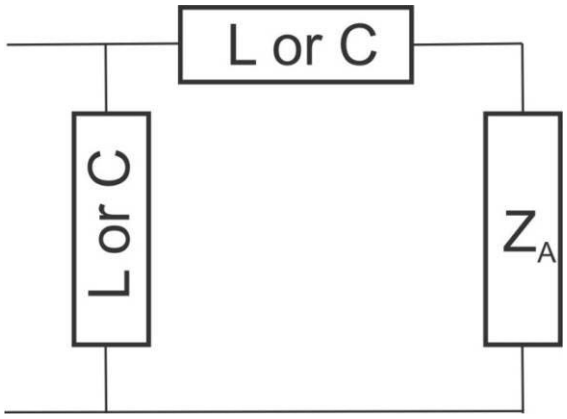

Fig. E. 2. L - Section matching network.

The antenna Quality factor, Q_a is approximated as,

$$Q_a(\omega = \omega_C) = \frac{|X(\omega = \omega_c)|}{R(\omega = \omega_c)} = \frac{|X(\omega = \omega_c)|}{R_r(\omega = \omega_c) + R_{loss}(\omega = \omega_c)} \tag{4}$$

We can use this approximation since we are clearly below the first resonance of the antenna. Since, losses in antenna structure have been assumed to be small, we get,

$$Q_a(\omega = \omega_C) = \frac{|X(\omega = \omega_c)|}{R_r(\omega = \omega_c)} \tag{5}$$

From [32], the radiation resistance of a small dipole is given to be,

$$R_{dp} = 20\pi^2 (l_A/\lambda)^2 \; \forall \quad \lambda/50 \le l_A \le \lambda/10 \tag{6}$$

and reactance can be derived as,

$$X_{dp} = -120\frac{\left[\ln\left(l_A/2a\right)-1\right]}{\left(kl_A/2\right)} \tag{7}$$

In Eq. (6), l_A is the dipole length, *a*, is the dipole radius, and $k = 2\pi/\lambda$ is the wavenumber.. In the case of a strip or blade dipole of width *t*, the equivalent radius is $a_{eq} = t/4$ [32]. The small dipole condition can be expressed in the frequency domain as $0.04 < f_c / f_{res} \le 0.2$, where, $f_{res} \equiv c_0/2l_A$ is the resonant frequency of a half wave resonant ideal dipole, c_0 is the speed of light and f_c is the center frequency. Note that the expression for reactance holds only within the dimension limits specified in Eq. (6). Similarly, for the circular loop, we have

$$R_{lp} = 20\pi^2\left(C/\lambda\right)^4 \forall\ C < \lambda/10 \tag{8}$$

and the loop inductance is,

$$L = \mu_0 r\left[\ln\left(8r/b\right) - 2\right] \tag{9}$$

RESULTS

We consider the following parameters for our numerical simulation.

Case I: *Electrically small dipole*

Table E. 1. Simulation Parameters.

PARAMETER	VALUE
f_{res}	1 GHz
l_A/d	[5 10 50]
Q $\{L_1,L_2\}$	55
f_c/f_{res}	[0.05:0.2]

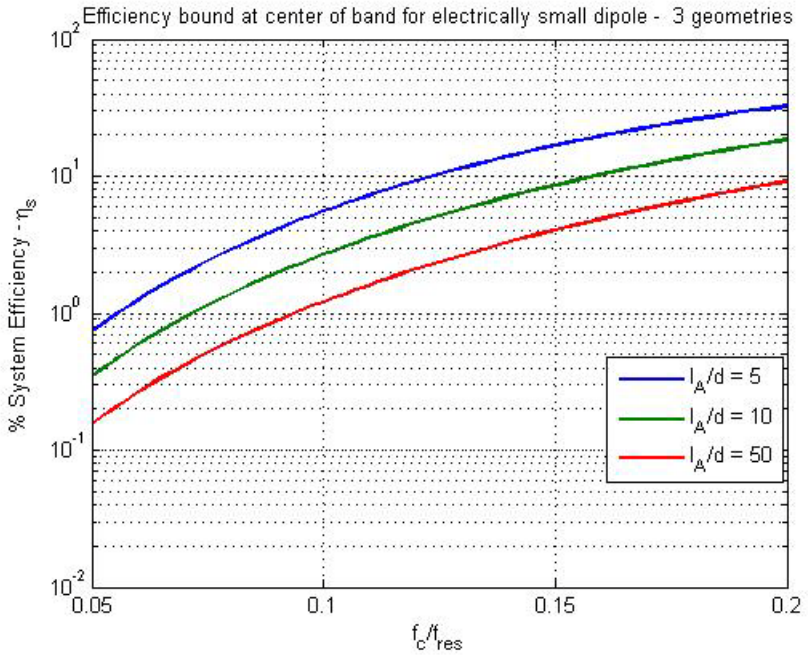

Fig.E. 3. Upper bound on achievable system efficiency for small dipole.

Case II: *Short dipole*

Considering a short dipole below the first resonance, such that the model for the impedance of the dipole is changed to,

$$Z_A = R(z) - j\left[120\left(\ln\frac{l_A}{2a} - 1\right)\cot z - X(z)\right]$$

$$R(z) \approx -0.4787 + 7.3246z + 0.3963z^2 + 15.6131z^3 \quad (10)$$

$$X(z) \approx -0.4456 + 17.00826z - 8.6793z^2 + 9.6031z^3$$

Table E. 2. Simulation parameters

PARAMETER	VALUE
f_{res}	1 GHz
l_A/d	[5 10 50]
Q {L_1,L_2}	55
f_c/f_{res}	[0.05:0.5]

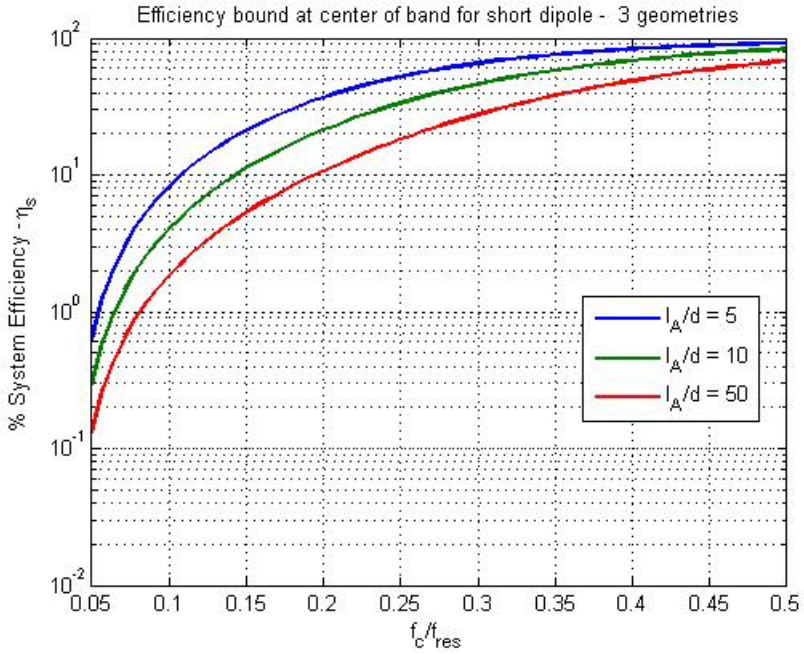

Fig. E. 4. The achievable system efficiency for short dipole.

Case III: *Electrically small circular loop*

Table E. 3. Simulation Parameters.

PARAMETER	VALUE
f_{res}	1 GHz
Ω(thickness factor[2])	[8 10 12]
Q {C_1,C_2}	1000
f_c / f_{res}	[0.05:0.1]

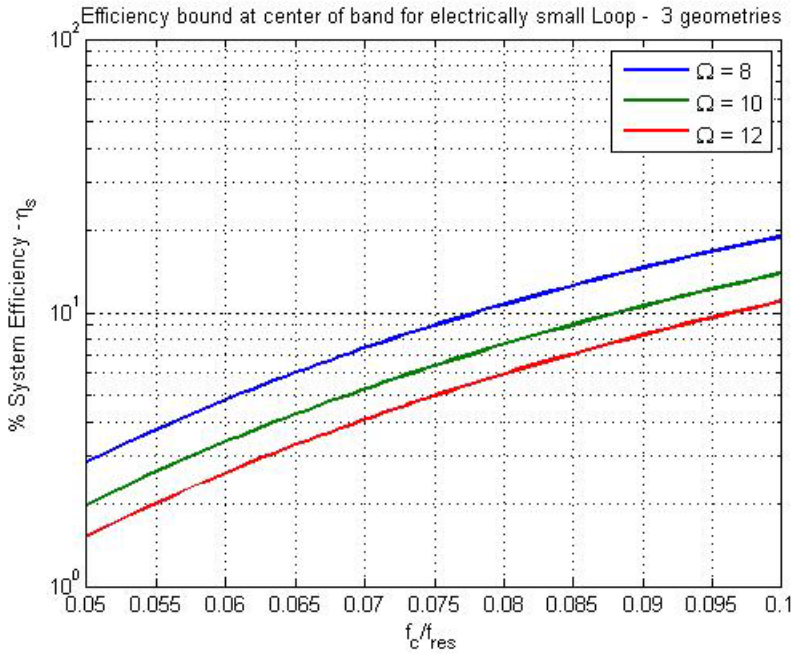

Fig. E. 5. The achievable system efficiency for an electrically small loop.

Case IV: *Electrically small circular loop*

The small loop approximation is changed to $r < \lambda/6\pi$ [32], and the results of the numerical simulation using the following parameters is shown,

Table E. 4. Simulation Parameters.

PARAMETER	VALUE
f_{res}	1GHz
Ω(thickness factor[2])	[8 10 12]
Q {C_1,C_2}	1000
f_c / f_{res}	[0.1:0.25]

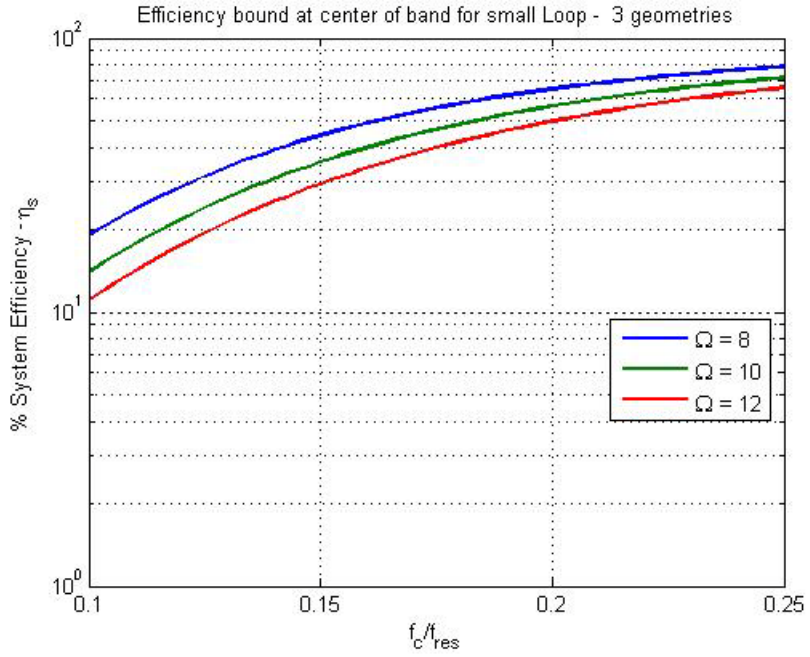

Fig. E. 6. The achievable system efficiency for small loop using approximation on radius

These results suggest that the small loop is capable of higher efficiency than the dipole

A look at the Q-factor approximation for dipole and loop antenna

The predicted efficiencies are close to 80- 95% for dipole and loop, at the upper frequencies. This can be explained by observing the Q factor of the antennas,

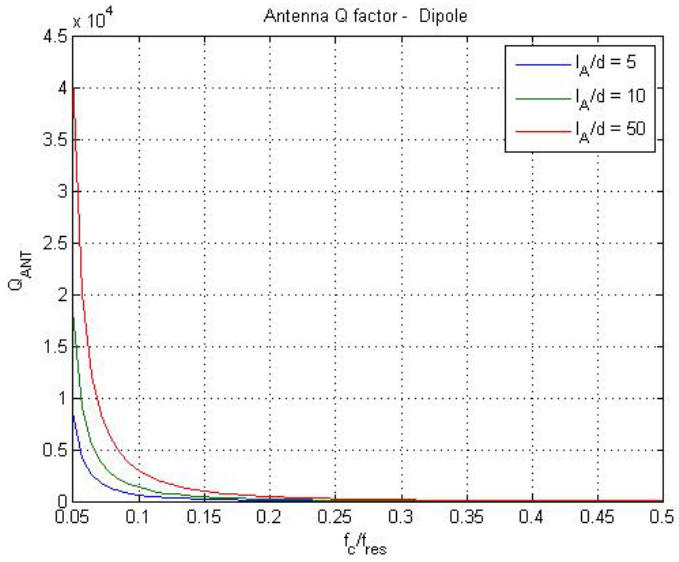

Fig. E. 7. The dipole quality factor as a function of center frequency of operation.

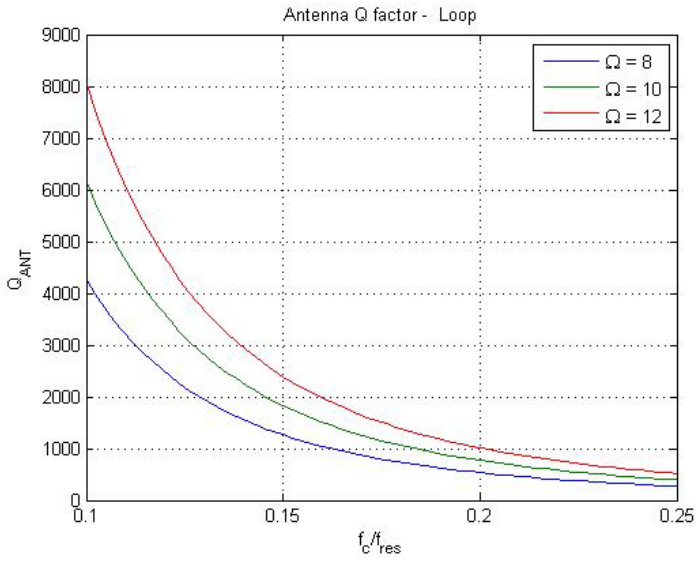

Fig. E. 8. The loop quality factor as a function of center frequency of operation.

The lower antenna Q implies a better radiation mechanism and hence improved efficiency.

Appendix F – Reflectionless equalizers for an electrically small monopole and a dielectrically (truncated hemisphere) loaded top-hat monopole antenna

I. ANTENNA TYPE

The antenna geometry is shown in Fig. F.1. The metal structure includes the feed, which protrudes the entire dielectric hemisphere and is closed by a metal top hat. The geometry and the feed position support the $TM_{01\delta}$ mode of the dielectric resonator (DR) with the electric field in the vertical direction. Simultaneously, it supports the monopole field of the standard top-hat monopole above the ground plane. Therefore, the present antenna is likely a mix of the short monopole and a $TM_{01\delta}$ dielectric resonator. It might be also viewed as a variation of the dielectric-loaded monopole. However, the dielectric body now extends further away from the monopole.

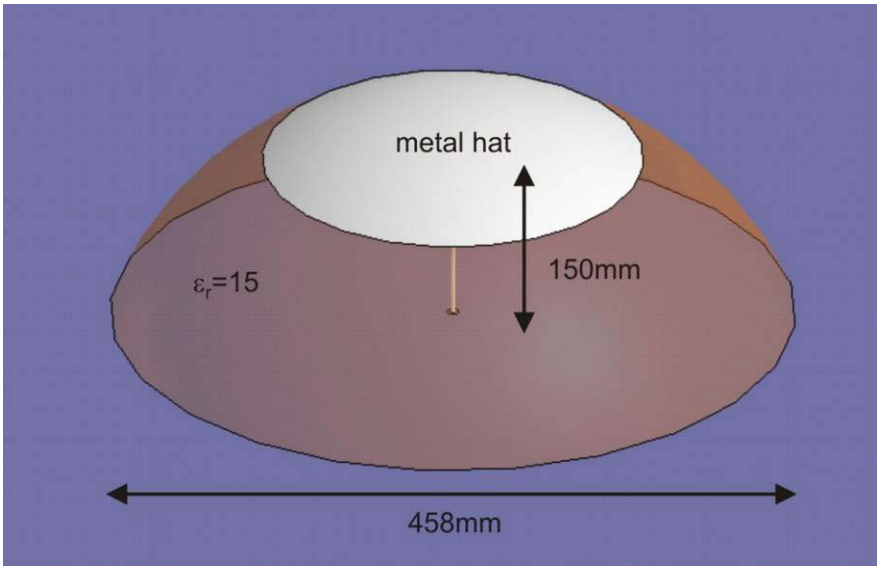

Fig. F. 1. A DR antenna in the form of a spherical sector (height - 150mm; width - 458mm) with a metal hat.

II. RADIATION PATTERN

The radiation pattern of the DR antenna as seen in Fig. F.2, indicates a monopole like behavior.

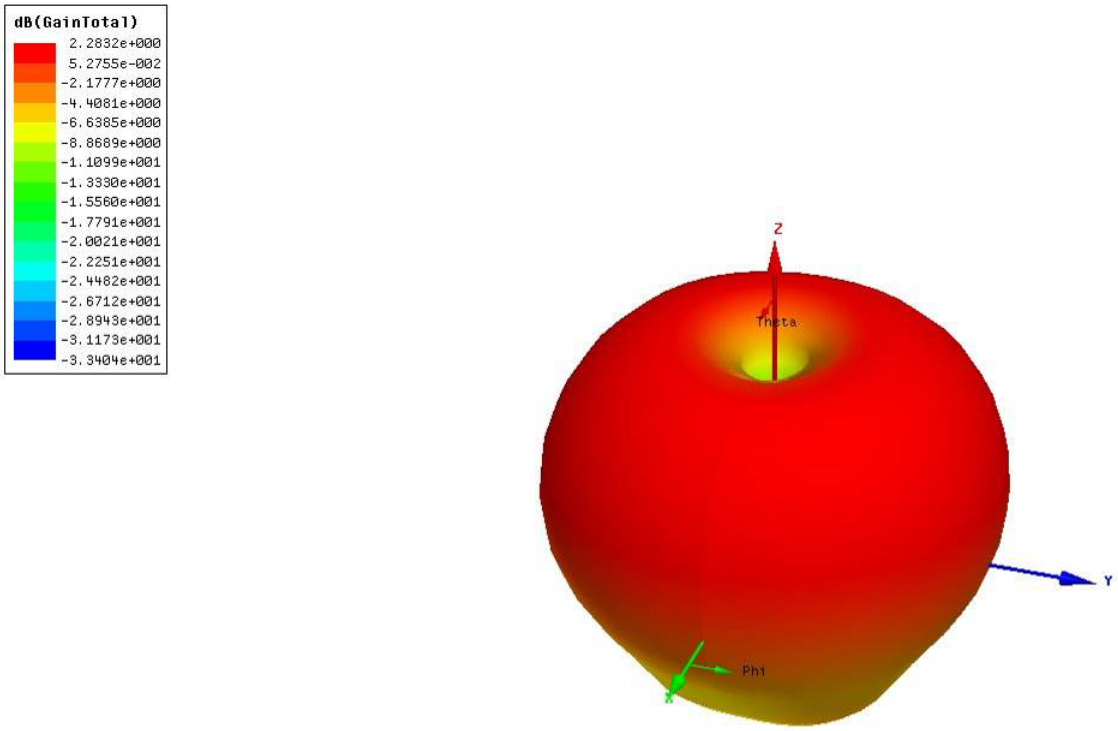

Fig. F. 2. The radiation pattern of the dielectrically loaded (truncated hemisphere) top-hat monopole antenna at 110 MHz. Note, that mismatch loss is not taken into account.

III. RESONANT FREQUENCY

The antenna shown in Fig. F. 1 has an interesting performance. It does resonate at about 50 MHz as Fig. F. 3 shows. The corresponding simulations in Ansoft HFSS have been done with a large PML box on the size of 5m×5m×5m (the PML thickness was 2.5m), with the lowest frequency of 30 MHz, and on fine meshes with about 100,000 tetrahedra and better. Note that the wavelength at resonant frequency of 50 MHz is 6m. Thus, the selected PML size guarantees us the good accuracy at low frequencies up to 30 MHz.

Only the discrete frequency sweep has been used. The computed resonant frequency of 50 MHz is

i. much lower than the resonant frequency of a stand-alone equivalent cylindrical dielectric resonator antenna in the $TM_{01\delta}$ mode (230 MHz) and;

ii. much lower than the resonant frequency of the stand-alone quarter-wave unloaded monopole (500MHz).

Therefore, it appears that we have a new combined effect of two basic resonant structures.

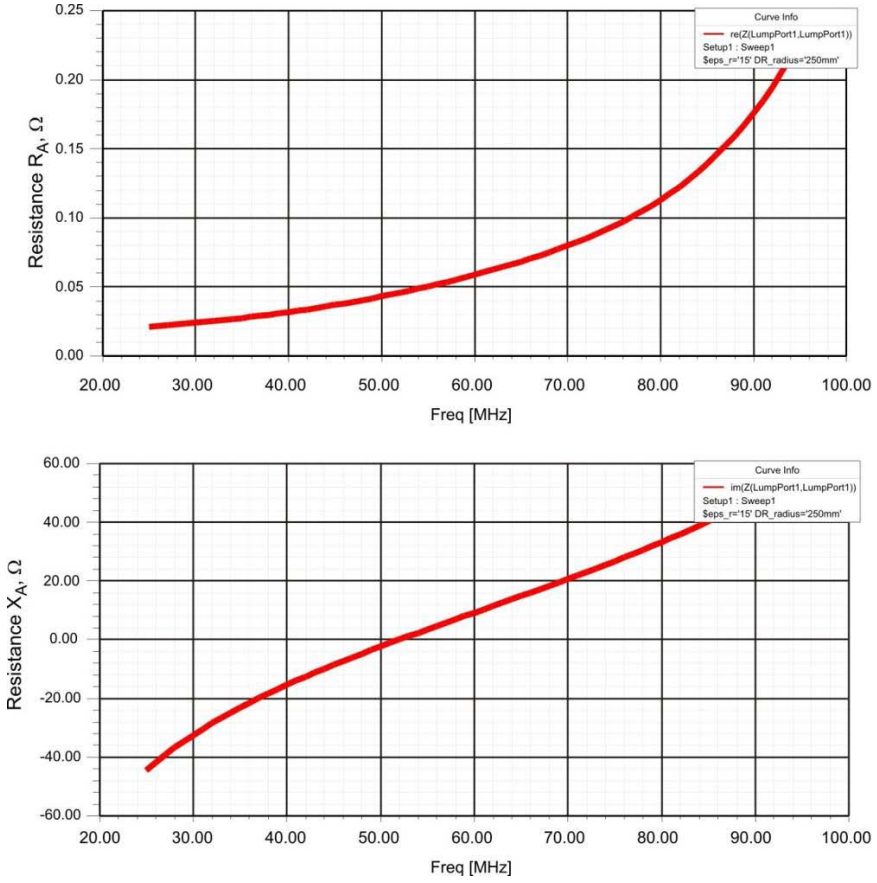

Fig. F. 3. Input impedance of the spherical-sector antenna. The resonance is observed at 50 MHz.

At the same time, the radiation resistance of the antenna in Fig. F.1 is very small, on the order of 0.1Ω and less at the resonance. Therefore, the antenna should be matched over the band using a dedicated lumped circuit - the equalizer.

IV. EXTRACTING MODEL PARAMETERS FOR A RESONANT ELECTRICALLY SMALL TOP-HAT DIELECTRICALLY (TRUNCATED HEMISPHERE) LOADED MONOPOLE ANTENNA

The LCR parameters of the series resonant circuit must be extracted for proper impedance matching and efficient equalizer design. The input impedance of the dipole using a series RLC circuit as the model is given by

$$Z(\omega) = R + sL + \frac{1}{sC} \tag{1}$$

Here, $s = j\omega$ is the complex frequency. Therefore we rewrite Eq. (1) in terms of ω shown in Eq. (2)

$$Z(\omega) = R + j\left(\omega L - \frac{1}{\omega C}\right) \tag{2}$$

Our goal is to extract the parameters R, L and C given the frequency dependent impedance $Z(\omega)$. In this case, the impedance data has been obtained through simulation of the antenna in Ansoft HFSS - see Fig. F.3. The impedance data is obtained in complex form, i.e. $Z(\omega) = R + jX$ at N frequency points. In order to extract L and C, we consider the following set of equations for the reactance obtained from Eq. (2),

$$\mathrm{Im}\{Z(\omega_n)\} = \frac{\omega_n^{\,2} LC - 1}{\omega_n C} = X(\omega_n) \quad \forall n = 1 \ldots N \tag{3}$$

If we expand this equation out we obtain

$$\omega_n{}^2 LC - \omega_n CX(\omega_n) - \mathbf{1} = \mathbf{0} \quad \forall n = \mathbf{1}\ldots N \tag{4}$$

For each frequency point, this equation needs to be satisfied, i.e.

$$\begin{array}{l} \omega_1{}^2 LC - \omega_1 CX(\omega_1) - \mathbf{1} = \mathbf{0} \\ \omega_2{}^2 LC - \omega_2 CX(\omega_2) - \mathbf{1} = \mathbf{0} \\ \vdots \qquad\qquad \vdots \qquad\qquad \vdots \\ \omega_N{}^2 LC - \omega_N CX(\omega_N) - \mathbf{1} = \mathbf{0} \end{array} \tag{5}$$

This can be written in matrix-vector notation as,

$$\begin{bmatrix} \omega_1^2 & -\omega_1 X(\omega_1) & -\mathbf{1} \\ \vdots & \vdots & \vdots \\ \omega_N^2 & -\omega_1 X(\omega_1) & -\mathbf{1} \end{bmatrix} \begin{bmatrix} LC \\ C \\ \mathbf{1} \end{bmatrix} = \begin{bmatrix} \mathbf{0} \\ \vdots \\ \mathbf{0} \end{bmatrix} \tag{6}$$

Eq. 6 is an overdetermined matrix equation that shall be solved by SVD. It can be written as

$$W\vec{x} = \vec{\mathbf{0}} \tag{7}$$

This implies that the solution $\vec{x}$ belongs to the null-space of *W*. If *W* were square, we could have computed the eigen-decomposition and this would have given us the necessary eigenvector solution. However, here we have a tall matrix, and so we use the SVD (Singular Value Decomposition) instead. The result of the SVD on the matrix *W* is shown in Eq. (8)

$$W = U\Sigma V \tag{8}$$

where, U and V are the matrices and the diagonal matrix Σ comprises the singular values of *W***.** Out of this result we need the right singular vector only, since this is the desired solution to Eq. 7. The column vectors of *V* are this exactly and we choose the vector that has all positive values and has its final entry closest to 1. The resistance value for this model is chosen to be the average value of resistance from the simulated impedance data. The model parameters are given below in Table 1 that follows.

Table F. 1. Model parameters of the input impedance.

R	**0.07 Ω**
L	**83.688 pF**
C	**114.41 nH**

The corresponding parameter approximation is given in Fig. F. 4.

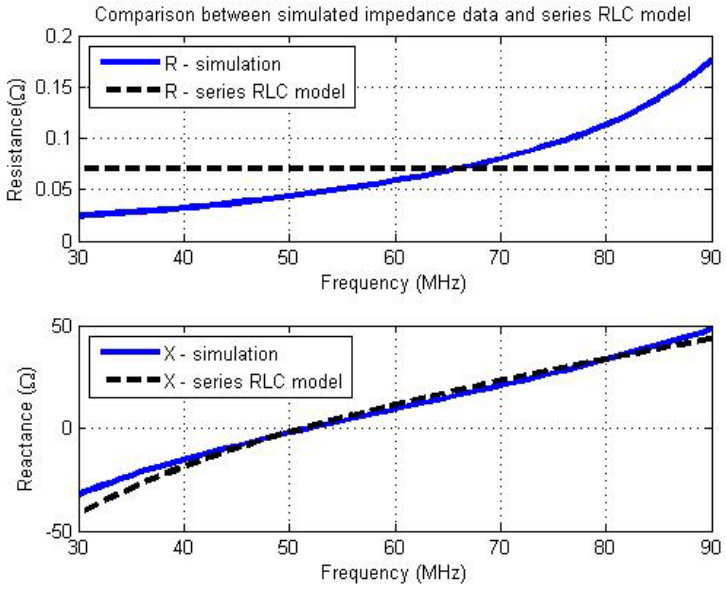

Fig. F. 4. Comparison between the extracted and exact antenna parameters - see Table F.1.

Note that the average resistance approximation might be good enough since the actual value are small enough.

V. IMPEDANCE MATCHING AT 30-80 MHZ FOR THE BLADE MONOPOLE

Geometry

In Fig. F.5 – a variation of the standard blade monopole, used commonly on aircraft, from Ref. [88] is shown and Fig. F.6 shows its radiation pattern.

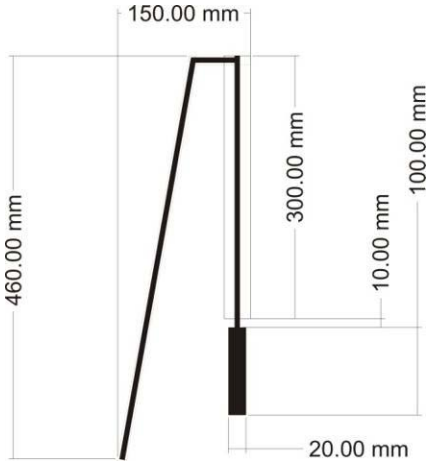

Fig. F. 5. The blade monopole from [88].

Radiation pattern

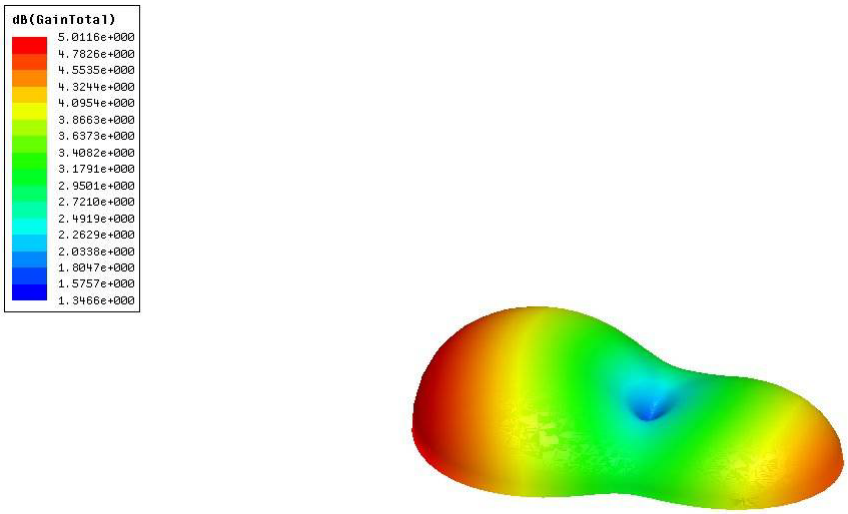

Fig. F. 6. Radiation pattern of the blade monopole at 110 MHz.

Matching network

A 4-component impedance-matching network [86], [87] shown in Fig. F.7, is used for the blade monopole geometry shown in Fig. F.5. The network is composed of a series inductor, a tank circuit in shunt, and a resistor. This network provides a consistent VSWR over the band. At the same time, the matching network is lossy: it includes a tank circuit in series with a resistor. The required resistor value is approximately equal to R_A.

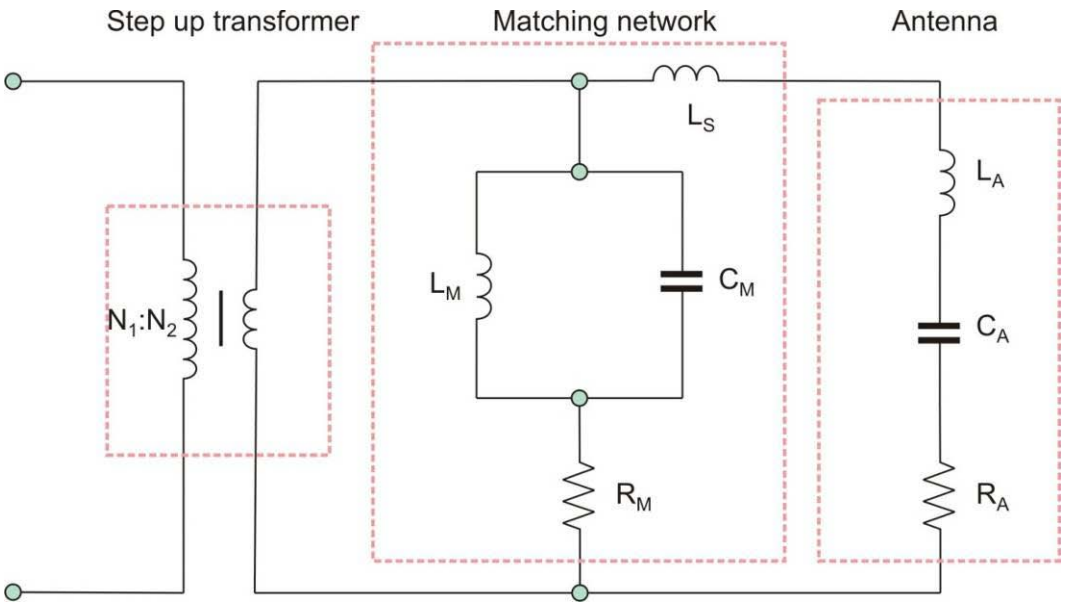

Fig. F. 7. Antenna matching: the impedance-matching network and a step-up transformer.

An equivalent circuit for such an antenna is the series LCR circuit. The DR antenna as well as the blade monopole introduced above in Fig. F. 4 belongs to exactly this type.

The matching network outputs a real, but still small impedance on the order of R_A uniformly over the band. Therefore, it should be followed by a step-up impedance transformer as shown in Fig. F.7. An alternative may be to switch the matching network and the low-loss transformer in the RX mode at least, which might, under certain conditions, result in a better overall power efficiency.

We calculate the transducer gain for this network as follows

$$T(\omega^2) = \frac{4R_T(\omega)R(\omega)}{\left|Z_A(\omega) + Z_T(\omega)\right|^2}$$

Here, we calculate the Thevenin equivalent for the network as shown in Fig. F.8. The antenna resistance $R = R_A$ from Fig. F. 7.

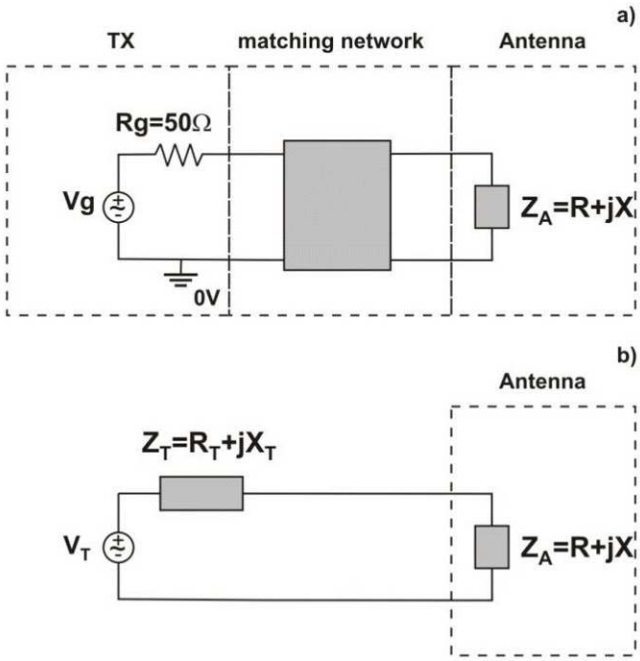

Fig. F.8. Transformation of the matching network: a) lossy matching network representation, b) Thévenin-equivalent circuit representation. The matching network does not include transformers.

Since the network in Fig. F. 7 is lossy, the one to one relationship between the transducer gain and the reflection coefficient doesn't exist. Therefore we calculate the reflection coefficient and hence, VSWR at the input to the network cascaded with the antenna's impedance.

The result of model parameter extraction for the blade monopole yielded the results shown in Fig. F. 9. Here we see that an acceptable agreement is present for the reactance

data while the resistance has been approximated to be constant over the band. This resistance value is indeed quite low and hence we determined a matching impedance of 1Ω to match for prior to the transformer. We note the presence of a resonance within the band at approximately 47 MHz. This resonance essentially validates the LCR model for the antenna as well.

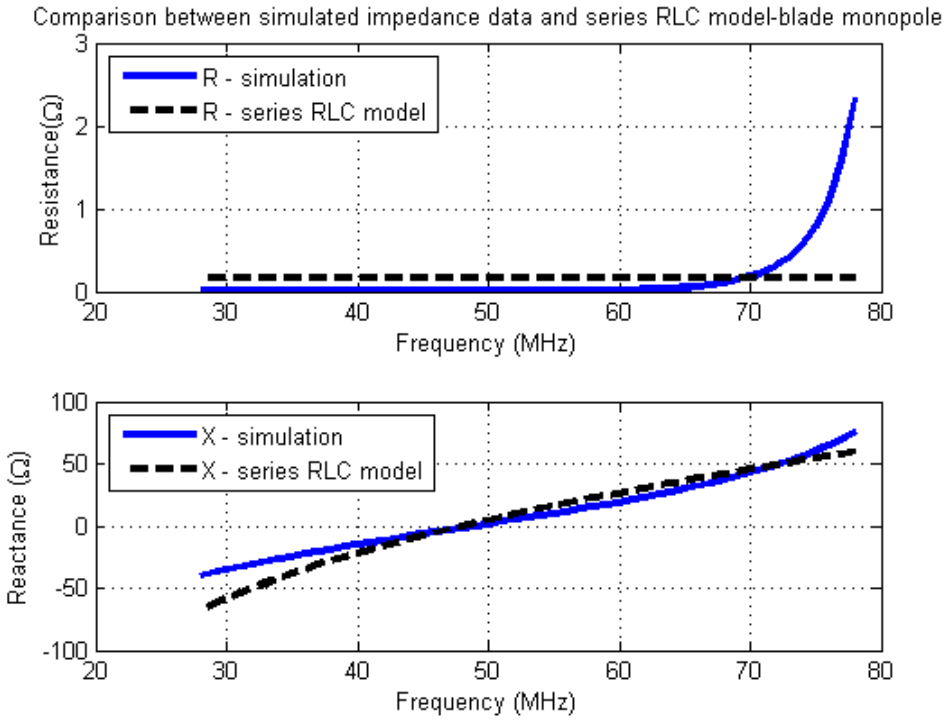

Fig. F. 9. Comparison of the impedance data from simulation and the extracted LCR model for the blade monopole.

Results

By using the appropriate matching network, we calculate the VSWR and the transducer gain as a function of frequency. The band to be matched over is 30 - 80 MHz. The use of the reflection-less equalizer gives a flat VSWR profile, while the transcuer gain behavior over the band shows the narrowband response.

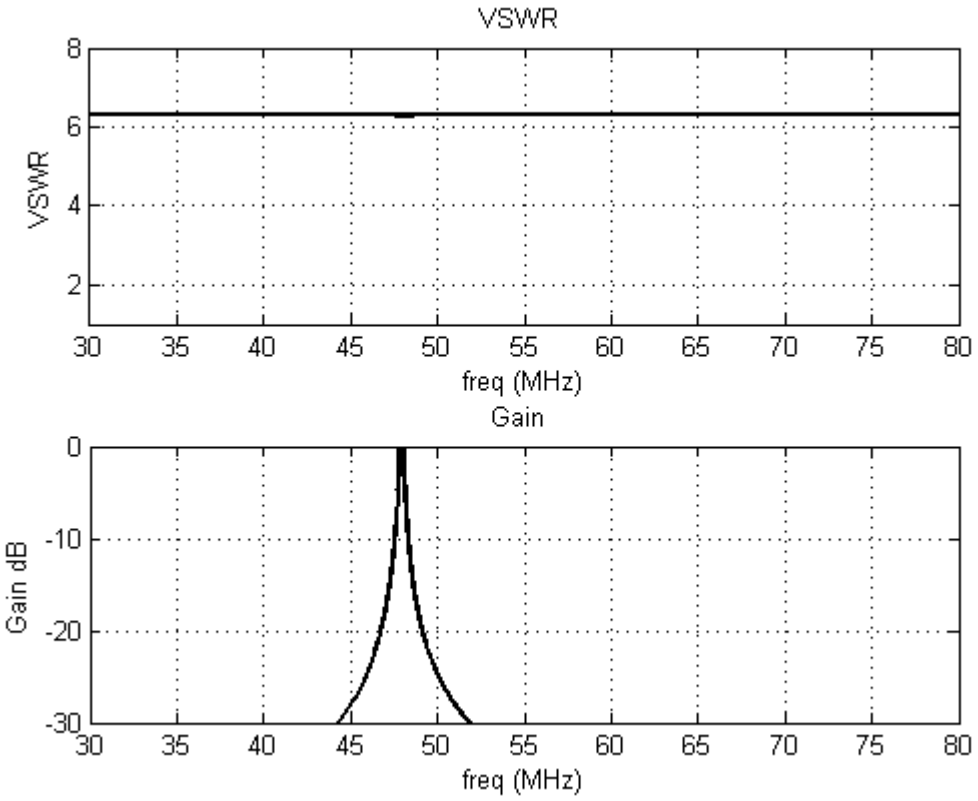

Fig. F. 10. VSWR at the input to the reflection less equalizer and transducer gain for the blade monopole antenna.

Appendix G – Code

```
function [ZA] = dipole(f, dipole_x, dipole_y);

%    Dipole self-impedance: analytical solution for the cylindrical or
strip dipole

%    C.-T. Tai and S. A. Long, “Dipoles and monopoles,” in: Antenna
Engineering Handbook,

%    John L. Volakis, Ed., Mc Graw Hill, 2007, fourth edition, pp. 4-3
to

%   4-32.

%   EM data

const.epsilon       = 8.85418782e-012;  %  ANSOFT HFSS value

const.mu            = 1.25663706e-006;  %  ANSOFT HFSS value

const.c             = 1/sqrt(const.epsilon*const.mu);

const.eta           = sqrt(const.mu/const.epsilon);

k   = 2*pi*f/const.c;

kl  = k*dipole_y/2;

a   = dipole_x/2;       %   equivalent radius

l   = dipole_y/2;

R   = -0.4787 + 7.3246*kl   + 0.3963*kl.^2 + 15.6131*kl.^3;

R(find(R < 0)) = 0;

X   = -0.4456 + 17.00826*kl - 8.6793*kl.^2 + 9.6031*kl.^3;

ZA  = R - j*(120*(log(l/a)-1)*cot(kl)-X);   %   Antenna impedance
```

```
function [ZA,L] = smallLoop(f,loop_a,loop_b)
% This function calculates the Impedance of a small circular loop based
on input parameters which are the frequency, loop radius and loop
conductor width.

%   EM data
const.epsilon       = 8.85418782e-012;  %  ANSOFT HFSS value
const.mu            = 1.25663706e-006;  %  ANSOFT HFSS value
const.c             = 1/sqrt(const.epsilon*const.mu);
const.eta           = sqrt(const.mu/const.epsilon);

lambda    = const.c./f;
Circ_umf  = 2*pi*loop_a;                    % loop circumference

Rr        = 20*(pi^2)*((Circ_umf./lambda).^4);    % Radiation resistance
of a small circular loop
L           = const.mu*loop_a*(log(8*loop_a/loop_b) - 2);   % Inductance
of small circular loop
Xl          = 2*pi.*f*L;

ZA          = Rr + 1i.*Xl;
```

```
%     A script for matching circuit estimation at different center
frequencies fc and bandwidths B. Saves the matching circuit parameters
and optimized performance dataset for every parameter set.

% S. Makarov and V. Iyer, ECE Dept., WPI Aug. 2008

dipole_y  = 230e-3;            %   dipole length (m)

Rg        = 50;                %   generator resistance

f_res     = 3e8/(2*dipole_y);  %    resonant frequency (ideal; half-wave
resonance)

Ls = [1 1 1 1 1]*eps;          %  lower initial bounds for the parameter
search

Us = [2e-6 1e-6 100e-12 1e-6 100e-12];  % upper initial bounds for the
parameter search

                               % (optimized for 150mm length)

Us = Us*(dipole_y/150e-3);     %  good for any length

dipole_lt   = [20];            %   length to width ratio

DCF         = [0.5];           %   relative center frequency vs. f_res

FB          = [0.5];                   %   fractional bandwidth


MeanGain    = zeros(   length(dipole_lt), length(DCF), length(FB));

VarGain     = zeros(   length(dipole_lt), length(DCF), length(FB));

CP_nHpF     = zeros(5, length(dipole_lt), length(DCF), length(FB));


for ilt = 1:length(dipole_lt)

    for iDCF = 1:length(DCF)

        for iFB = 1:length(FB)

            dcf = DCF(iDCF); fb  = FB(iFB);

            run.center_freq     = dcf;

            run.bandwidth       = fb;

            run.dipole_lt       = dipole_lt(ilt);

       %-----------------------------------------------------------------
```

```
            [temp1  temp2 CP] = ...
            optimizer02_function(dipole_y, dipole_lt(ilt), Rg, dcf, fb,
Ls, Us);
            MeanGain(ilt, iDCF, iFB)    = temp1;
            VarGain (ilt, iDCF, iFB)    = temp2;
            CP_nHpF(:, ilt, iDCF, iFB)  = CP.*[1e9 1e9 1e12 1e9 1e12]';
            run.gain = temp1; run

%%%%%%%%%%%%%%%%%%%%%%%%%%%%%%%%%%%%%%%%%%%%%%%%%%%%%%%%%%%%%%%%%%%%%%%%
            %   Post-processing (plot)
            thisfile = strcat('fig_lt_', num2str(dipole_lt(ilt)), ...
                                    '_FB_',   num2str(fb),   '_DCF_'   ,
      num2str(dcf));
            if temp1 >0
                dipole_x      =  dipole_y/dipole_lt(ilt); %dipole  width
(m)
                F            = linspace(0.01*f_res, 1.0*f_res, 2e5);  %
full spectrum
                ZA               = dipole(F, dipole_x, dipole_y); RL =
real(ZA);
                s           = j*2*pi*F;
%-------------------------------------------------------------------
                Zg   =  s*CP(4).*(Rg  +  1./(s*CP(5))./(s*CP(4)  +  (Rg  +
1./(s*CP(5)))) +...
                                                        1./(s*CP(3));
                ZT  = s*CP(2).*Zg./(s*CP(2) + Zg) + s*CP(1);
%-------------------------------------------------------------------
                Gain = (4*RL).*real(ZT)./((abs(ZA+ZT)).^2);
                ind    =  find(abs(F/f_res-dcf)<fb*dcf/2  +  0.5*(F(2)-
F(1))/f_res);
                GM     =  mean(Gain(ind));  GV  =  100*max(abs(Gain(ind)-
GM)/GM);  %  just checking on a finer grid
```

```
                h = figure; semilogy(F/f_res, Gain, 'LineWidth', 2);
grid on; hold on;

                line([dcf-fb*dcf/2    dcf-fb*dcf/2], [1e-4 1], 'Color',
'g');

                line([dcf+fb*dcf/2    dcf+fb*dcf/2], [1e-4 1], 'Color',
'g');

                line([dcf,                dcf],             [1e-4 1],
'LineWidth', 2, 'Color', 'r');

                title(strcat('Average gain, a.u. = ', num2str(GM), ';
Variation(%) =', num2str(GV)));

                xlabel('f/f_{res}');        ylabel('Gain,        a.u.');
axis([min(F/f_res) max(F/f_res) 1e-4, 1]);

                saveas(h, strcat(thisfile, '.fig'));

            end


%%%%%%%%%%%%%%%%%%%%%%%%%%%%%%%%%%%%%%%%%%%%%%%%%%%%%%%%%%%%%%%%%%%%%%%%

            close all;

        end

    end

end

save;
```

```
function [MeanGain VarGain CP] = optimizer02_function(dipole_y,
dipole_lt, Rg, DCF, FB, Ls, Us);
%   Matching circuit optimizer for a dipole - a reflective equalizer
%   Direct search on 1D arrays; the search here is limited to 5 circuit
%   elements
%
%   dipole_y  - dipole length
%   dipole_lt - length-to-width or length-to-radius ratio
%   DCF       - relative center frequency fc/f_res
%   FB        - fractional bandwidth vs. center frequency
%   Ls        - lower bound of search parameters
%   Us        - upper bound of search parameters
%   There are no output arguments; the function saves all data in a mat
%   file.
%
%   1D Array assembly in parameter space:
%   (M(1) = 3; M(2) = 2; M(3) = 2; M(4) = 2; M(5) = 1)
%    [1 2 3][1 2 3][1 2 3][1 2 3][1 2 3][1 2 3][1 2 3][1 2 3]     M(1)
A(1, :)
%    [1 1 1][2 2 2][1 1 1][2 2 2][1 1 1][2 2 2][1 1 1][2 2 2]     M(2)
A(2, :)
%    [1 1 1][1 1 1][2 2 2][2 2 2][1 1 1][1 1 1][2 2 2][2 2 2]     M(3)
A(3, :)
%    [1 1 1][1 1 1][1 1 1][1 1 1][2 2 2][2 2 2][2 2 2][2 2 2]     M(4)
A(4, :)
%    [1 1 1][1 1 1][1 1 1][1 1 1][1 1 1][1 1 1][1 1 1][1 1 1]     M(5)
A(5, :)
%   S. Makarov and V. Iyer, ECE Dept., WPI Aug. 2008
```

```
%   Antenna/generator/bandwidth

dipole_x        = dipole_y/dipole_lt;   %   dipole width (m)

f_res            = 3e8/(2*dipole_y);     %   resonant frequency (ideal;
half-wave resonance)

B                  = 4;                        %    number of frequency
observation points over the bandwidth

f_center         = DCF*f_res;             %   absolute center frequency
vs. f_res

bandwidth       = FB*f_center;          %   absolute bandwidth


%   Bandwidth  discretization for initial and final search

f      = linspace(f_center-bandwidth/2, f_center+bandwidth/2, B);     %
initial search

s     = j*2*pi*f;                                                          %
initial search

ZA     = dipole(f, dipole_x, dipole_y); RL = real(ZA);                %
initial search

f1      = linspace(f_center-bandwidth/2, f_center+bandwidth/2, 16*B); %
final search

s1     = j*2*pi*f1;                                                         %
final search

ZA1    = dipole(f1, dipole_x, dipole_y); RL1 = real(ZA1);             %
final search


%   Equalizer circuit

M(1) = 128;                          %   first parameter search space

M(2) = 064;                          %   second parameter search space

M(3) = 032;                          %   third parameter search space

M(4) = 016;                          %   fourth parameter search space

M(5) = 016;                          %   fifth parameter search space

A     = complex(zeros(5, prod(M)));    %   all parameter values assembled
in linear arrays
```

```
Gain = zeros(1, prod(M));            %   the generator gain

Par_min = Ls;                          %   lower initial bounds for the
parameter search

Par_max = Us;                          %   upper initial bounds for the
parameter search

%    main loop over the seach domains (the domain is refined at every
step)

VarGain          = 0;                      %   controls gain variation
over the band (global)

MeanGain        = 0;                     %   controls mean gain over the
band (global)

TGain           = 0;                     %   controls max mean gain over
the band (loop)

TGain_plot      = TGain;                 %   visualize gain improvement
over the seach

CP                = zeros(length(M), 1);  %   circuit parameters to be
found (global)

search_domains  = 7;                    %   number of domain iterations

for search_domains_ind = 1:search_domains

    StopGain = 0; tic                       %    controls the current
iteration

    %   Circuit parameters (cell arrays)

    par(1)    = {linspace(Par_min(1), Par_max(1),  M(1))};  %    L1 here
(0)

    par(2)    = {linspace(Par_min(2), Par_max(2),  M(2))};  %    L2 here
(inf)

    par(3)    = {linspace(Par_min(3), Par_max(3),  M(3))};  %    C3 here
(inf)

    par(4)    = {linspace(Par_min(4), Par_max(4),  M(4))};  %    L4 here
(inf)

    par(5)    = {linspace(Par_min(5), Par_max(5),  M(5))};  %    C5 here
(inf)

    %   Fill out the 1D arrays

    temp  = 1;
```

```
    for m = 1:length(M)
        if m >1
            temp = prod(M(1:m-1));
        end
        block_length  = temp;
        no_of_blocks  = prod(M(m+1:end));
        A(m,  :)              =  reshape(repmat(par{m},  block_length,
no_of_blocks), 1, prod(M));
    end
    %     Find  min  power  over  the  entire  frequency  band  for  every
particular parameter set
    for m = 1:length(s)
        %-------------------------------------------------------------
----
        Zg  = s(m)*A(4, :).*(Rg + 1./(s(m)*A(5, :))./( s(m)*A(4, :) +
(Rg+1./(s(m)*A(5, :))) ) +...
                                                1./(s(m)*A(3, :));
        ZT  = s(m)*A(2, :).*Zg./(s(m)*A(2, :) + Zg) + s(m)*A(1, :);
        %-------------------------------------------------------------
----
        if m ==1
            Gain =(4*RL(m))*real(ZT)./((abs(ZA(m)+ZT)).^2);
        else
            Gain = min(Gain,(4*RL(m))*real(ZT)./((abs(ZA(m)+ZT)).^2));
        end
    end
    %   Sort that power (most CPU time-involved step)
    [dummy index] = sort(uint16(1e6*Gain), 'descend');
    %     Check  if  the  +/-25%  criterion  of  gain  variation  is  really
satisfied on a finer grid
```

```
    for p = 1:round(prod(M)/128)     %   a critical point: only initial
values are examined

        temp    = index(p);         %   index into arrays

        a         = A(:, temp);         %    obtain particular circuit
parameters

        %--------------------------------------------------

        Zg_             =  s1*a(4).*(Rg  +  1./(s1*a(5))./(  s1*a(4)  +
(Rg+1./(s1*a(5))) ) +...

                                            1./(s1*a(3));

        ZT_       = s1*a(2).*Zg_./(s1*a(2) + Zg_) + s1*a(1);

        %--------------------------------------------------

        Gain_ = (4*RL1).*real(ZT_)./((abs(ZA1+ZT_)).^2);

        MGain = mean(Gain_);                                          %
local mean gain

        VGain  =  100*max(abs(Gain_-MGain)/MGain);                    %
local gain variation

        if  (VGain <= 25)                                          %   +/-
25% satisfied

            if (MGain> TGain)                                         %
search for a higher average gain

                VarGain = VGain; MeanGain = MGain; CP = a;

                TGain       = MGain;                                  %
TGain controls the loop

                StopGain    = MGain;                                  %
StopGain controls the loop iteration

                TGain_plot  = [TGain_plot  TGain];                    %
Convergence history

                plot(TGain_plot, '-bs',...;                           %
Plot converegence history

                'MarkerEdgeColor',    'k',    'MarkerFaceColor',    'g',
'MarkerSize',10);

                title('Gain convergence'); hold on; grid on; drawnow;

            end
```

```
        end

    end

    if TGain    == 0 return; end;                    %   found none -
exit this function

    if StopGain == 0 break; end;                      %   found none
for this iteration (no more iterations)

    %     Find  the  bettter  search  range  based  on  the  found  circuit
parameters (+/- 50%)

    Par_min   = 0.50*CP;

    Par_max   = 1.50*CP; toc

End
```

```
%   Bode-Fano criterion for the dipole

%   Dipole parameters
dipole_y        = 230e-3;             %   dipole length (m)
dipole_lt       = 10;
dipole_x        = dipole_y/dipole_lt; %   dipole width (m)
f_res           = 3e8/(2*dipole_y)
f_center        = [0.05:0.01:0.5]*f_res;

b = figure;
z   = pi/2*f_center/f_res;
a   = dipole_x/2;       %   equivalent radius
l   = dipole_y/2;       %   half-length
R   = -0.4787 + 7.3246*z   + 0.3963*z.^2 + 15.6131*z.^3;
R = R./2; % Monopole impedance is half of dipole
GBP = 4*pi^2*R./480.*(f_center/f_res)/(log(l/a)-1);

B = 0.50;
G   = 1- exp(-GBP*(1-(B^2)/4)/B);
semilogy(f_center/f_res, G, 'r', 'LineWidth', 2);
grid on;
hold on

axis([min(f_center/f_res), max(f_center/f_res), 1e-3, 1])
```

```
% This script calculates the upper bound on system efficiency for antennas (below first resonance) and matching network combination. The antenna is assumed to be lossless and its Q is approximated using Q(w=w_0) = X(w=w_0)/R_r(w=w_0). This upper bound holds under the following conditions
%
% 1. All elements in network of the same type electric/magnetic have equal Q
% 2. These elements store energy in a form opposite to the antenna
% 3. Generator  is lossless

% Author: V. Iyer, S. Makarov, WPI, Oct.2008
%

%%  SMALL DIPOLE CALCULATION
dipole_y        = 150e-3;               %   dipole length (m)
Rg              = 50;                   %   generator resistance
f_res            = 3e8/(2*dipole_y);     %   resonant frequency (ideal; half-wave resonance)
dipole_lt       = [5 10 50];                %   length to width ratio
DCF                 = [0.05:0.05:0.5];              %    relative center frequency vs. f_res
f_center         = DCF*f_res;             %   absolute center frequency vs. f_res
f    = linspace(f_center(1), f_center(end), 64);
figure
Antenna_Q = zeros(3,length(f));

for loop = 1:length(dipole_lt)
    dipole_x = dipole_y/dipole_lt(loop);
    ZA  = dipole(f, dipole_x, dipole_y);
    R   = real(ZA);
    X   = imag(ZA);
    % Q approximation for antenna
    Q_a  = abs(X)./R;
    eta_a = 1;
```

```
    % component Q - Matching Network  comprising of L section L1, L2 -
% CHANGE TO 55
    Q_mn    = 55;
    eta_mn  = 1./(1 + (Q_a./Q_mn));
    % System Efficiency
    eta_s = eta_a*eta_mn*100;
    Antenna_Q(loop,:)  = Q_a;
    semilogy(f/f_res, eta_s,'LineWidth',2)
    grid on
    xlabel('f_c/f_r_e_s')
    ylabel('% System Efficiency - \eta_s')
    title('Efficiency bound at center of band for short dipole -   3
geometries')
    hold all
end
legend('l_A/d = 5','l_A/d = 10','l_A/d = 50')

axis([min(f/f_res) max(f/f_res) 1e-2 1e2])
figure
for loop = 1:length(dipole_lt)
    plot(f/f_res,Antenna_Q(loop,:));
    hold all
end
grid on
xlabel('f_c/f_r_e_s')
ylabel('Q_A_N_T')
title('Antenna Q factor -  Dipole')
legend('l_A/d = 5','l_A/d = 10','l_A/d = 50')

%% SMALL CIRCULAR LOOP CALCULATION

f_res           = 1e9;
loop_a          = 3e8/(2*pi*f_res);     % loop radius
Circ_umf        = 2*pi*loop_a;          % loop circumference
Rg              = 50;                   %   generator resistance
Omega           = [8 10 12];               % Conductor thickness factor
f_min           = 3e8/(10*Circ_umf);
f_max           = 3e8/(4*Circ_umf);
```

```
f_min           = f_min/f_res;f_max = f_max/f_res;
DCF              = f_min:f_min/2:f_max;             %   relative center
frequency vs. f_res
f_center         = DCF*f_res;              %   absolute center frequency
vs. f_res
% Set of Center Frequencies
f                = linspace(f_center(1), f_center(end), 64); %    final
search
figure
Antenna_Q = zeros(3,length(f));
for loop = 1:length(Omega)
    loop_b        = Circ_umf*exp(-Omega(loop)/2);    %    loop conductor
width (m)
    ZA          = smallLoop(f, loop_a, loop_b);
    R           = real(ZA);            %    final search
    X           = imag(ZA);
    % Q approximation for antenna
    Q_a  = abs(X)./R;
    eta_a = 1;

    % component Q - Matching Network  comprising of C section C1, C2
    Q_mn    = 1000;
    eta_mn  = 1./(1 + (Q_a./Q_mn));
    % System Efficiency
    eta_s = eta_a*eta_mn*100;
    % Plots
    semilogy(f/f_res, eta_s,'LineWidth',2)
    grid on
    xlabel('f_c/f_r_e_s')
    ylabel('% System Efficiency - \eta_s')
    title('Efficiency bound at center of band for small Loop -   3
geometries')
    hold all
    Antenna_Q(loop,:) = Q_a;
end

legend('\Omega = 8','\Omega = 10','\Omega = 12')
axis([min(f/f_res) max(f/f_res) 1 1e2])
```

```
figure
for loop = 1:length(dipole_lt)
    plot(f/f_res,Antenna_Q(loop,:));
    hold all
end
grid on
xlabel('f_c/f_r_e_s')
ylabel('Q_A_N_T')
title('Antenna Q factor -  Loop')
legend('\Omega = 8','\Omega = 10','\Omega = 12')
```

```
% Matching Circuit design for a dipole -  Reflective Equalizer
% HYBRID GA
    %   Using Genetic Algorithm -  Vectorized
    %   Using Pattern Search to refine
% Both Low pass and High pass + L - section are available for design
% The population size has been reduced and a no. of independent GA runs
are used to determine the best candidate
% STATUS : Currently, it uses pattern search on the best starting
% point candidate after a certain number of GA runs have occurred.
%
% Authors : - Vishwanath Iyer, Sergey Makarov, ECE Dept.,WPI,Aug. 2008
%

%%   Antenna/generator/bandwidth
DCF              = 5/12;                  %   relative center frequency
vs. f_res
FB               = 0.4;                %   fractional bandwidth
dipole_y         = 500e-3;              %   dipole length (m)
dipole_lt        = 0.5/0.001;           %   length to width ratio
dipole_x         = dipole_y/dipole_lt;  %   dipole width (m)
f_res            = 3e8/(2*dipole_y);     %   resonant frequency (ideal;
half-wave resonance)
Rg               = 50;                  %   generator resistance
B                  = 32;                        %    number of frequency
observation points over the bandwidth
f_center         = DCF*f_res;             %   absolute center frequency
vs. f_res
bandwidth        = FB*f_center;         %   absolute bandwidth

%   Bandwidth  discretization for initial and final search
f      = linspace(f_center-bandwidth/2, f_center+bandwidth/2, B);     %
initial search
s     = j*2*pi*f;                                                     %
initial search
ZA     = dipole(f, dipole_x, dipole_y); RL = real(ZA);                %
initial search
```

```
%% GA SECTION - Read Genetic algorithm examples in help
M  = 5;                                    % no. of elements in matching
network
nw_choices = {'LP' 'HP'};                  % choose between Low pass and
High pass network
nw_choice = 2;
LB = eps*ones(1,M);                          % lower bound on component
values
if strcmp(nw_choices(nw_choice),'LP')
    UB = [2e-6 1e-6 1e-6 100e-12 1e-6];      % upper bound on component
values - LP (L1 L2 L3 C4 L5)
else
    UB = [2e-6 1e-6 100e-12 1e-6 100e-12];  % upper bound on component
values - HP (L1 L2 C3 L4 C5)
end
popinitRange = [LB;UB];                    % initial range for component
values
N  = 50;                                    % search space -  Population
Size
GAruns = 30;                              % number of independent GA runs

%% For vectorized fitness function
RLvec     = RL.'*ones(1,N);
ZAvec     = ZA.'*ones(1,N);
ZAvec     = ZAvec.';

%% Allocate Memory
LCvals          = zeros(GAruns,M);      % candidate component values in
each run
tempfval          = zeros(1,GAruns);       % to store fitness function
value at each run
tempfinalpop     = zeros(N,M,GAruns);     % to store final population at
each run
%% Core      -  test crossover function choices
% Set options structure for GA
gaoptions = gaoptimset('PopInitRange',popinitRange,...
                       'Generations',100,...
                       'PopulationSize',N,...
```

```
                        'EliteCount',round(N/2),...
                        'MutationFcn',{@mutationadaptfeasible},...
                        'MigrationDirection','forward',...
                        'MigrationInterval',2,...
                        'MigrationFraction',0.35,...
                        'SelectionFcn',@selectionremainder,...
                        'PenaltyFactor',20000,...
                        'TolFun',1e-9,...
                        'StallTimeLimit',inf,...
                        'StallGenLimit',inf,...
                        'Display','iter',...
                        'Vectorized','on',...
                        'PlotFcns', @gaplotbestf);

% Set options structure for Pattern Search
afterN_GA_runs = 5;                                % No. of GA runs after
which to refine result
PSoptions = psoptimset('CompletePoll','on',...
                       'CompleteSearch','on',...
                       'SearchMethod',{@MADSPositiveBasisNp1},...
                       'InitialMeshSize',1e-14,...
                       'MaxIter',30*M,...
                       'TolMesh',1e-16,...
                       'TolCon',1e-16,...
                       'TolX',1e-16,...
                       'TolFun',1e-16,...
                       'PenaltyFactor',100,...
                       'Cache','on',...
                       'PlotFcns',{@psplotbestf},...
                       'Vectorized','off');

FitnessFunction                                    =       @(tempLCvals)
GAfitnessFunc_Vec(tempLCvals,s,Rg,ZAvec,RLvec,nw_choice);
numberOfVariables   = M;
indx_prev = 0;
tic
for loop2 = 1:GAruns
```

```
    [tempLCvals,fval,exitflag,output,final_pop]                          =
ga(FitnessFunction,numberOfVariables,[],[],[],[],LB,UB,[],gaoptions);
    tempfval(loop2) = fval;
    tempfinalpop(:,:,loop2) = final_pop;
    LCvals(loop2,:) = tempLCvals;

%       Refinement loop -  Pattern Search is used to obtain a better
result by taking the best GA candidate point as initial point.
    if (mod(loop2,afterN_GA_runs)==0)
        indx = max(find(tempfval(1:loop2)==min(tempfval(1:loop2))));
        if(indx~=indx_prev)
            initial_pt = LCvals(indx,:);
            RLps     = RL.'*ones(1,size(initial_pt,1));
            ZAps     = ZA.'*ones(1,size(initial_pt,1));
            ZAps     = ZAps.';
            [tempLCvals,    fvalps]    =    patternsearch(@(initial_pt)
GAfitnessFunc_Vec(initial_pt,s,Rg,ZAps,RLps,nw_choice),...

initial_pt,[],[],[],[],LB,UB,[],PSoptions);
            LCvals(loop2,:) = tempLCvals;
            indx_prev = indx;
        end
    end
end
toc
close all;

%-------------------------------------------------------------------------
---
%% Post Processing
%-------------------------------------------------------------------------
---
disp('-----------GA RESULT---------')
[m,n] = size(LCvals);
F       = linspace(0.01*f_res, 1.0*f_res, 2e5);  %   full spectrum
ind1    = min(find(F>min(f))); ind2 =  max(find(F<max(f)));
ind     = [ind1:ind2];
ind     = find(abs(F/f_res-DCF)<FB*DCF/2 + 0.5*(F(2)-F(1))/f_res);
```

```
[ZA]    = dipole(F, dipole_x, dipole_y);
RL      = real(ZA);
s       = j*2*pi*F;
tempGain = zeros(m,length(F));
GainInfo = zeros(m,2);
% Compute the response of the Equalizer across the full spectrum for
each
% case of GA run
for loop = 1:m
    if strcmp(nw_choices(nw_choice),'LP')
        %-------------------------------------------------------------
----
        k1     = 1./(LCvals(loop,4)*s);
        k2     = LCvals(loop,5)*s;
        k3     = LCvals(loop,3)*s;
        Zg     = ((k1.*(Rg+k2))./(k1+(Rg+k2))) + k3;
        ZT          =  s*LCvals(loop,2).*Zg./(s*LCvals(loop,2)  +  Zg)  +
s*LCvals(loop,1);
        %-------------------------------------------------------------
----
    else
        %-------------------------------------------------------------
----
        Zg          =  s.*LCvals(loop,4).*(Rg+1./(s.*LCvals(loop,3))./(
s.*LCvals(loop,4) +...
            (Rg+1./(s.*LCvals(loop,3))) ) + 1./(s.*LCvals(loop,5));
        ZT          =  s*LCvals(loop,2).*Zg./(s*LCvals(loop,2)  +  Zg)  +
s*LCvals(loop,1);
        %-------------------------------------------------------------
----
    end
    tempGain(loop,:)  = 4*RL.*real(ZT)./((abs(ZA+ZT)).^2);
    Gain = tempGain(loop,:);
    GainInfo(loop,1)  = mean(Gain(ind));
    GainInfo(loop,2)                    =         100*max(abs(Gain(ind)-
mean(Gain(ind)))/mean(Gain(ind)));  % percentage

end
```

```
% Find which cases satisfy Gain Variation criterion
best_cases      = find(GainInfo(:,2)<25);
GainData        = GainInfo(best_cases,:);
Gainbest        = tempGain(best_cases,:);
LCval_best      = LCvals(best_cases,:);

% Plot 2 cases and save important parameters to file
if (GainData(:))

%-------- Find the best case for least average gain variation ---------
----------
    ind = find(GainData(:,2)==min(GainData(:,2)));
    Gain1 = GainData(ind,1)
    leastGainVar = GainData(ind,2)

% ------- Find the highest acheived average gain (less than 25% still
valid) --------------------------------
    ind2 = find(GainData(:,1)==max(GainData(:,1)));
    highestGain = GainData(ind2,1)
    GainVar2 = GainData(ind2,2)



% -------Plot both cases ----------------------------------------------
--
    figure
    plot(F/f_res, 10*log10(Gainbest(ind,:)),'LineWidth', 2); grid on;
    title(strcat('Average Gain, a.u. for ',' ',nw_choices(nw_choice),'
n/w -(Least variation) = ' ,num2str(Gain1) ,' ;Gain variation (%) =
',num2str(leastGainVar)));
    line([DCF-FB*DCF/2 DCF-FB*DCF/2], [-30 0], 'Color', 'g');
    line([DCF+FB*DCF/2 DCF+FB*DCF/2], [-30 0], 'Color', 'g');
    line([DCF,         DCF],          [-30 0], 'LineWidth', 2, 'Color',
'r');
    xlabel('f/f_res');
    ylabel('Gain, dB');
    axis([min(F/f_res) max(F/f_res) -30, 0]);
```

```
    figure
    plot(F/f_res, 10*log10(Gainbest(ind2,:)),'LineWidth', 2); grid on;
    title(strcat('Average gain, a.u. for ',' ',nw_choices(nw_choice),'
n/w -(Highest avg. gain) = ',num2str(highestGain), ' ;Gain variation(%)
= ', num2str(GainVar2)));
    line([DCF-FB*DCF/2 DCF-FB*DCF/2], [-30 0], 'Color', 'g');
    line([DCF+FB*DCF/2 DCF+FB*DCF/2], [-30 0], 'Color', 'g');
    line([DCF,          DCF],           [-30 0], 'LineWidth', 2, 'Color',
'r');
    xlabel('f/f_res');
    ylabel('Gain, dB');
    axis([min(F/f_res) max(F/f_res) -30, 0]);

% ----------------------Display circuit parameters and Save File -----
---------------------------------
if strcmp(nw_choices(nw_choice),'LP')

    % Component values
    circuit.L1 = LCval_best(ind,1)*1e6;
    circuit.L2 = LCval_best(ind,2)*1e6;
    circuit.L3 = LCval_best(ind,3)*1e6;
    circuit.C4 = LCval_best(ind,4)*1e12;
    circuit.L5 = LCval_best(ind,5)*1e6;
    disp(strcat('------Component values for LP n/w with least avg gain
variation'))
    circuit

        % Component values
    circuit2.L1 = LCval_best(ind2,1)*1e6;
    circuit2.L2 = LCval_best(ind2,2)*1e6;
    circuit2.L3 = LCval_best(ind2,3)*1e6;
    circuit2.C4 = LCval_best(ind2,4)*1e12;
    circuit2.L5 = LCval_best(ind2,5)*1e6;
    disp(strcat('------Component values for LP n/w with highest avg
gain'))
    circuit2
    filename = strcat('GA_circuit5LP_DCF=',num2str(DCF));
```

```
    filename = strcat(filename,'_FB=');
    filename = strcat(filename,num2str(FB));
    filename = strcat(filename,'.mat');
    save(filename, 'DCF', 'FB', 'GainData', 'Gainbest', 'LCval_best',
'F','gaoptions','PSoptions');
else
    % Component values
    circuit.L1 = LCval_best(ind,1)*1e6;
    circuit.L2 = LCval_best(ind,2)*1e6;
    circuit.C3 = LCval_best(ind,3)*1e12;
    circuit.L4 = LCval_best(ind,4)*1e6;
    circuit.C5 = LCval_best(ind,5)*1e12;
    disp(strcat('------Component values for HP n/w with least avg gain
variation'))
    circuit
        % Component values
    circuit2.L1 = LCval_best(ind2,1)*1e6;
    circuit2.L2 = LCval_best(ind2,2)*1e6;
    circuit2.C3 = LCval_best(ind2,3)*1e12;
    circuit2.L4 = LCval_best(ind2,4)*1e6;
    circuit2.C5 = LCval_best(ind2,5)*1e12;
    disp('------Component values for HP n/w with highest avg gain')
    circuit2


    filename = strcat('GA_circuit5HP_DCF=',num2str(DCF));
    filename = strcat(filename,'_FB=');
    filename = strcat(filename,num2str(FB));
    filename = strcat(filename,'.mat');
    save(filename, 'DCF', 'FB', 'GainData', 'Gainbest', 'LCval_best',
'F','gaoptions','PSoptions');
end
else
    disp('---------No Matching network found------')
end
```

```
function output = GAfitnessFunc_Vec(LCvals,s,Rg,ZA,RL,nw_choice)
% Handles both Low pass and high pass cascades to the L- section.
% Vectorized fitness function;
% LCvals - is of the population size, s is a vector
% ZA and RL have to be supplied as matrices of size NX popsize where N
% is no. of freq points when used by GA

if (nw_choice==1)
    % Impedance calculation for Low pass T network
    k1     = 1./(LCvals(:,4)*s);
    k3     = LCvals(:,3)*s;
    k2     = LCvals(:,5)*s;

    Zg     = ((k1.*(Rg+k2))./(k1+(Rg+k2))) + k3;

    ZT             =   (LCvals(:,2)*s).*Zg./((LCvals(:,2)*s)   +   Zg)   +
(LCvals(:,1)*s);

else
    % Impedance calculation for high pass T network
    k1     = (LCvals(:,4)*s);
    k2     = (Rg + 1./(LCvals(:,3)*s));
    k3     = 1./(LCvals(:,5)*s);

    Zg     = ((k1.*k2)./(k1+k2)) + k3;

    ZT             =   (LCvals(:,2)*s).*Zg./((LCvals(:,2)*s)   +   Zg)   +
(LCvals(:,1)*s);
end

% Gain calculations
tempZ       = real(ZT)./((abs(ZA+ZT)).^2);
Gain        = 4*RL.*tempZ.';
```

```
%% COST FUNCTION CHOICES

% Average reflection coefficient in passband
% output = max(10.*log10(abs((ZT - conj(ZA))./(ZT + ZA))));         %
Works
% output = max((abs((ZT - conj(ZA))./(ZT + ZA))));                  %
Works
output = -min(Gain);                                                %
Works
% output = -mean(Gain);                                          % No

% From Cuthbert
refl_coeffMag = abs((ZT - conj(ZA))./(ZT + ZA));

% Choice - 1 (SWR)
SWR = (1 + refl_coeffMag)./(1 - refl_coeffMag);

% Choice - 2 (SWR^2)
% SWR2 = (1 + (refl_coeffMag.^2))./((1 - (refl_coeffMag.^2)));

% Choice -3 Poincare Metric
P = atanh(refl_coeffMag);

% Choice - 4
% Tx_gain = 10.*log(1 - (refl_coeffMag.^2));
%
% output = max(refl_coeffMag.');
% output = max(SWR');                                               %
Works
% output = max(P');                                                 %
Works
% output = max(SWR2');                                              %
works
```

```
% This script attempts to calculate the R,L and C values of a antenna
model directly from the simulated impedance data

% Author: Vishwanath Iyer, Antenna Lab, WPI, 2008

%%

% Load csv data from file

strip4Z                                                                 =
csvread('Z:\Vishwanath\DRA_materials\DR_deepSearch\Brian_DR\strip4.csv'
);

%%%%%%%%%%%%%%%%%%%%%%%%%%%%%%%%%%%%%%%%%%%%%%%%%%%%%%%%%%%%%%%%%%%%%%%
```

Strip 4

```
freq        = strip4Z(:,1);

Z_A4        = strip4Z(:,2) + 1i.*strip4Z(:,3);

% Set up matching band and extract data

f_min       = 28;                   % MHz

f_max       = 78;                   % MHz

f_c         = (f_min + f_max)/2;

indx_min    = find(freq>=f_min);indx_min = indx_min(1);

indx_max    = find(freq>=f_max);indx_max = indx_max(1);

freqs       = freq(indx_min:indx_max);

Z_A         = Z_A4(indx_min:indx_max);

omega       = 2*pi*freqs.*1e6;

s           = 1i.*omega;                % Complex frequency

%% Form the spectral matrix with reactance data from simulation and
compute SVD

A                                   =   [omega.^2   -imag(Z_A).*omega   -
1.*ones(length(freqs),1).*1];

[U,S,V]     = svd(A);

%% Picking the third column of V  (all positive values and last is
close to 1)

% This column is one of the right singular vectors and spans the null
space of S.

coeffs        = V(:,3)
```

```
params.R      = mean(real(Z_A));
params.C      = coeffs(2);
params.L      = coeffs(1)./params.C;
params
%% Verifying the model
% Impedance of model
Z_model     = params.R + s.*params.L + 1./(s.*params.C);
figure
subplot(211)
plot(freqs,real(Z_A),'LineWidth',3)
hold on
plot(freqs,real(Z_model),'k--','LineWidth',3)
grid on
xlabel('Frequency (MHz)')
ylabel('Resistance(\Omega)')
title('Comparison between simulated impedance data and series RLC
model-STRIP 4')
legend('R - simulation','R - series RLC model','Location','NorthWest')
subplot(212)
plot(freqs,imag(Z_A),'LineWidth',3)
hold on
plot(freqs,imag(Z_model),'k--','LineWidth',3)
xlabel('Frequency (MHz)')
ylabel('Reactance (\Omega)')
legend('X - simulation','X - series RLC model','Location','NorthWest')
grid on
hold off
hold on
```

```
%% This script finds the component value for a reflectionless
matching circuit using the impedance data from HFSS.
% Author: V. Iyer, S. Makarov Antenna Lab, WPI, 2009
%%
f_min       = 30;                   % MHz
f_max       = 80;                   % MHz
f_c         = (f_min + f_max)/2;
freqs       = linspace(f_min,f_max,10000);
omega       = 2*pi*freqs.*1e6;
s           = 1i.*omega;                % Complex frequency
params.R= 0.1592
params.C= 5.5502e-011
params.L= 1.9772e-007
 %% Matching Network  values
L_s        = 1e-9;
L_m        = params.C*(params.R^2);
C_m        = (L_s + params.L)./(params.R^2);
%% Sweep radiation resistance to see change in Transducer gain
res        = 1;
% params.R   = linspace(params.R,100,res);
%% Main
Rg         = 1;
gamma      = zeros(res,length(freqs));
Gain       = zeros(res,length(freqs));
for loop    = 1:res
    % Impedance of model
```

```
    Z_model                    =  params.R(loop)  +  s.*params.L  +
1./(s.*params.C);

    RL                  = real(Z_model);

    % Input Impedance with matching network

    tank_Z                     =  s.*L_m.*(1./(s.*C_m))./(s.*L_m  +
1./(s.*C_m));

    shunt_Z                          =  tank_Z  +  params.R(loop);
% shunt LC tank + R in series

    Z_in                = shunt_Z.*(Z_model + s.*L_s)./(shunt_Z +
Z_model + s.*L_s);



    gamma(loop,:)       = (Z_in - Rg(loop))./(Z_in + Rg(loop));


% ----------------VSWR and Transducer Gain ----------------------
--- %

    Zg                           =  Rg(loop).*shunt_Z./(Rg(loop)  +
shunt_Z);

    ZT                  = Zg + s.*L_s;

    Gain(loop,:)                                                  =
((4*RL).*real(ZT)./((abs(Z_model+ZT)).^2));

    GaindB(loop,:)      = 10*log10(Gain(loop,:));

    VSWR(loop,:)               =  (1  +  abs(gamma(loop,:))./(1  -
abs(gamma(loop,:)));



    % ------------------------------------------------------------
----------

    % Plot

    hold on

    subplot(211)

    plot(freqs,VSWR(loop,:),'k','LineWidth',2)
```

```
    hold on
    xlabel('freq (MHz)')
    ylabel('VSWR')
    title('VSWR ')
    axis([min(freqs) max(freqs) 1 8])
    grid on
    subplot(212)
    plot(freqs,GaindB(loop,:),'k','LineWidth',2)
    xlabel('freq (MHz)')
    ylabel('Gain dB')
    title('Gain ')
%     axis([min(freqs) max(freqs) -30 0])
    grid on
    drawnow;
    pause(0.3)
    hold on
end
```

References

[1] R. M. Foster, “A reactance theorem,” *Bell Sys. Tech. Journal*, vol. 3, pp. 259-267; April, 1924.

[2] J. R. Carson, “Electromagnetic theory and the foundations of electric circuit theory,” *Bell Sys. Tech. Journal*, vol. 6, pp. 1-17, January, 1927.

[3] O. Brune, “Synthesis of a finite 2-terminal network whose driving-point impedance is a prescribed function of frequency,” J. *Math. Phys.*, vol. 10, pp. 191-236, August, 1931.

[4] C. M. son Gewertz, “Synthesis of a finite four-terminal network from its prescribed driving point functions and transfer function,” *J. Math. Phys.*, vol.12, pp. l-257, 1933.

[5] E. A. Guillemin, “Communication Networks V 2,” John Wiley and Sons, Inc., New York, 1935.

[6] S. Darlington, “Synthesis of reactance 4-poles which produce prescribed insertion loss characteristics,” *J. Math. Phys.*, vol. 28, pp. 257-353, September, 1939.

[7] W. L. Everitt, "Output Networks for Radio-Frequency Power Amplifiers," *Proceedings of the IRE*, vol.19, no.5, pp. 723- 737, May 1931.

[8] A. Papoulis, "Foster's Reactance Theorem," *Transactions of the IRE Professional Group on Circuit Theory*, vol. 2, no. 1, pp.106-106, December 1953 doi: 10.1109/TCT.1953.1085212.

[9] W. Geyi, P. Jarmuszewski, Y. Qi, "The Foster reactance theorem for antennas and radiation Q," *IEEE Transactions on Antennas and Propagation*, vol. 48, no. 3, pp.401-408, Mar 2000. doi: 10.1109/8.841901.

[10] S. R. Best, "The Foster reactance theorem and quality factor for antennas," *IEEE Antennas and Wireless Propagation Letters,* vol.3, pp.306-309, 2004 doi: 10.1109/LAWP.2004.839240.

[11] F. E. Terman, "Network Theory, Filters, and Equalizers," *Proceedings of the IRE*, vol.31, no.4, pp. 164- 175, April 1943

[12] A. V. Eastman, "The Application of Filter Theory to the Design of Reactance Networks," *Proceedings of the IRE*, vol.32, no.9, pp. 538- 546, Sept. 1944

[13] H. W. Bode, “Network Analysis and Feedback Amplifier Design,” D. Van Nostrand Company, Inc., Princeton, N. J.; 1945.

[14] S. Roberts, "Conjugate-Image Impedances," *Proceedings of the IRE*, vol.34, no.4, pp. 198p- 204p, April 1946.

[15] F. D. Bennett, P. D. Coleman, A. S. Meier, "The Design of Broad-Band Aircraft-Antenna Systems," *Proceedings of the IRE* , vol.33, no.10, pp. 671- 700, Oct. 1945.

[16] R. M. Fano, *Theoretical Limitations on the Broadband Matching of Arbitrary Impedances*, Technical Report No. 41, Research Laboratory of Electronics, MIT, Jan. 2, 1948, 44 pages.

[17] D. C. Youla, “A new theory of broadband matching,” *IEEE Trans. Circuit Theory*, vol. CT-11, pp. 30-50, March 1964.

[18] W.-K. Chen, “Explicit formulas for the synthesis of optimum broad-band impedance-matching networks,” *IEEE Trans. on Circuits and Systems*, vol. CAS-24, no. 4, pp. 157-169, April 1977.

[19] W.-K. Chen and K. G. Kourounis, “Explicit formulas for the synthesis of optimum broad-band impedance-matching networks II,” *IEEE Trans. on Circuits and Systems*, vol. CAS-25, no. 8, pp. 609-620, Aug. 1978.

[20] W.-K. Chen, *Broadband Matching: Theory and Implementations*, World Scientific, Singapore, 1988, second ed.

[21] R. Gudipati and W.-K. Chen, “Explicit formulas for the design of broadband matching bandpass equalizers with Chebyshev response,” 1995 *IEEE International Symposium on Circuits and Systems*, ISCAS 1995, 28 April – 3 May, Seattle, Washington, USA, vol. 3, pp. 1644-1647.

[22] T. T. Ha and T. H. Dao, “Application of Takahasi’s results to broad-band matching for microwave amplifiers,” *IEEE Trans. on Circuits and Systems*, vol. CAS-26, no. 11, pp. 970-973, Nov. 1979.

[23] H. J. Carlin, “A new approach to gain bandwidth problems,” *IEEE Trans. on Circuits and Systems*, vol. CAS-24, no. 4, pp. 170-175, April 1977.

[24] H. J. Carlin and B. S. Yarman, *Wideband Circuit Design*, CRC Press, Boca Raton, FL, 1997.

[25] T. R. Cuthbert, “A real frequency technique optimizing broadband equalizer elements,” *2000 IEEE International Symposium on Circuits and Systems*, ISCAS 2000, May 28-31, Geneva, Switzerland, vol. 5, pp. 401-404.

[26] E. H. Newman, “Real frequency wide-band impedance matching with nonminimum reactance equalizers,” *IEEE Trans. Antennas and Propagation*, vol.53, no. 11, pp. 3597-3603, Nov. 2005.

[27] D. F. Bowman and E. F Kuester, “Impedance matching, broadbanding, and baluns,” in: *Antenna Engineering Handbook*, John L. Volakis, Ed., Mc Graw Hill, 2007, fourth edition, pp. 52-1 to 52-31.

[28] D. M. Pozar, *Microwave Engineering*, Wiley, New York, 2005, third edition, Chapter 5.

[29] S. N. Yang, H.Y. Li, M. Goldberg, X. Carcelle, F. Onado, and S. M. Rowland, “Broadband impedance matching circuit design using numerical optimization techniques and field measurements,” *2007 IEEE International Symposium on Power Line Communications and Its Applications*, ISPLC '07, 26-28 March 2007, pp. 425 – 430.

[30] Melvin M. Weiner, *Monopole Antennas*, Marcel Dekker, Inc., New York, 2003, pp. 114-118.

[31] C.-T. Tai and S. A. Long, “Dipoles and monopoles,” in: *Antenna Engineering Handbook*, John L. Volakis, Ed., McGraw Hill, 2007, fourth edition, pp. 4-3 to 4-32.

[32] C. A. Balanis, *Antenna Theory. Analysis and Design*, Wiley, New York, 2005, third edition.

[33] L. J. Chu, “Physical limitations of omni-directional antennas,” *J. Appl. Physics*, vol. 19, pp. 1163-1175, 1948.

[34] A. Hujanen, J. Holmberg, and J. C.-E. Sten, “Bandwidth limitation of impedance matched ideal dipoles,” *IEEE Trans. Antennas and Propagation*, vol.53, no. 10, pp. 3236-3239, Oct. 2005.

[35] H. F. Pues and A. R. Van de Capelle, “An impedance matching technique for increasing the bandwidth of microstrip antennas,” *IEEE Trans. Antennas and Propagation*

[36] D. E. Goldberg, *Genetic Algorithms in search, optimization and machine learning*, Addison-Wesley, Reading, MA, 1989.

[37] R. L. Haupt, “Thinned arrays using genetic algorithms,” *IEEE Trans. Antennas and Propagation*, vol. 42, no. 7, pp. 993-999, Nov.1994.

[38] J. M. Johnson and Y. Rahmat-Samii, “Genetic algorithms in electromagnetics,” vol. 45, no. 3, pp. 343-353, Nov.1997.

[39] Alona Boag, Amir Boag, Eric Michielssen, and Raj Mittra, “Design of electrically loaded wire antennas using genetic algorithms,” *IEEE Trans. Antennas and Propagation*, vol. 44, no. 5, pp. 687-695, May 1996.

[40] *GADS* user's guide, The Mathworks, Natick,MA. [Online]. Available: http://www.mathworks.com/access/helpdesk/help/toolbox/gads/

[41] K. Pahlavan, Xinrong Li, J. P. Makela, "Indoor geolocation science and technology," *IEEE Communications Magazine*, vol.40, no.2, pp.112-118, Feb 2002.

[42] D. Cyganski, J. A. Orr and W. R. Michalson, “A Multi-Carrier Technique for Precision Geolocation for Indoor/Multipath Environments”, *Institute of Navigation Proc. GPS/GNSS*, Portland, OR, September 9-12 2003.

[43] S. J. Ingram, D. Harmer, M. Quinlan, "UltraWideBand indoor positioning systems and their use in emergencies," *Position Location and Navigation Symposium, 2004. PLANS 2004* , vol., no., pp. 706- 715, 26-29 April 2004.

[44] Liuqing Yang; G. B. Giannakis, "Ultra-wideband communications: an idea whose time has come," *IEEE Signal Processing Magazine,* vol.21, no.6, pp. 26- 54, Nov. 2004.

[45] J. Mitola III, "Cognitive radio for flexible mobile multimedia communications," *IEEE International Workshop on Mobile Multimedia Communications, (MoMuC '99),* vol., no., pp.3-10, 1999.

[46] J. Mitola III, "Software radio architecture: a mathematical perspective," *IEEE Journal on Selected Areas in Communications,* vol.17, no.4, pp.514-538, Apr 1999.

[47] Andrea Giorgetti, Marco Chiani, Davide Dardari, Riccardo Minutolo, Montanari, Mauro, "Cognitive Radio with Ultra-Wide Bandwidth Location-capable Nodes," *IEEE Military Communications Conference, 2007,* pp.1-7, 29-31 Oct. 2007.

[48] V. H. Rumsey, “Frequency independent antennas,” 1957 IRE National Convention Record, pt. 1, pp. 114 – 118.

[49] J. D. Dyson, “The equiangular spiral antenna,” IRE Trans. on Antennas and Propagation, Vol. AP-7, pp.181-187, April 1959.

[50] R. H. DuHamel and D. E. Isbell, “Broadband logarithmically periodic antenna structures,” 1957 IRE National Convention record, pt.1 pp. 119-128.

[51] Seong-Youp Suh, A. E. Waltho, V. K. Nair, W. L. Stutzman, and W. A. Davis , "Evolution of broadband antennas from monopole disc to dual-polarized antenna," IEEE Antennas and Propagation Society International Symposium 2006, pp.1631-1634, 9-14 July 2006.

[52] http://www.fas.org/spp/military/program/track/cobra_dane.htm

[53] A. A. Oliner and R. G. Malech, “Mutual Coupling in Infinite Scanning Arrays,” in R. C. Hansen (ed.), Microwave Scanning Antennas, Volume II, New York, Academic Press, 1966, Chapter 3, pp. 301-306.

[54] A. K. Bhattacharyya, Phased Array Antennas: Floquet Analysis, Synthesis, and Active Array Systems, New York, Wiley, 2006.

[55] H. Steyskal, "Mutual coupling in a finite planar array antenna," Antennas and Propagation Society International Symposium, 1972, vol.10, pp. 165- 168, Dec 1972.

[56] H. Steyskal, "Mutual coupling analysis of a finite planar waveguide array," IEEE Transactions on Antennas and Propagation, vol.22, no.4, pp. 594- 597, Jul. 1974.

[57] W. Kahn, "Impedance-match and element-pattern constraints for finite arrays," IEEE Transactions on Antennas and Propagation, vol.25, no.6, pp. 747- 755, Nov. 1977.

[58] D. Pozar, "Finite phased arrays of rectangular microstrip patches," IEEE Transactions on Antennas and Propagation, vol.34, no.5, pp. 658- 665, May 1986.

[59] T. S. Bird, "Mutual coupling in finite coplanar rectangular waveguide arrays," Electronics Letters, vol.23, no.22, pp.1199-1201, Oct. 1987.

[60] K. M. Lee, R.-S. Chu, "Analysis of mutual coupling between a finite phased array of dipoles and its feed network," IEEE Transactions on Antennas and Propagation, vol.36, no.12, pp.1681-1699, Dec. 1988.

[61] J. Ashkenazy, P. Perlmutter, D. Treves, "A modular approach for the design of microstrip array antennas," IEEE Transactions on Antennas and Propagation, vol.31, no.1, pp. 190- 193, Jan. 1983.

[62] R. P. Owens, A. C. Smith , "A dual band, dual polarised array antenna of modular construction," IEE Colloquium on Circularly Polarised Elements and Arrays, vol., no., pp.6/1-6/5, Jun. 1991.

[63] D. H. Werner., W. Kuhirun, P. L. Werner, "A new design methodology for modular broadband arrays based on fractal tilings," IEEE Topical Conference on Wireless Communication Technology, pp. 267- 268, 15-17 Oct. 2003.

[64] M. W. Elsallal, D. H. Schaubert, "Electronically scanned arrays of dual-polarized, doubly-mirrored balanced antipodal Vivaldi antennas (DmBAVA) based on modular elements," IEEE Antennas and Propagation Society International Symposium 2006, pp.887-890, 9-14 July 2006.

[65] T. G. Spence, D. H. Werner, "Modular broadband planar arrays based on generalized Peano-Gosper curves," IEEE Antennas and Propagation Society International Symposium, pp.1-4, 5-11 July 2008.

[66] M. C. Van Beurden, R. Dirks, A. G. Tijhuis, "Modular modeling and optimization for large antenna arrays," 38th European Microwave Conference, pp.825-828, 27-31 Oct. 2008.

[67] W. J. Otter, B. P. Pirollo, R. I. Henderson, R. A. Lewis, "Multi-octave BAVA radiating elements for use in modular phased array antennas," 3rd European Conference on Antennas and Propagation, pp.1324-1328, 23-27 March 2009.

[68] M. King and R. Thomas., “Gain of large scanned arrays,” IRE Trans. on Antennas and Propagation, vol. 8, no.6, pp.635-636, November 1960.

[69] C. A. Balanis, Antenna Theory. Analysis and Design, Wiley, New York, 2005, third edition.

[70] V. Iyer, S. N. Makarov, D. D. Harty, F. Nekoogar, and R. Ludwig, "A lumped circuit for wideband impedance matching of a non-resonant, short dipole or monopole antenna," *IEEE Trans. Antennas and Propagation*, vol. 58, no. 1, Jan.2010.

[71] R. C. Hansen, Phased Array Antennas, New York, Wiley, 1998, Chapter 2, pp.41-45.

[72] E. J. Wilkinson, "An N-way hybrid power divider," IRE Trans. on Microwave Theory and Techniques, vol.8, no.1, pp.116- 118,Jan.1960.

[73] G. Marocco, "RFID antennas for the UHF remote monitoring of human subjects," *IEEE Trans. on Antennas and Prop.*, vol.55, no.6, pp .1862-1870, June 2007.

[74] R. S. Sangwan, R. G. Qiu, D. Jessen, "Using RFID tags for tracking patients, charts and medical equipment within an integrated health delivery network," *IEEE Intern. Conf. Networking Sensing and Control*, 2005, pp. 1070-1074.

[75] R. Want, "An introduction to RFID technology," *IEEE Pervasive Computing*, vol.5, issue 1, pp. 25-33, Jan-Mar 2006.

[76] Y. Z. Zhao, O. P. Gan, "Distributed design of RFID network for large scale RFID deployment," *IEEE Int. Conf. on Industrial Informatics*, 2006, pp.44-49.

[77] G. Yang, M. Xiao, C. Chen, "A simple energy-balancing method in RFID sensor networks," *IEEE Intern. Workshop on Anti-counterfeiting, Security, Identification*, 2007, pp 306-310.

[78] K. V. S. Rao, P. V. Nikitin, S. F. Lam, "Antenna design for UHF RFID tags: A review and a practical application," *IEEE Trans. on Antennas and Prop.*, vol.53, no.12, pp. 3870-3876, Dec. 2005.

[79] H. W. Son, J. Yeo, G. Y. Choi, C.S. Pyo, “A low-cost, wideband antenna for passive RFID tags mountable on metallic surfaces,” in *Proc. 2006 IEEE Antennas and Prop. Society Intern. Symp.,* Albuquerque, NM, pp. 1019-1022.

[80] J. Nummela, L. Ukkonen, L. Sydanheimo, M. Kivikoski, “13,56 MHz RFID for cell phone integrated reader,” in *Proc. 2007 IEEE Antennas and Prop. Society Intern. Symp,* Hawaii, pp. .1088-1091.

[81] A. Galehdar, D. V. Thiel, S.G. O’Keefe, “Antenna efficiency calculations for electrically small, RFID antennas,” *IEEE Antennas and Prop. Letters*, vol. 6, 2007.

[82] H. An, B. Nauwelaers, A, Van De Capelle, “Matching network design of microstrip antennas with simplified real frequency technique,” *Electronic Letters*, vol. 27, Issue 24, pp. 2295 – 2297, 21 Nov. 1991.

[83] B. S. Yarman, M. Sengul, P. Lindberg ,A Rydberg, “A single matching network design for a double band PIFA antenna via simplified real frequency technique,” Asia Pacific Microwave Conference, pp.1325-1328, Dec. 2006.

[84] L. Zhu, Y. Qi, "A novel approach to evaluating the gain-bandwidth potential of antennas," *Antennas and Prop. Society International Symposium, 1996. AP-S. Digest* , vol.3, no., pp.2058-2061 vol.3, 21-26 Jul 1996

[85] G. S. Smith, “Efficiency of electrically small antennas combined with matching networks,” *IEEE Transactions on Antennas and Propagation,* vol.25, no.3, pp. 369-373, May 1977.

[86] R. La Rosa, H. J. Carlin, *A General Theory of Wideband Matching with Dissipative 4- Poles*, Technical report, Polytechnic Inst Brooklyn, NY: Defense Tech. Info. Center, AD0002980, Feb. 1953.

[87] Steve Stearns, *New results on Antenna Impedance Models and Matching*, Technical Presentation, ARRL Pacificon Antenna Seminar, San Ramon, CA, Oct 19-21, 2007.

[88] B. Josephson "The quarter-wave dipole," WESCON/57 Conference Record, vol. 1 part 1, pp. 77-90, 1957.